University of Stavanger

Faculty of Science and Technology

MASTER'S THESIS

Study programme/ specialisation: Petroleum Engineering:/ Natural Gas Technology	Spring/ Autumn semester, 2019 Open/Confidential
Author: Nonso Nwankwo Ihebuzor	…… (signature of author)
Supervisor(s): Dmitry Shogin	
Title of master's thesis: The Impact of Brine Salinity/Concentration on Small Amplitude Oscillatory Shear (SAOS) Flow Material Functions of EOR Polymers.	
Credits (ECTS): 30	
Keywords: Non-Newtonian Storage Modulus Loss Modulus Complex Viscosity C-FENE-P Polymer Rheology Salinity Concentration Small Amplitude Oscillatory Shear (SAOS) Material Functions	Number of pages: 112 Stavanger, June/ 2019 Date/Year

Title page for master's thesis
Faculty of Science and Technology

Abstract

Flopaams polymers are water-soluble polymers which display a significant degree of sensitivity to salinity changes as they consist of negative charges along their molecular chains. Electrostatic charges present along the backbone of a polymer molecule causes stretching (which results from repulsion of electrons) of the polymeric chains in water. The repulsion of these charges extends the molecular chain and gives it a rigid structure which results in high viscosities. When these polymers are exposed to a saline environment, the opposite charged cations present in salts makes the polymers loose their charges and the molecules loose their rigidity and become flexible. This drastically changes the physical properties of the solution of which a reduced polymer viscosity is easily noticed.

Small Amplitude Oscillatory Shear (SAOS) material functions such as: Complex Viscosity Coefficients (alternatively, storage and loss moduli) were measured for four (4) Flopaam polymers. Sensitivity analysis were carried out to determine how these material functions depend on the polymer concentration and brine salinity. Comparisons were made with predictions made by an advanced non-Newtonian fluid model (C-FENE-P).

Results show that the C-FENE-P dumbbell model is capable of understanding the effects of salinity in Small Amplitude Oscillatory Shear (SAOS) flow . At the same time, it should be extended to a more realistic Bead-Spring-Chain model variant in order to resolve the quantitative relations between SAOS flow material functions.

Acknowledgement

I would love to express my profound gratitude to my thesis supervisor, Associate Professor Dmitry Shogin for being a mentor and a role model to look up to, continually challenging me, explaining complicated concepts in the most easy-to-understand manner, painstakingly scrutinizing this work, and spontaneously creating time for my unscheduled visits. Many thanks to the Department of Energy and Petroleum Engineering, University of Stavanger, Norway, and the management of the National Improved Oil Recovery (IOR) Center of Norway led by Professor Merete Vadla Madland, for providing the resources and laboratories used in his research work. My deepest appreciation goes to the Federal Government of Nigeria, for providing the funds for my studies through the Petroleum Technology Development Fund (PTDF) Overseas Scholarship Scheme. Thank you Kim Vorland for your super human skills in polymeric fluid rheology laboratory and your counsel in other matters as well. Without your patience and understanding, this work wouldn't have been successful. Thank you for giving me unlimited access to key equipment used in your laboratory. My appreciation goes to Eystein Opsahl for providing the polymers used in this work.

My heart felt gratitude goes to my father Engr A.I Nwankwo, and for the emotional support, my mother , Mrs. Ngozi Nwankwo, my siblings Sistogee, Chibueze, Kelechi and Chinedu for their love. To my family, friends and colleagues Micheal Ofei, Trond, Jonylyn, Annemay and Kenneth Gjedrem, Ingeborg Annet, Peder, Olav and Liv Saerheim, Roy-Even, Menyinah Gold, Alexellis, Olayinka, Lucas, Usman, Zowam, Kehinde, Tavares, Ebuka, Boyle, Leesi, Priscilla. And finally to all whose contribution to my life has made me a better person, from the innermost depth of my heart I say, Thank you!

Table of contents

List of Tables

List of Figures

CHAPTER ONE

Introduction

1.Background of the Study

An oil well undergoes important phases in which different techniques are used to ensure that crude oil is economically produced at maximum levels. The main goal of these techniques is to optimally recover as much oil as possible. On the Norwegian continental shelf (NCS), the recovery factor averages about 47 percent which is high when compared with the average global figures which are slightly below 40 per cent [NPD, 2018]. Enhanced oil recovery, used at the third stage significantly improved the recovery efficiency.

2.Polymer Flooding

Polymer flooding is an Enhanced Oil Recovery technique that improves the recovery of oil by controlling the mobility of aqueous phase of reservoir fluid to that of oil phase. It is sub-categorized under chemical flooding [Du et al., 2004]. This technique positively affects both volumetric and displacement sweep efficiencies. Polymers achieve these effects partly due to the nature of their molecular size and structure, thus, increasing the apparent viscosity of the aqueous phase. Polymers achieve this by travelling far and radially inside the reservoir thereby having contact with an appreciable surface area [Falode and Afolabi, 2011]. Polymer flooding is considered to be a technically and commercially viable method of Enhanced Oil Recovery (EOR) method due to its recent successes in the large scale application in the Daqing field in Northern China where about 300,000 barrels of incremental oil per day is attributed to polymer flooding [Wang et al., 2009]. Polymers consist of long chained organic molecules formed from the joining together of smaller molecules called monomers. Two types of polymers commonly used for Enhanced oil recovery (EOR) are the Xanthan gums and the Partially Hydrolysed polyacrylamide (HPAM) [Wever et al., 2011].

3.Polymeric Fluids

Polymeric liquids consist of macromolecules, made up of more or less identical molecular smaller structural units which could either be branched or linear sub-units. Polymeric fluids are classified as non-Newtonian fluids. The relationship between the force per unit area (shear stress) and the rate at which deformation occurs (shear rates) is not linear. They are sometimes called viscoelastic fluids because they posses both viscous and elastic properties [Bird et al., 1987a]. Polymeric fluid viscosity depends on shear rate. Laboratory experiments have demonstrated that polymers exhibit shear thinning/pseudo-plastic behaviours as their viscosities decreases with increasing shear rates [Bird et al., 1987a]. However, studies shows that HPAM polymers [page 44], a common EOR polymer exhibits pseudo-dilatant (shear thickening) characteristics in porous media as well as in viscometers at relatively high shear rates [Seright et al., 2009].
Polymeric fluids flows have been modelled with models such as the Carrea-Yasuda models [Page 37] which describes the dependency of viscosity on shear rate. However this models is very simplistic in nature and do not account for other complex flow phenomena of polymers such as normal stresses and time dependent flows.

4.Polymeric Fluid behaviours

4.1.Tube Flow

Simple laboratory experiments performed on polymeric fluids as illustrated in the Figure 2. Two fluids, Glycerine which is Newtonian, (N) and the second, a polymeric fluid (P) are placed in two separate tubes and a plate is used to stop the fluids from flowing out, downwards in figure (a). The fluids were measured to have the same viscosity at low shear rates. Once the plate was removed as shown in figure b, and the fluid is allowed to flow downward by the gravitational forces, it is observed that the polymeric fluid drains out of the tube faster than the Newtonian fluid. This simple experiment [Bird et al., 1987a], illustrates the importance of shear thinning effects in polymeric fluids. Shear thinning is the decrease in viscosity with increasing shear rate, and the fluid is said to be pseudo-

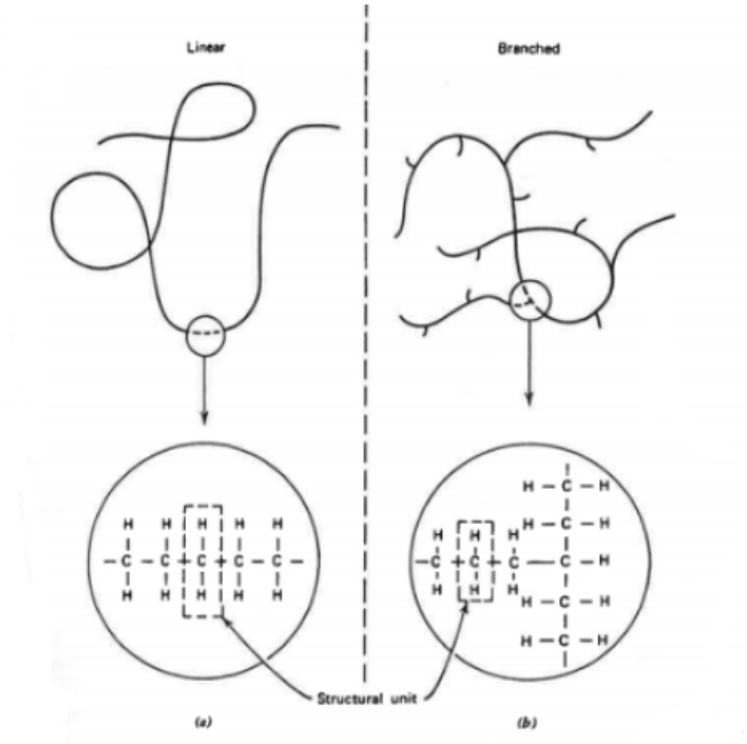

Figure 1: Symbolic Representations of Linear and Branched Polymer Molecules [Bird et al., 1987a]

plastic.

4.2.Weissenberg Rod climbing effects

When rotating stirrers are placed in two fluids, one a Newtonian and the second a polymeric fluid, in a beaker. The Newtonian fluid forms a vortex as the stirrer is being rotated as the centrifugal forces in the fluid are greater than the normal forces even at relatively low speeds. The fluid moves towards the edge of the beaker, away from the stirring rod. However, for polymeric fluids the fluid moves in a totally opposite direction. The normal forces in the fluid are so large and significant as they are greater than the centrifugal forces and the Weissenberg rod climbing effect is observed as shown in the figure 3 and 4 [Bird et al., 1987a]. The polymeric fluid moves towards the center of the beaker and climbs the stirring rod.

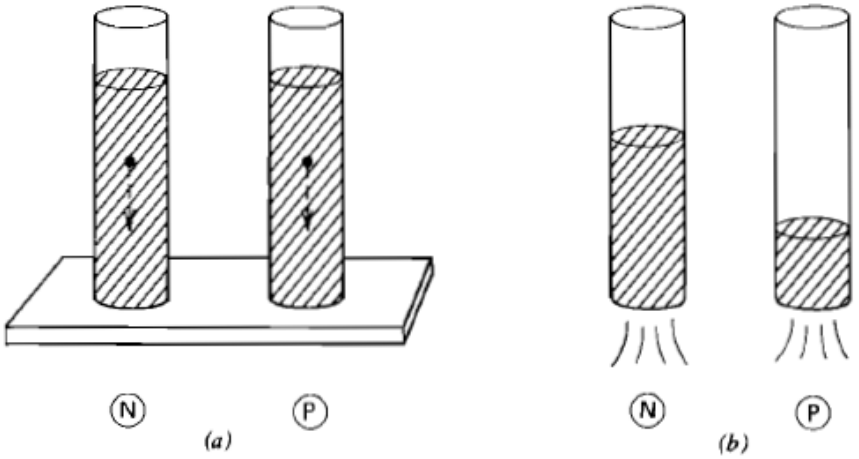

Figure 2: Tube flow and "shear thinning." In each part, the Newtonian behaviour is shown on the left (N); the behaviour of a polymer on the right (B). (a) A tiny sphere falls at the same rate through each of the fluids; (b) the Newtonian fluid flows out slower than the polymer fluid [Bird et al., 1987a]

.

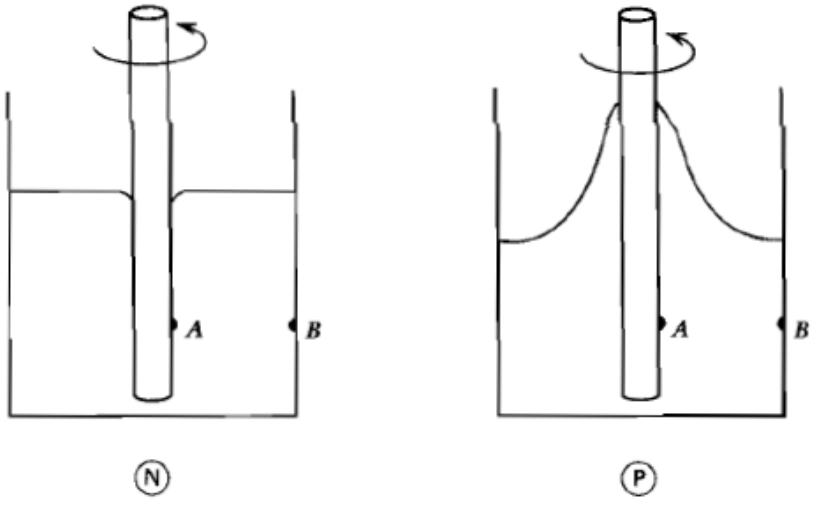

Figure 3: Weissenberg rod climbing effects for a Newtonian fluid (N) and a Polymeric Fluid (P).[Bird et al., 1987a]

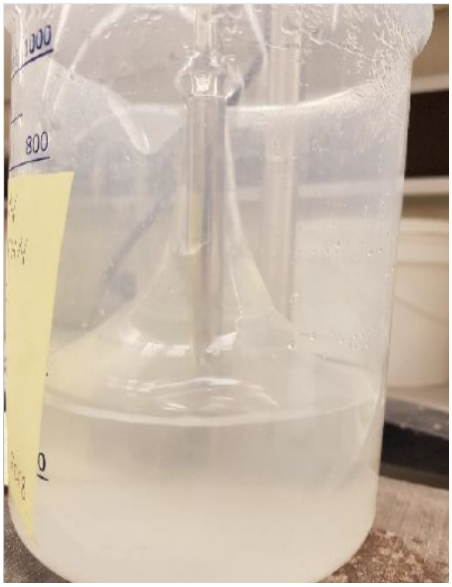

Figure 4: Weissenberg rod climbing effects for a polymeric Fluid observed in the Laboratory (P)

4.3.Extrudate Swell Effects

When Newtonian (N) and polymeric fluids (P) are being extruded from a pipette orifice as shown in the Figure 5, it is observed that the polymeric fluid expands and increases in diameter as it fall out of the pipette far more than the Newtonian fluid. This increase in diameter or expansion is attributed to the presence of significant normal stresses in polymeric fluids. Extrudate diameters of up to three or four times the tube diameter are possible with some polymers [Bird et al., 1987a] .

5.Statement of the Problem

Flopaams, which are partially Hydrolyzed Polyacrylamides (HPAM) are one of the most common polymers used commercially for polymers floods. These water-soluble polymers display a significant degree of sensitivity to salinity changes as they consist of negative charges along its molecular chains. From the general theory of polyelectrolyte solutions [Stokes and Evans, 1997], the presence of electrostatic charges along a polymer backbone is responsible for prominent stretching (due to electric repulsion) of the polymeric chains in water. The repulsion of these charges extends the molecular chain and gives it a

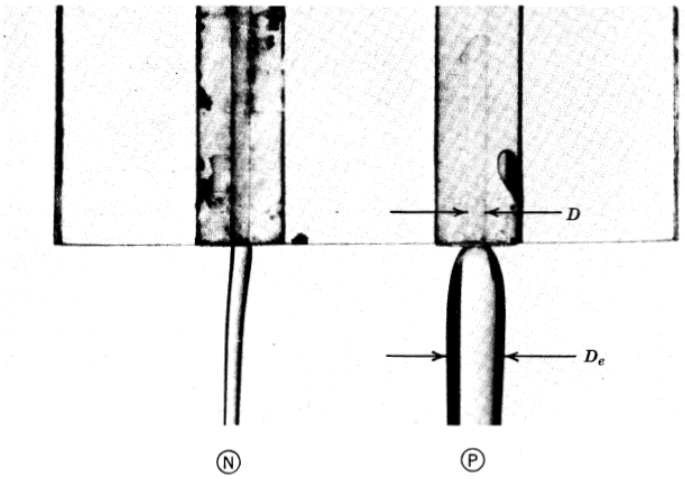

Figure 5: Behaviour of fluids issuing from orifices. Newtonian fluid shows no diameter increase upon emergence from the capillary tube; an increase in diameter is observed for polymeric fluid as it flows downward out of the tube [Bird et al., 1987a].

.

rigid structure which results in high viscosities. When these polymers are exposed to a saline environment, the opposite charged cations present in salts makes the polymers loose their charges and the molecules loose their rigidity and become flexible. This drastically changes the physical properties of the solution of which a reduced polymer viscosity is easily noticed [Borthakur et al., 1995], [Ait-Kadi et al., 1987], [Dupuis et al., 1994]. A significant amount of literature is available on the effects of salinity on polymer shear viscosity. However, knowledge of the effect of salinity on Small Amplitude Shear Oscillatory (SAOS) material functions such as: Complex Viscosity Coefficients (alternatively, storage and loss moduli), Complex First Normal Stress components, and First Normal Stress Displacement Coefficient is relatively unknown.

A deeper understanding of the physics of polymeric fluid flow, coupled with advanced modelling needs to adopted to fully explain this phenomenon.

6.Aim and Scope of the Study

In this research, the focus is on the small-amplitude oscillatory shearing (SAOS) flow experiment, which is one of the ways to investigate the behaviour of non-Newtonian fluids

in time-dependent flows. The polymer sample is subjected to harmonically oscillating shear rate at different frequencies, while the fluid's response in terms of shear stress and normal forces is being measured. This response is then described with various SAOS material functions: complex viscosity coefficients, storage and loss moduli.

The SAOS material functions for different EOR polymers are measured in a rheometer and further investigated on how they depend on the polymer concentration and on the brine salinity. The results would be compared with predictions made by an advanced non-Newtonian fluid model, the recent C-FENE-P dumbbell model, which takes the salinity effects into account.

CHAPTER TWO

Literature Review

7.Basic Concepts and Theories

7.1.Scalar, Vector and Tensor Notations

Physical quantities that are used in the studies of polymeric fluids can be categorized into scalars, vectors and tensors.

A scalar is any physical quantity that can be expressed by a single element of a number field like a real number. Examples of Scalars include: temperature, shear rate, energy, volume, time.

A vector is a geometric object that has both magnitude and direction. Examples include force, momentum, acceleration and velocity.

A tensor (second order) is a geometric object that is more general than a vector and it is represented by an array of components that are functions of the coordinates of space. Examples of tensors encountered in polymeric fluid dynamics include stress, rate of strain and vorticity tensors.

For the purpose of this thesis, we adopt the following mathematical notations for the representing and distinguishing scalars, vectors and tensors.

Normal font = Scalar

Bold Latin = Vectors

Bold Greek = Tensors

Specific notations are extended in the use of brackets.

Quantities inside round brackets (...) = Scalars

Quantities inside square brackets [...] = Vectors

Quantities inside curly brackets {...} = Tensors

7.2.The Navier-Stokes Equation

The fundamental equations used to describe the motion of fluids, Navier-Stokes equation, is derived from the conservation laws of mass, momentum and energy. Assuming that a fluid travelling at a velocity $\boldsymbol{v}$ across a surface as shown in Figure (6) dS with the volume of the surface as V. The volumetric flow rate of fluid through the surface dS is given by $(\boldsymbol{n} \cdot \boldsymbol{v})$ dS and the mass flow rate is given by $\rho(\boldsymbol{n} \cdot \boldsymbol{v})dS$ where $\boldsymbol{n}$ is the unit normal vector [Bird et al., 1987a].

7.2.1.Conservation of Mass

Carrying out a mass balance; the rate of change of mass inside the volume is equal to the total mass flow out of the volume

$$\frac{\mathrm{d}}{\mathrm{dt}} \int_V \rho dV = -\int_S (\boldsymbol{n} \cdot \rho \boldsymbol{v}) \mathrm{d}S \tag{7.1}$$

For the different integrals of area and volume, we apply the Gaussian diversion theorem to homogenize equation 10.1 in terms of volume integral, we obtain the following

$$\frac{\mathrm{d}}{\mathrm{dt}} \int_V \rho \mathrm{d}V = -\int_V (\boldsymbol{\nabla} \cdot \rho \boldsymbol{v}) \mathrm{d}V \tag{7.2}$$

Simplifying further, we use the Leibnitz rule to differentiate the integral, and combining the terms under a common integral sign, we obtain,

$$\int_V \left[\frac{\partial \rho}{\partial t} + \boldsymbol{\nabla} \cdot (\rho \boldsymbol{v}) \right] \mathrm{d}V = 0 \tag{7.3}$$

The Equation 7.3 is the conservation equation of mass over an arbitrary volume in a flowing. Setting the integral equal to zero since the limits of the integral are the boundaries

of the volume V which are arbitrary [Bird et al., 1987a].

$$\frac{\partial \rho}{\partial t} + (\boldsymbol{\nabla} \cdot \rho \boldsymbol{v}) = 0 \tag{7.4}$$

The above equation is the continuity equation and the main idea of the equation is that mass is conserved. This is true for any volume. For liquids, we assume incompressibility which implies that ρ is constant. Therefore equation (7.4) becomes

$$\boldsymbol{\nabla} \cdot \boldsymbol{v} = 0 \tag{7.5}$$

7.2.2.Conservation of Momentum

The laws of conservation of momentum is derived from the Newtons second law of motion. The law simply says that force applied on a body changes the momentum of the body.

$$\sum F_i = \frac{d(m\boldsymbol{v})}{dt} = 0 \tag{7.6}$$

The above equation shows that the momentum is conserved. There is no net gain or loss of momentum in the system, only changes of momentum between different parts of the system [Morrison et al., 2001]. Total momentum transfer in fluid flow is a sum total of the momentum contributions by the bulk flow and by molecular motion of the fluid particles. The law of conservation of momentum states that the total momentum of the fluid within a volume V, increases because of a net influx of momentum across the bounding surface and also because of external forces of gravity acting on the fluid [Bird et al., 1987a]. Mathematically,

$$\frac{\mathrm{d}}{\mathrm{dt}} \int_V \rho \boldsymbol{v} \mathrm{d}V = -\int_S [\boldsymbol{n} \cdot \rho \boldsymbol{v}\boldsymbol{v}] \mathrm{d}S - \int_S [\boldsymbol{n} \cdot \boldsymbol{\pi}] \mathrm{d}S + \int_V \rho \boldsymbol{g} \mathrm{d}V \tag{7.7}$$

where:

$[\boldsymbol{n} \cdot \rho \boldsymbol{v}\boldsymbol{v}]\mathrm{d}S$ = Local momentum across S by bulk flow contribution

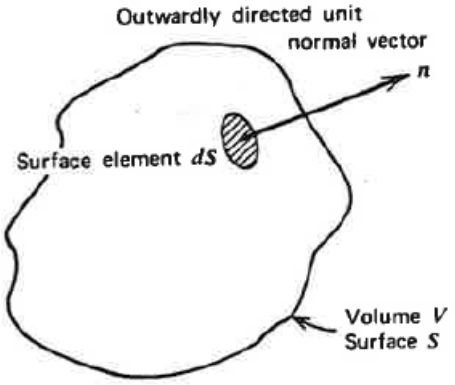

Figure 6: Arbitrary "control volume", fixed in space, over which mass, momentum and energy balances are made [Bird et al., 1987a].

$[\boldsymbol{n} \cdot \boldsymbol{\pi}]\mathrm{d}S$ = Local momentum across S due to molecular transport

$\boldsymbol{g}$ = Force per unit mass due to gravity.

Applying the Gaussian diversion theorem;

$$\int_V \left(\frac{\partial}{\partial t} \rho \boldsymbol{v} + \boldsymbol{\nabla} \cdot \rho \boldsymbol{v}\boldsymbol{v} + \boldsymbol{\nabla} \cdot \boldsymbol{\pi} - \rho \boldsymbol{g} \right) \mathrm{d}V = 0 \tag{7.8}$$

If V is an arbitrary volume, Then

$$\frac{\partial}{\partial t} \rho \boldsymbol{v} + [\boldsymbol{\nabla} \cdot \rho \boldsymbol{v}\boldsymbol{v}] + [\boldsymbol{\nabla} \cdot \boldsymbol{\pi}] - \rho \boldsymbol{g} = 0 \tag{7.9}$$

Equation 7.9 is an equation of motion

7.3.Stress Tensors

To better describe the Equation 7.9 above, we define the nature of the molecular forces described by $\boldsymbol{\pi}$ in the equation. The most important fluid properties are found in "$\boldsymbol{\pi}$".It is called the total stress tensor of the fluid. There are two major contributions to the total stress tensor $\boldsymbol{\pi}$: the thermodynamic pressure and a second portion that originates in the deformation of the fluid (equilibrium and non- equilibrium part). [Morrison et al., 2001]. Mathematically,

$$\boldsymbol{\pi} = P\boldsymbol{\delta} + \boldsymbol{\tau} \tag{7.10}$$

Where:

P = Thermodynamic pressure

$\boldsymbol{\delta}$ = Unit Tensor

$\boldsymbol{\tau}$ = Anisotropic Stress tensor ($\tau = 0$ at equilibrium conditions).

The thermodynamic pressure P is an isotropic contribution and it has an equal magnitude in all directions.it is related to the density ρ and temperature T through the "thermodynamic equations of state" $P = P(\rho, T)$ [Bird et al., 1987a].This pressure acts only normally (perpendicularly) to a give surface [Morrison et al., 2001]. The contributions of pressure can be expressed as a tensor proportional to the unit tensor. Mathematically

$$\text{Pressure contribution} = \begin{bmatrix} P & 0 & 0 \\ 0 & P & 0 \\ 0 & 0 & P \end{bmatrix} = P\boldsymbol{\delta} \tag{7.11}$$

As can be seen from figure 7, the stress tensor at a point needs to be defined by nine components. These component are defined not only by the direction in which it acts upon, but the orientation of the surface upon which it is acting is taken into consideration.

$$\text{Stress Tensor}, \boldsymbol{\tau_{i,j}} = \begin{bmatrix} \tau_{xx} & \tau_{xy} & \tau_{xz} \\ \tau_{xy} & \tau_{yy} & \tau_{yz} \\ \tau_{xz} & \tau_{yz} & \tau_{zz} \end{bmatrix} \tag{7.12}$$

The first index i defines the orientation of the surface upon which it is acting while The second subscript j shows the direction in which the stress component acts. Therefore, $\tau_{i,j}$ is the force per unit area (stress) acting in the j direction on a surface that is perpendicular to the i direction [Bird et al., 1987a] .The diagonals of the matrix in equation 7.12 represents the normal stresses while other components contained in the matrix represents the shear stresses.

An equation specifying $\boldsymbol{\tau}$ is called a constitutive equation. It is an intrinsic property of a fluid that makes it distinctly different from another fluid because it depends on the nature of the fluid. $\boldsymbol{\tau}$ is equal to zero at equilibrium (when the fluid is at rest). For a parallel

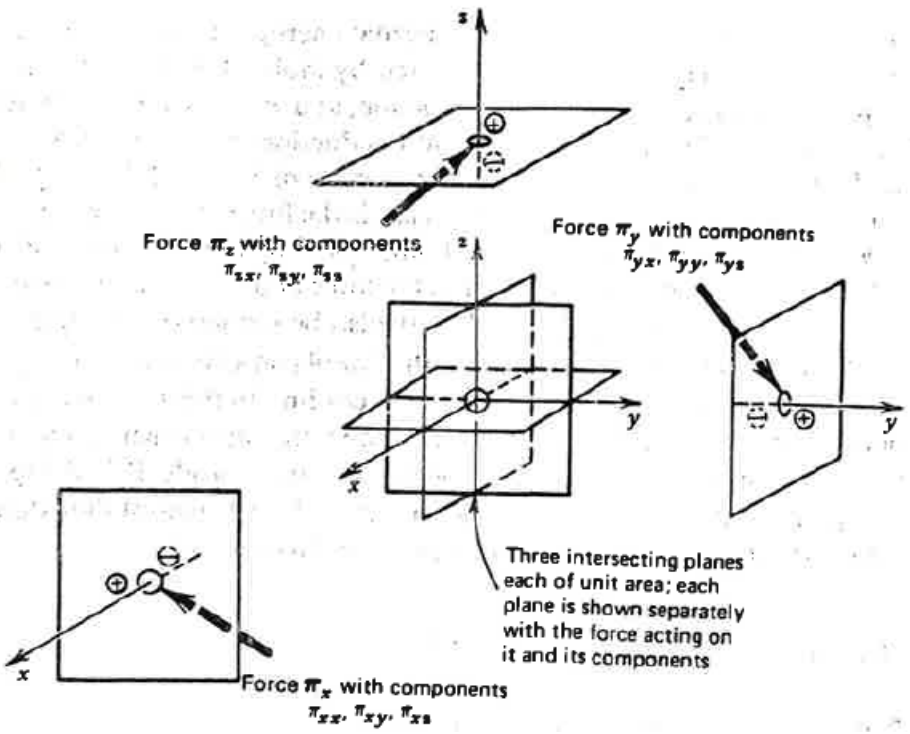

Figure 7: Sketch showing the sign convention and the index convention for the component of the stress tensor π [Bird et al., 1987a].

reference frame velocity, $\boldsymbol{\tau}$ is equal to zero.

For Newtonian fluids, $\boldsymbol{\tau}$ obeys the following equation:

$$\boldsymbol{\tau} = -\mu\left\{\boldsymbol{\nabla v} + \boldsymbol{\nabla v}^{\boldsymbol{T}}\right\} + \left(\frac{2}{3}\mu - \kappa\right)(\boldsymbol{\nabla \cdot v})\boldsymbol{\delta} \tag{7.13}$$

Where:

μ = Shear viscosity constant

κ = Bulk (Dilatational) viscosity

This is the most general linear velocity gradient equation that has been experimentally verified to be correct across a broad range of fluids. In ideal and mono-atomical gasses, the dilatational viscosity is assumed to be zero, while for incompressible liquids, $\boldsymbol{\nabla \cdot v} = 0$ [Bird et al., 1987a]. Therefore, for most Newtonian fluid of practical interest,

$$\boldsymbol{\tau} = -\mu\left\{\boldsymbol{\nabla v} + \boldsymbol{\nabla v}^{\boldsymbol{T}}\right\} = -\mu\dot{\boldsymbol{\gamma}} \tag{7.14}$$

where $\dot{\boldsymbol{\gamma}} = -\mu\left\{\boldsymbol{\nabla v} + \boldsymbol{\nabla v}^{\boldsymbol{T}}\right\}$, is defined as the rate of strain tensor.

Substituting the above stress tensor equation into the the conservation of momentum

equation, we obtain the Naiver stokes equation for an incompressible Newtonian fluid as

$$\rho\left[\frac{\partial \boldsymbol{v}}{\partial t}+\boldsymbol{v}\cdot\boldsymbol{\nabla}\boldsymbol{v}\right]+\boldsymbol{\nabla}p-\mu\boldsymbol{\nabla}^2\boldsymbol{v}-\rho\boldsymbol{g}=0 \tag{7.15}$$

8.Types of Flows and Material Functions

Fluid flow behaviours depends not only on the functions of the fluid, but also on the medium/material in which they flow through. Material functions are functions of kinematic parameters that describe the rheological behaviour of fluids. They are either predicted or measured directly from laboratory experiments while their form must be predicted by reliable fluid models. Simple flows enable the characteristics of fluids to be determined and aids in the testing of models [Shogin, 2019].
Two main types of simple flows that are easy to describe experimentally are the simple shearing flow and shear free flow. It should be noted however that real flows are typically neither of these. The experiments performed in this theses is more focused on the simple shearing flows, hence we would concentrate on this type of flow and we would give a cursory overview of the shear free flows in the subsections below.

8.1.Shearing flows

In this flow, it is assumed that the fluid layers slide past each other and that they do not mix. Locally at any at any point in the flow, we have three (3) orthogonal directions, the flow direction, the direction in which the velocity changes and the neutral direction which is equal to zero as shown in figure 8 [Shogin, 2019]. The simplest flow of this kind can be shown by the velocity field.

$$v_x=\gamma_{yx}y; \qquad v_y=0; \qquad v_z=0 \tag{8.1}$$

Where the velocity gradient $\dot{\gamma}_{yx}$ can be a function of time. The absolute value of $\dot{\gamma}_{yx}$ is called shear rate [Bird et al., 1987a]. A good analogy of this type of flow is a pack of poker cards slide on top each other. This flow type can be produced by two parallel plates and a fluid in between the plates, with the bottom plate static while the top plate moves at a constant velocity in one direction.

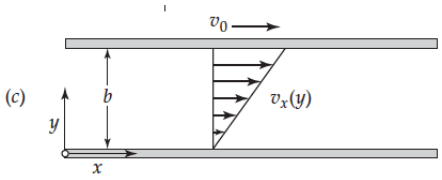

Figure 8: Simple shear flow [Chegg, 2019]

8.1.1.Stress Tensors for Steady Shear Flows

For shear flows in Newtonian fluids, it is only the shear stress $\boldsymbol{\tau}_{yx}$ that is non zero, the rest components are zero as shown in the equation 8.2.

$$\tau_{xx} = -2\mu\frac{\partial v_x}{\partial x} = 0 \tag{8.2}$$

since $V_x = V_x(y)$.

However in non-Newtonian fluids, the assumption is made that in an unknown case of a constitutive equation that any flow all the six independent components of the stress tensor may be non-zero. [Bird et al., 1987a]. The shear stress tensors have always been assumed to be symmetrical for amorphous liquids ($\tau_{xy} = \tau_{yx}$), However simulation studies conducted by [Rigelesaiyin et al., 2018] on various material systems demonstrates that the stress tensor can be asymmetric near dislocation cores, phase boundaries, holes and even in homogeneous material under a shear loading.

Mathematically, stress tensors for simple shearing flow is

$$\boldsymbol{\pi} = p\boldsymbol{\delta} + \boldsymbol{\tau} = \begin{pmatrix} P + \tau_{xx} & \tau_{xy} & 0 \\ \tau_{yx} & P + \tau_{yx} & 0 \\ 0 & 0 & P + \tau_{zz} \end{pmatrix} \tag{8.3}$$

When we assume that a fluid is incompressible, It is impossible to separate the pressure and the normal stress contributions in normal force measurements on surfaces by using simple experiments. Therefore the only quantities that are of experimental interest are the shear stress and the two normal stress difference. There are just three independent , experimentally accessible quantities in simple shear flows [Bird et al., 1987a]. they are

Shear stress: τ_{yx}

First Normal stress difference: τ_{xx} - τ_{yy}

Second Normal Stress difference: τ_{xx} - τ_{yy}

It is important to note that Newtonian fluids have no normal stresses and hence, the stress components of the diagonal in equation 8.3 is equal to zero and only the pressure components are non-zero [Bird et al., 1987a]. Therefore , Newtonian fluids are being described alone by viscosity. However this is not the case for non-Newtonian in steady state shearing flows as they are described by the following material function equations.

$$\tau_{yx} = -\eta(\dot{\gamma})\dot{\gamma}_{yx} \tag{8.4}$$

$$\tau_{xx} - \tau_{yy} = -\psi_1(\dot{\gamma})\dot{\gamma}_{yx}^2 \tag{8.5}$$

$$\tau_{yy} - \tau_{zz} = -\psi_2(\dot{\gamma})\dot{\gamma}_{yx}^2 \tag{8.6}$$

The non- Newtonian viscosity η in equation 8.4 which is a function of shear rate, is similar to the viscosity μ found in Newtonian fluids. ψ_1 and ψ_2 are called the first and second normal stress coefficients respectively. η, ψ_1, ψ_2 are known as the steady shear flow material functions [Bird et al., 1987a]. For Newtonian fluids; $\eta(\dot{\boldsymbol{\gamma}}) = \mu = constant$, while $\psi_1(\dot{\boldsymbol{\gamma}}) = \psi_2(\dot{\boldsymbol{\gamma}}) = 0$ signifying that there is no normal stress.

Plots of viscosity $\eta(\dot{\boldsymbol{\gamma}})$ showed that at low shear rates from Figure 9, the shear stress is proportional to $(\dot{\boldsymbol{\gamma}})$ and viscosity approaches a constant value η_0 called the zero-shear rate viscosity. When we have higher shear rates, the polymer viscosity decreases with corresponding increase in shear rates. this phenomenon, called shear thinning is a predominant property of polymers solutions and melts [Bird et al., 1987a].

From a plot of log η versus log $\dot{\gamma}$, it was observed that the plotted viscosity against shear rate curve showed a linear region at relatively high shear rates which could persist for a broad range of decreasing viscosity. this slope, also called the power law region was determined experimentally to be between -0.4 to -0.9 for polymeric fluids [Bird et al., 1987a]. The rate at which the ranges of shear rates transits from from η_0 to the power law region is directly proportional to the molecular weight distribution of the polymer. An increase in the molecular weight of the polymer gives a broader transition region that shifts closer to

lower shear rates [Graessley, 1974]. At sufficiently high shear rates, the effect of viscosity becomes insignificant and would approach η_∞, called the infinity-shear-rate viscosity as shown in Figure 9. [Bird et al., 1987a]

8.2.Shear free flows

Shear free flows show more symmetry than simple shear flows and it is unaffected by 180 degrees rotation about the x, y or z axis.shear free flows matrix hence reduces to the form

$$\pi = p\boldsymbol{\delta} + \boldsymbol{\tau} = \begin{pmatrix} P+\tau_{xx} & 0 & 0 \\ 0 & P+\tau_{yy} & 0 \\ 0 & 0 & P+\tau_{zz} \end{pmatrix} \tag{8.7}$$

Simple shear free flows can be described by the velocity profile

$$v_x = -\frac{1}{2}\dot{\epsilon}(1+b)x \tag{8.8}$$

$$v_y = -\frac{1}{2}\dot{\epsilon}(1-b)y \tag{8.9}$$

$$v_z = +\dot{\epsilon}z \tag{8.10}$$

where $0 \leq b \leq 1$. and $\dot{\epsilon}$ is the elongation rate. Values of b and $\dot{\epsilon}$vary depending on the type of shear free flow encountered [Bird et al., 1987a].These flow types include:

Elongation flow: $(b = 0, \dot{\epsilon} > 0)$

Biaxial stretching flow: $(b = 0, \dot{\epsilon} < 0)$

Planar elongation flow: $(b = 1)$

For incompressible fluids, there are only two normal stress difference of practical importance [Bird et al., 1987a].

$$\tau_{zz} - \tau_{xx} \tag{8.11}$$

$$\tau_{yy} - \tau_{xx} \tag{8.12}$$

The equations for the material functions in elongational flow is given by

$$\tau_{zz} - \tau_{xx} = -\hat{\eta}_1(\dot{\epsilon}, b)\dot{\epsilon} \tag{8.13}$$

$$\tau_{yy} - \tau_{xx} = -\hat{\eta}_2(\dot{\epsilon}, b)\dot{\epsilon} \tag{8.14}$$

Note that in the case of steady shear flows, where $b = 0$, $\eta = \hat{\eta}_1(\dot{\epsilon})$ and $\hat{\eta}_2(\dot{\epsilon}) = 0$.

$\hat{\eta}$ is called the Trouton or elongational viscosity [Bird et al., 1987a].

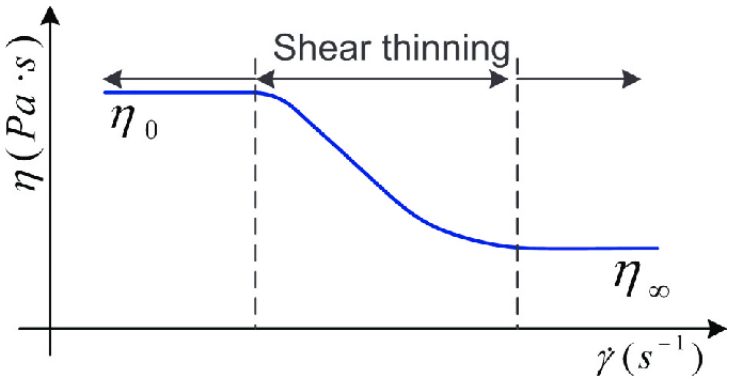

Figure 9: Linear plot of viscosity against shear rate. showing the zero-shear rate viscosity region η_0, power law region and the infinity-shear-rate viscosity η_∞ [Martínez-Vázquez et al., 2010]

.

8.3.Unsteady Shear flow

Unsteady shear flow are flows that depend on time (frequency) as well as shear rates and there are three stress properties that can be measured. These properties describe the flow and they include the shear stress and the two normal stress differences [Bird et al., 1987a]. There are various standardized laboratory flow experiments used in rheology that are conducted to evaluate these measurable stress properties, however for the purpose and scope of this work, the focus is on the Small-Amplitude Oscillatory Shear (SAOS) experiments.

8.3.1.Small Amplitude Oscillatory Shear(SAOS)

Oscillatory shear is used to define viscoelastic fluids. SAOS is a non- destructive test that is used to investigate changes in the structure of complex fluids at an early stage. This test requires that that deformation should occur at very small strain amplitudes within the Linear Viscoelastic Region (LVE). Strain amplitudes used in SAOS are generally very small in the order of 10^{-2} to 10^{-1} [Hyun et al., 2011]. It involves the measurement of of the unsteady response of a sample that is contained between two parallel plates where the upper plate undergoes small-amplitude sinusoidal osculations in its own plane with a frequency ω [Bird et al., 1987a].

In Polymeric fluids, the shear stress that oscillates at a certain frequency ω is not always

in phase with either the shear rate or shear strain. This is illustrated by the figure 10.

Mathematically,

$$\gamma_{yx}(0,t) = \gamma^0 \sin \omega t \tag{8.15}$$

$$\dot{\boldsymbol{\gamma}}_{\boldsymbol{yx}}(t) = \gamma^0 \omega \cos \omega t = \dot{\boldsymbol{\gamma}}^{\mathbf{0}} \cos \omega t \tag{8.16}$$

to find the shear stress, the amplitude and and phase angle shift are written as functions of the frequency.

$$\tau_{yx} = -A(\omega)\gamma^o \quad \sin(\omega t + \delta) \qquad (0 \leq \delta \leq \frac{\pi}{2}) \tag{8.17}$$

$$\tau_{yx} = -B(\omega)\dot{\gamma}^0 \quad \cos(\omega t - \Phi\delta) \qquad (0 \leq \delta \leq \frac{\pi}{2}) \tag{8.18}$$

Where $\Phi = \dfrac{\pi}{2} - \delta$.
If we write equation 8.17 and 8.18 in terms of the in-phase and out-of-phase parts of shear stress, we can show the the equivalent sets of viscoelastic material functions G' and G''.

$$\tau = -G'(\omega)\dot{\gamma^o} \quad sin\omega t - G''(\omega)\dot{\gamma^o} \quad cos\omega t \tag{8.19}$$

$$\tau = -\eta'(\omega)\dot{\gamma^o} \quad sin\omega t - \eta''(\omega)\dot{\gamma^o} \quad cos\omega t \tag{8.20}$$

Taking the equivalence by combining equations 8.19 and 8.20 with equations 8.17 and 8.18, we find that G', G'' are related to A, δ and also, η' , η'' are related to B, Φ be the following relationship

$$A(\omega) = \sqrt{G'^2 + G''^2} = |G^*|, \qquad tan\delta = \frac{G''}{G'} \tag{8.21}$$

$$B(\omega) = \sqrt{\eta^2 + \eta''^2} = |\eta^*|, \qquad tan\Phi = \frac{\eta''}{\eta'} \tag{8.22}$$

Where $|G^*|$ and $|\eta^*|$ are magnitudes for the complex modulus G^* and complex viscosity η^* respectively.

Storage modulus G' and loss modulus G'' are called the linear viscoelastic properties and they are used to determine the behaviour of a material undergoing a small deformation. They are discussed in details in the subsequent sections

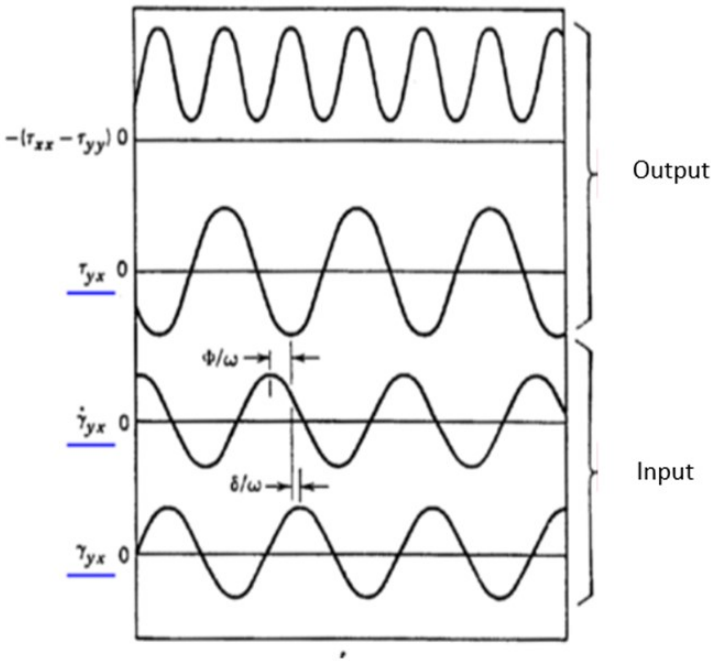

Figure 10: Oscillatory shear strain,shear rate,shear stress and First normal stress difference in small-amplitude oscillatory shear flow [Bird et al., 1987a]

8.4.Shear Modulus

The storage modulus $G'(\omega)$ is a measure of the deformation energy stored and recovered per cycle, when different systems are compared at the same strain amplitude [Ferry, 1980]. After the load is removed, this energy is completely available and would act as a driving force to restore the fluid either partially of completely to the previously obtained deformation structure [Mezger, 2011]. A study of storage modulus G' as a function of angular frequency ω of colloid samples by [Okubo et al., 2001] showed that at significantly large phase angle ϕ, the storage modulus G' was insensitive to frequency ω. At low sphere concentrations of 0.022 and 0.043 in volume fraction, the phase transition from "crystal" to "liquid" was observed. While measuring the elongational relaxation modulus of polystyrene, [Ninomiya and Fujita, 1957] observed that at the end of a terminal zone where $G(\omega)$ approaches zero with decreasing frequency, G' becomes proportional to ω^2 instead of being exponentially dependent on t. They concluded that the proportionality constant $A_G = G'/\omega^2$ depends strongly on the molecular weight distribution.

Loss modulus G'', is defined as the stress 90^o out of phase with the strain divided by the strain and it is a measure of the deformation energy that is used up or lost as heat per cycle of sinusoidal deformation, when different systems are compared at the same strain amplitude. At low frequencies, G'' for a viscoelastic liquid is directly proportional to ω, with a slope of 1 on a logarithmic plot [Ferry, 1980]. [Winter and Chambon, 1986] in analysing the linear viscoelasticity of a cross-linked polymer,showed that both loss and storage moduli were found to be congruent and proportional to $\omega^{0.5}$ at gel point.

The loss factor or damping factor, is calculated as ratio of the lost and storage moduli. it gives an idea of the ratio of the viscous and elastic portions of the viscoelastic deformation behaviour.Mathematically,

$$\tan\delta = \frac{G''}{G'} \tag{8.23}$$

Ideally elastic behaviour is shown where $\delta = 0^o$ or where $\tan\delta = 0$. In this scenario, the storage modulus G' dominates G''. Ideally viscous behaviour is shown when $\delta = 90$ or as $\tan\delta = \infty$. This scenario depicts that the loss modulus G'' completely dominates the storage modulus G'.When the viscous and the elastic characteristics of the fluid are exactly balanced, i.e $G' = G''$, then $\tan\delta = 1$ or $\delta = 45$ [Mezger, 2011].
For dilute solutions, $\tan\delta$ is usually very high because both solvent and solute contribute G'' but only the solute contributes to G'. At low frequencies, $\tan\delta$ is large for uncross-linked polymers and it is inversely proportional to the frequency [Ferry, 1980].

8.5.Complex Viscosity

The complex viscosity η^* is expressed as a complex number having a real and imaginary part. It is totally different from normal shear viscosity η. They are measured and analysed from oscillatory tests. The real and imaginary part of the complex viscosity are written mathematically in terms of sine and cosine functions.

$$\eta' = \frac{G''}{\omega} = \frac{(\tau_A \sin\delta)}{(\gamma_A \omega)} \tag{8.24}$$

$$\eta'' = \frac{G''}{\omega} = \frac{(\tau_A \cos\delta)}{(\gamma_A \omega)} \tag{8.25}$$

where η' and η'' represents the viscous and elastic behaviours respectively and are both measured in pascals-seconds [Pa.s].

Complex viscosity can be represented as the vector sum of both individual parts by using the Pythagoras theorem.

$$|\eta^*| = \sqrt{(\eta')^2 + (\eta'')^2} = \frac{\sqrt{(G')^2 + (G'')^2}}{\omega} \tag{8.26}$$

9.Generalized Newtonian Fluid Models

This class is the most widely used fluid model because it is simple, describes shear dependent viscosity and it works well in steady shear flows. Here, shear stress is a function of shear rate but it is independent of the history of deformation. The constitutive equation has the form of the generalized Newtonian fluid.

$$\tau = \eta(\dot{\gamma})\dot{\gamma} \tag{9.1}$$

Where:

μ = Viscosity

τ = Shear stress

$\dot{\gamma}$ = Shear rate

This model is however too simplistic as it does not account for complex fluid flows such as normal stresses and time dependent effects. The only non-Newtonian feature of this fluid model is the shear dependent viscosity. There are other variants of the Generalized Newtonian models. The power law model and the Carreau-Yasuda models are briefly reviewed in the subsequent sections.

9.1.Power Law Model

Proposed by Ostwald and De Waele in 1929, the power law model, which is a variant of the generalized Newtonian fluid model, relates the shear stress of a Newtonian fluid to its shear rate of deformation using the following relationship.

$$\eta(\dot{\gamma}) = K\dot{\gamma}^{n-1} \tag{9.2}$$

Where:

$\eta(\dot{\gamma})$ = viscosity

K = Constant called consistency constant

$\dot{\gamma}$ = Shear rate

n = Power Law index

When $n < 1$, = shear thinning fluid; $n > 1$, = shear thickening fluid while for Newtonian fluids, n= 1. One of the main disadvantage of the power law model is that it is valid only in simple shear flows and it fails to describe the viscosity non-Newtonian fluids in very low and very high shear rate regions [Bird et al., 1987a].

9.2.Carreau-Yasuda Model

This is another varriant of the generalized Newtonian fluid model. In this model, the effective viscosity depends on the shear rate by the following equation.

$$\eta_{eff}(\dot{\gamma}) = \eta_{\infty} + (\eta_o - \mu_{\infty}) \left(1 + (\dot{\gamma}\lambda)^2\right)^{\frac{n-1}{2}} \tag{9.3}$$

Where:

$\eta_{eff}(\dot{\gamma})$ = viscosity depending on the shear rate

η_o = Viscosity at Zero shear rate (Pa·s)

η_{∞} = Viscosity at infinity shear rate(Pa·s)

n = Power Law index

λ = Relaxation time/ on set of shear thinning

The Carreau Yasuda model is quite more successful than the power law due to its flexibility. At low shear rates ($\dot{\gamma} << 1/\lambda$), the model reduces to the normal Newtonian fluid model. At intermediate shear rates ($\dot{\gamma} \geq 1/\lambda$), it behaves like the power law model while at relatively high shear rates which is dependent on the power law index n and infinite shear rate viscosity μ_∞ it behaves like a Newtonian fluid again. However the Carreau-Yasuda model has certain limitations as it fails in its prediction of unsteady flow and it does not account for normal stresses [Bird et al., 1987a].

10.Physical Non-Newtonian Fluid Models

These models are based on physical theory as various assumptions about the molecular interactions at the microscopical levels are made and being up scaled. Dilute solution implies that the individual molecules of the polymer do not interact with each other however, they interact with the solvent that they are dissolved in. For concentrated solutions, the polymer molecules interact with each other. In dilute solutions and in concentrated solutions, different physics works and different phenomena dominates, hence as of now there is no single model that is valid for all the range concentrations. There are models which applicable to concentrated while others are applicable to dilute solutions [Bird et al., 1987b].

Dumbbell models which assumes two beads connected with a chain are the models predominantly used in the modelling of dilute solutions while Bead Spring Chain models which assumes several chains with beads at various lengths of the chains, are used for concentrated solution [Bird et al., 1987b]. These models are realistic because polymer molecules have the ability to take different orientations in space just like real molecules and they can deform, expand and contract exactly like real molecules. These properties of the real molecules are well represented by these models [Shogin, 2019]. A good example of the bead spring chain model is the Phan-Tier Than model which is discussed in the subsequent chapters. For the purpose of this study, much emphasis is being placed on the

diluted solutions.

10.1.Hookean Dumbbell Models

The most simple kinetic theory model for a dilute solution of linear flexible polymers consists of a Hookean dumbbell, that is two beads connected by a Hookean spring, suspended in an incompressible Newtonian fluid [Bird et al., 1987b]. The beads represent molecular segments of several monomers and the spring describe the entropic effects to which the end-to-end vector of the polymer is subject [Herrchen and Öttinger, 1997]. The beads accounts for the viscous forces while the spring accounts for the elastic forces in the molecules [Larson, 1999]. The system is approximated as a system of oscillations between the molecules. This is shown in the Figure 11.

A major pitfall of this model is that It is assumed that the spring obeys Hooks law, however the Hookean spring force is only realistic for small deformations from equilibrium and the spring has absolutely no limit to the extent in which it can be extended [Herrchen and Öttinger, 1997]. This model does not account for shear thinning, non-linearity and also, elongational viscosity approaches infinity at infinite shear rates. Hookean dumbbell models predicts shear independent viscosity, first normal stresses coefficients.

$$\boldsymbol{F} = H \cdot \boldsymbol{Q} \tag{10.1}$$

Where:

$\boldsymbol{F}$ =Force

$\boldsymbol{Q}$= Connector vector

10.2.FENE Dumbbell Model

The Finite Elongated Non-Linear Elastic (FENE) model, proposed by [Warner Jr, 1972], attempts to correct the problems of infinite extension in the Hookean dumbbell model by introducing a concept of finite extensibility [Bird et al., 1987b] as shown in the equation.

Figure 11: A Simple dumbbell Model

$$\boldsymbol{F} = \frac{H\boldsymbol{Q}}{1 - \dfrac{Q^2}{Q_o^2}} \tag{10.2}$$

Where:

$\boldsymbol{F}$= Warner Force

$\boldsymbol{Q}$ = Three dimensional connector vector of the beads

Q_o = Maximum possible spring length

H = Spring Constant

For small values of Q, it reduces to the Hookean model. If the Q grows, it cannot be extended far more than than Q_O. This limit corrects the pitfall of the Hookean model. This model gives a good qualitative prediction of all non-Newtonian flow . The major disadvantage of this model, owing to the non-linearity of the spring force, is that no closed constitutive equation for the polymeric stress tensor exists and no simple analytical solutions are possible [Bird et al., 1987b]. Attempts by [Warner Jr, 1972, Armstrong, 1974], have been made to compute perturbation and numerical solutions for steady shear flows, steady homogeneous flows and high amplitude oscillatory flows respectively.

10.3.FENE-P Dumbbell Model

The FENE-P model, introduced by Peterlin, is an analytical model that leads to a close constitutive equation. It is derived by replacing the configuration dependent non-linear

factor in the FENE spring force by a self consistently averaged term [Bird et al., 1987b].

The constitutive equation is derived as composing of two components: The polymer and the solvent which dissolves the polymer [Shogin et al., 2017]. It can thus be written as

$$\boldsymbol{\tau} = \boldsymbol{\tau_s} + \boldsymbol{\tau_p} \tag{10.3}$$

Where τ_s is assumed to be a Newtonian fluid and τ_P is written as :

$$\frac{b}{3} Z \boldsymbol{\tau}_p + \lambda \boldsymbol{\tau}_{p(1)} - \lambda \{\boldsymbol{\tau}_p - nkT\boldsymbol{\delta}\} \mathrm{D}_t \ln Z = -nkT\lambda\dot{\boldsymbol{\gamma}} \tag{10.4}$$

Where

λ = Time constant

nkT = Ideal gas pressure

b = Degree of non-Linearity

$\boldsymbol{\tau}_{p(1)}$ = Oldroyd derivative of $\boldsymbol{\tau}_p$ [Bird et al., 1987b].

Z = Polymer contribution to the stress tensor, given by

$$Z = 1 + \frac{3}{b}\left(1 - \frac{\mathrm{tr}(\tau_p)}{nkTb}\right) \tag{10.5}$$

The FENE-P model behaves like the FENE Dumbbell due to the self-consistent linearisation, the diffusion equation of the end to end vector of the dumbbell has a Gaussian solution in any homogeneous flow [Bird et al., 1987b]. This model has been successful in predicting all complex flow behaviours that is required. However, the quantitative values of the material functions may not be numerically correct. There are various modification and variants of the FENE-P dumbbell model such as the FENE-PM model by [Wedgewood et al., 1991]. [Chilcott and Rallison, 1988] proposed the FENE-CR model which was used to compute to numerically complex flows . The model is based on Peterlin approximation, however it eliminates the shear rate dependence of the steady state viscosity in order to describe Boger fluids [Herrchen and Öttinger, 1997] which is out of the scope of this work.

10.4.C-FENE-P Dumbbell Model

The C-FENE-P [**?**], shall model polyelectrolytes solutions and explain the salt sensitivity. This dumbbell model builds on the success of the FENE-P Model, however it further attempts to model the effect of charge repulsion between ionization groups in the polymer [Dunlap and Leal, 1984]. Mathematically, the connector force for this model is given by the equation

$$\boldsymbol{F_c} = \frac{H \cdot \boldsymbol{Q}}{1 - \left(\frac{Q}{Q_o}\right)^2} - \boldsymbol{F_e} \tag{10.6}$$

F_e is the repulsive force that exist between the charges given by the relation

$$\boldsymbol{F_e} = -\frac{q^2}{4\pi\epsilon_o\epsilon}\frac{\boldsymbol{Q}}{Q^3} \tag{10.7}$$

Where:

ϵ_o is the permittivity of the vacuum and

q = Effective charge

ϵ = Relative permittivity of the solvent to be.

The main constitutive equation is similar with the constitutive equation for the FENE-P Dumbbell model. The main difference is found in the Z factor which is dependent on the E. for the C-FENE-P, the Z factor is given as:

$$Z = (Z_0 - 1)\mathcal{F}(Z_0 - 1, E/b) \tag{10.8}$$

Where:

E = Non-negative Electric to Elastic ratio.

$\mathcal{F}$= A special function introduced by [Shogin and Amundsen, 2019].

A higher value of E corresponds to a larger electric repulsive force. Also, an increase in salt concentration gives a corresponding decrease in E. At $E = 0$, the model reverts back to the original FENE -P Dumbbell model, while at $E \to \infty$, the rigid dumbbell model is attained [**?**].

10.5.Rigid Dumbbell Model

These models are similar to the Hookean models however they work on an assumption that the connecting rod between the polymer molecules are rigid and not flexible. They are used mainly in the modelling of stiff bio-polymers such as protein molecules and DNA. Further references [**?**, Bird et al., 1987b] gives a detailed discussion of this model.

10.6.Phan Tien -Tanner Model PTT

Unlike the FENE-P model that is being built using the kinetic theory, the Phan Tien Tanner model is based on the neuron network principles [Thien and Tanner, 1977]. It is a model that focusses on modelling concentrated polymer solutions and melts. The model includes material functions that can describe the extensional and shear responses of flow and it can be solved analytically for its viscometric functions.

the model can be shown as

$$Z(\mathrm{tr}\boldsymbol{\tau})\boldsymbol{\tau} + \lambda\boldsymbol{\tau}_{(1)} = -\eta_o\dot{\gamma} \tag{10.9}$$

Where: for Linear model (LPTT)

$$Z = 1 - \epsilon\lambda \mathrm{tr}\tau/\eta_o \tag{10.10}$$

and for Exponential model (EPTT)

$$Z = \exp[-\epsilon\lambda \mathrm{tr}\tau/\eta_o] \tag{10.11}$$

Where:

η_o = Viscosity,

λ= parameter of time

ϵ = extensional parameter

An interesting feature of the EPTT is the poly-logarithmic shear thinning where the thinning increases with the shear rate and there is no power law region [Thien and Tanner, 1977].

The three parameters listed above are to be determined from experiments. The linear model (LPTT) is very much identical to the FENE-P model for simple shear flow scenarios.

11.EOR Polymers

11.1.Partially hydrolyzed polyacrylamide (HPAM)

This is the most popular polymer used for EOR applications and it is a copolymer of Polyacrylic acid (PAA) and Polyacrylamide (PAM). It is gotten from the partial hydrolysis of PAM [Morgan and McCormick, 1990] or by the co-polymerization of sodium acrylate with acrylamide . The thickening capability of HPAM is largely depends on its high molecular weight and also in the electrostatic repulsion between polymer coils and between polymeric segments in the same coil [Lake, 1989]. HPAM polymers are polyelectrolytes and when they are dissolved in water that contain electrolytes (salts) a significant reduction in viscosity is observed [Borthakur et al., 1995], and the specific viscosity of HPAM solutions depends on the amount of salt present [Sukpisan et al., 1998]. HPAM polymers are preferred in EOR application because they have the capacity to tolerate high mechanical forces that are present during the flooding process. It is relatively cheap and withstands bacteria attack [Lake, 1989].

11.1.1.Flopaams

Produced by SNF, these poly acrylamide water soluble flocculants exist in different forms such as powder, beads, solutions, emulsions and dispersions. Molecular weights could range from 2 million to 22 million Dalton and ionic charge ranges from 0 to 100 per cent [SNF, 2004]. Molecular weight also depends on the hydrolysis level while maximum molecular weight could be achieved at 40 mole. Partially hydrolysed polyacrylamide is a synthetic straight chain polymer of acrylamide monomers of which some has been hydrolysed [SNF, 2004]. For the purpose of this experiment, four (4) Flopaam polymers were studied. They include:

1. Flopaam 5115 Very High Molecular weight (VHM)
2. Flopaam 5115 Very Low Molecular weight (VLM)
3. Flopaam AN-125 Very High Molecular weight (VHM)
4. Flopaam AN-125 Very Low Molecular weight (VLM)

12.Effects of Salinity

The effects of salts on HPAM polymers and other polymers has been well studied . Studies by [Ait-Kadi et al., 1987] on the salt on solution viscosity of HPAM polymers showed that below the critical shear rate, addition of salts (NaCl) reduced the extent of shear thinning, while above the critical shear rate the amplitude of shear thickening is increased. A study of the effect of salinity, polymer concentration and sulfonation degree on the viscosity and solubility effect of the various PAMS copolymers by [Rashidi et al., 2010] showed that polymer solution viscosity decreases in the presence of NaCl. This decrease rate after a certain NaCl concentration levels off, a small increase rate due to the increase viscosity of the solvent was seen up to 20 wt per cent NaCl concentration. It was concluded that with regards to the salinity effect on the shear rate dependence, PAMS copolymers behave almost like Newtonian fluids at high NaCl concentration.

[Lee et al., 2009] developed a comprehensive rheological database for floppams EOR polymers .The shear rate viscosity and the dynamic oscillatory viscosity for a number of HPAM polymers were measured in terms of shear rate/frequency, polymer concentration, salinity, hardness and temperature and their effects on various parameters in the Carreau model. They found out that the effects of salinity on the parameters in the Carreau model is quite different from that for polymer concentration. An increase in the salinity leads to a corresponding increase in n but decreases other parameters. They further observed that divalent ions have a similar effect on the Carreau model parameters as compared salinity, however the magnitude of dependence is much larger that that for NaCl salinity. They concluded that the effects of polymer concentration and salt concentration on shear viscosity can be accurately quantified by using the Martins equation and that empirical

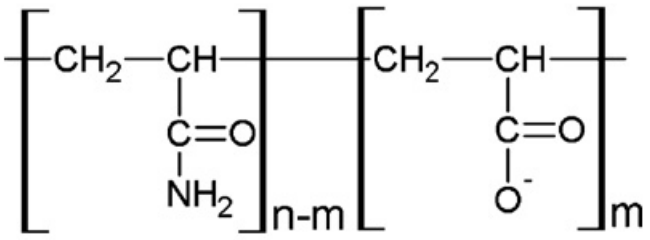

Figure 12: Chemical structure of HPAM [Wever et al., 2011]

correlations developed by fitting the measured data describes the effects of key process variables polymer shear viscosity accurately and reliably except for very low salinity.

[Tam and Tiu, 1990] studied the effects of salts on the steady shear behaviour of HPAM. They established that the addition of divalent salts in a solution reduces the viscosity at the zero-shear-rate limit by about 5 to 6 times more than mono-valent salts. They further showed that addition of salts shifts the position of the critical shear rate (where the onset of shear thinning occurs) to a higher value, and causes a reduction in in the slope of the shear thinning region. After testing various kinds of monovalent and divalent salts, they concluded that the magnitude of viscosity reduction is affected by the valency of the salt and not by the species.

[Stavland A., 2013] studied the effects of salinity on polymer viscosity of two EOR plymers , one HPAM and one AMPS. The polymers were dissolved in brines with different concentrations of NaCl and $CaCl_2$. Results shows that HPAM polymers are generally slightly more salt sensitive than AMPS polymers . They concluded that for polymers where the viscosity depends on salinity, the controlling parameter is the effective salinity and that the intrinsic viscosity decreases as the effective salinity increases. In a different study although not on polymers, [Jeldres et al., 2018] studied the effect of salinity on the dynamic moduli of flocculated kaolinite sediments and found out that salinity causes a non-monotonous effect on the yield stress, which reaches a maximum value at 0.001 M NaCl.They concluded that it is a consequence of the electrolytes present that on the one hand, shield the electric charges and on the other cause the winding of the flocculant chains. However, the phase angle increases monotonically with the salinity of the system. They suspected that the gel structure at high salt concentrations may be different from that at low salt concentrations, and that gels formed by kaolinite particles are more

solid-like at low salinity and more liquid-like as the salt concentration increases.

CHAPTER THREE

Methodology

The aim of these experimental research is to study the effects of salinity and concentration on the Small Amplitude Oscillatory Shear (SAOS) material functions of various Enhanced Oil Recovery (EOR) polymers in the Small Amplitude Oscillatory Shear (SAOS) or otherwise known as the linear viscoelastic (LVE) range. Furthermore, compare the experimental results to predictions made by the C-FENE- P mathematical model. In this experiment, the effects of temperature/temperature shifts were not considered as experiments were carried out at isothermal temperatures of 20^oC. The methodology employed in this experiment was designed to suit the objectives. The following template was used to carry out the experiment.

1. A polymer stock standard solution of a specific concentration was prepared with de-ionized water at Zero Salinity (Base Solution).

2. This Base Solution was further diluted with deionized water to different concentrations and rheometric readings were measured.

3. A second polymer stock standard solution of the same concentration as (1) above was prepared with brine solution that has a salinity corresponding to the salinity of sea water (35 grams per litre). This second solution was diluted with sea water to different polymer concentrations and rheometric readings were measured.

4. Subsequent polymer stock solutions of were prepared with brine concentrations of 10, 20 and 30 g respectively and measurements were recorded.

13.Method for determining G' and G'', and Complex Viscosity Coefficients

13.1.Amplitude Sweeps

Shear strain amplitude or strain sweeps were conducted at a controlled shear strain. Here, the period of time for each one of the oscillations cycles of the measuring bob is kept constant , only the maximum value of the bobs deflection angle (amplitude) is increasing continuously. [Mezger, 2011]. The screen shot in Figure 13 shows the amplitude sweep setting on the Anton Paar rheometer. Amplitude sweeps were performed to determine the Small Amplitude Oscillatorry Shear (SAOS) region for each polymer sample tested. At low amplitudes, both the $G'(\gamma)$ and $G''(\gamma)$ are constant and display plateau values, mostly on different levels within the SAOS region [Mezger, 2011].

13.2.Frequency Sweeps

Frequency sweeps , which are oscillatory tests were then performed at variable frequencies, with a constant amplitude value that falls with the SAOS region [Mezger, 2011]. The region was estimated from the amplitude sweep tests previously conducted. Values of the storage G' and loss G'' modulus, and complex viscosity $\eta*$ were obtained from this test. The Anton Paar rheometer settings for this test are shown in the screen of Figure 14.

14.Brine Sample Preparation

Four different brine solutions with concentrations of 10, 20, 30 and 35 grams per litre of sodium chloride (NaCl) respectively was dissolved each, in 1 litre flask containing distilled water. The solutions were mixed at a speed of 60 rpm in a magnetic stirrer for 2 hours to ensure proper mixing and dissolution of the solute in the solution. .

The solutions were filtered in a filter paper membrane set-up of pore diameter 22 μm, connected to a vacuum pump as shown in Figure 15. This was carried out to remove

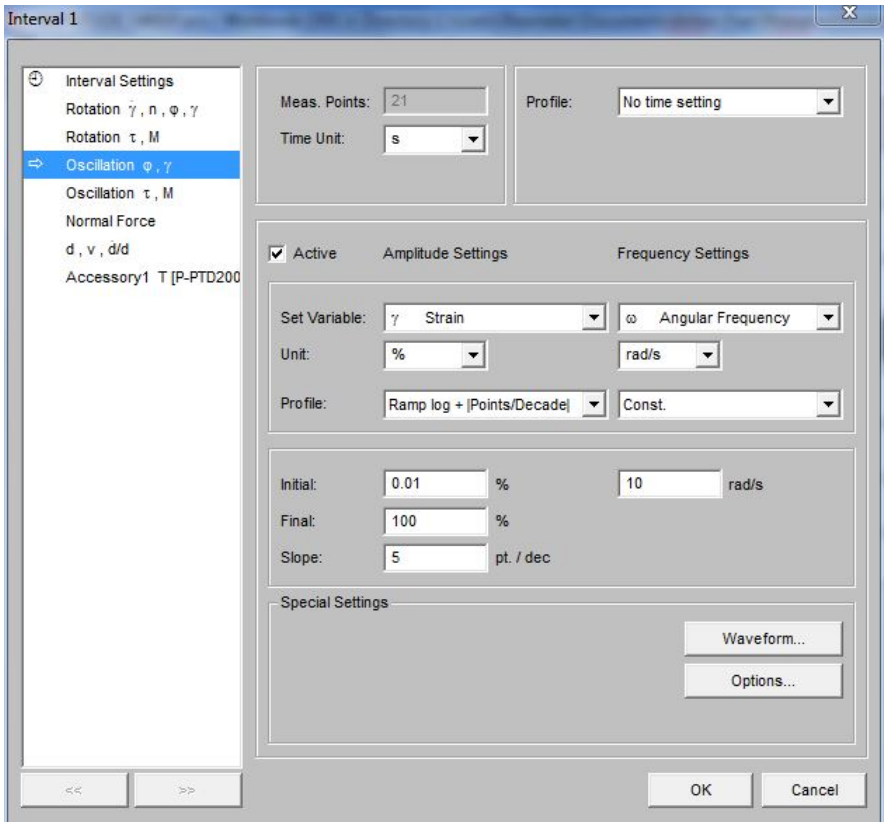

Figure 13: Screen shot of the Amplitude Sweep settings on the Anton Paar Rheometer

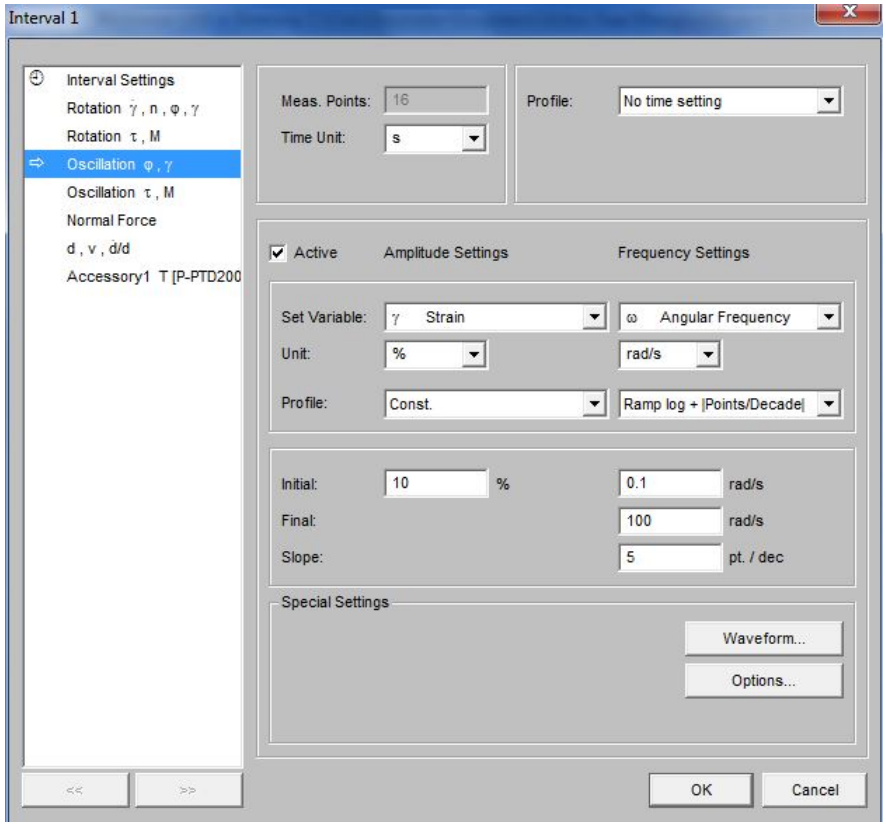

Figure 14: Screen shot of the Frequency Sweep settings on the Anton Paar Rheometer

undissolved (NaCl) solid particles and debris which could alter the rheometer readings.

These solution (10, 20, 30 and 35 g/l) were used to dilute polymer stock solutions into varying concentrations as required.

15.Polymer Sample Preparation

Polymer samples obtained from the chemical laboratory were weighed on the electronic weighting balance which was always reset to the zero point whenever a new measurement was to be made; the required theoretical and practical calculations were made with respect to Equations (A.1) and (A.2) to prepare the concentrated stock solutions of 10,000 ppm at 0 g/l and 35 g/l salt concentrations as shown in the Tables 1 and **??** [see Appendix A] respectively. These stock solutions, prepared in laboratory beakers were put in the Heidof propeller mixer and mixed for 2 hours. In order to achieve a homogeneous mixed solutions, the polymer powders were poured on the shoulder of the vortex created by the Heidof propeller mixer to prevent the formation of fish-eyes which are formed when polymers powder wetting is not homogeneous .

They were further transferred to the magnetic stirrer where they were stirred for 24 hours which gave sufficient time for the polymers to hydrate homogeneously, thereby eliminating air pockets/bubbles which could alter rheometer readings. During this period, various complex non-Newtonian fluid behaviours such as the Weissenberg rod climbing effects are easily observed. These solutions were further diluted to obtain concentrations of 200, 500, 1000, 1500 and 2000 ppm solutions of polymers respectively using Equation (A.3), (A.4), (A.5). To minimize the risk of mechanical shear degradation, the polymers were mixed at relatively low mixer and magnetic stirrer velocities and a mixing propeller rod blade having two blades was selected for mixing.
The solutions were put in well-labelled plastic containers and stored in temperature controlled refrigerators.

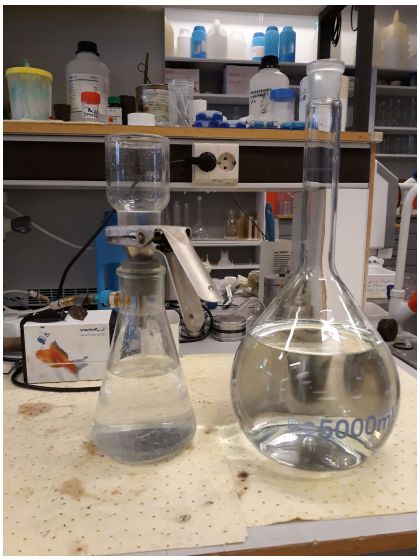

Figure 15: Filtration set-up showing the Vacuum Pump(Left) Filter(Middle) and Stock solution (right)

16.Rheometer

An Anton par Modular Compact Rheometer (MCR) was used for this experiment. It is a flexible instrument that can be used with all temperature devices and can be interchangeable within different categories of accessories. All geometry dimensions, safety limitations and safety limitations and calibration constants are saved in a chip called the $Toolmaster^{TM}$ located in the coupling of every measuring system [Paar, 2011]. The measuring systems are optimized regarding compliance, thermal expansion, and thermal conductivity and they are made from different a diverse range of materials, featuring different surfaces and dimensions.

Some measuring systems include $TruGap^{TM}$ which measures the gap and adjusts precisely to the desired position independently of temperature and thermal expansion, The $T-Ready^{TM}$ which employs the $TruGap^{TM}$ functionality to determine precisely when the required temperature is reached [Paar, 2011]. The MCR has the possibility of being connected to a network or PC.

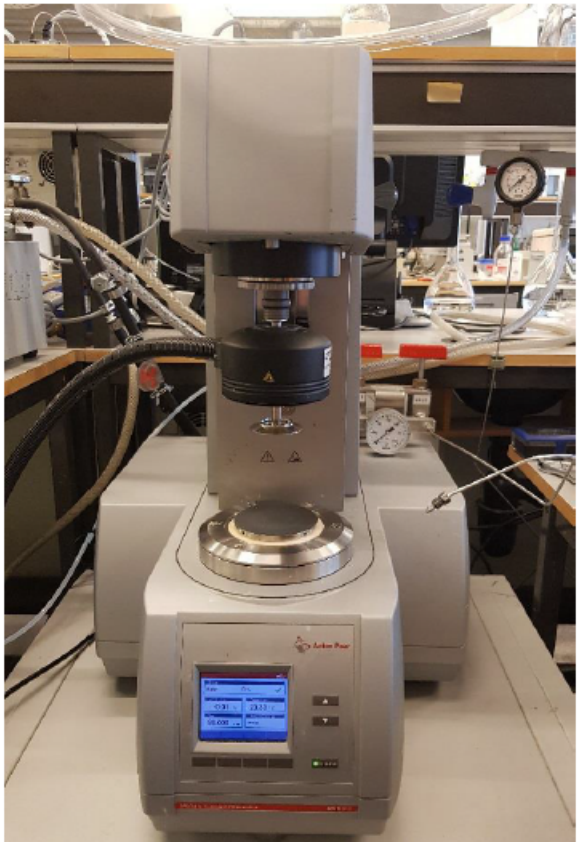

Figure 16: MCR-302 Anton Paar Rheometer

16.1.Cone-Plate System

A cone plate system accessory is used for this experiment. It consists of a stationary plate and a low angle inverted cone that rotates at a an angular frequency ω in specific regimes with the tip of the cone resting on the plate. The polymer that were measured was filled in the gap between the cone and the plate as shown in the Figure 16. It has several advantages such as having a constant shear rate within the entire gap due to the cone shape geometry. This implies that we measure the real material functions. It can handle small volumes which is easy to fill up and clean and it takes a shorter time for temperature to equalize. The cone-plate system has equal disadvantages of gap leakages of the fluid at extremely high shear rates, stability issues due to its fixed gap width, measurement disruption due to the presence of particles, and sample drying effects [Paar, 2011].

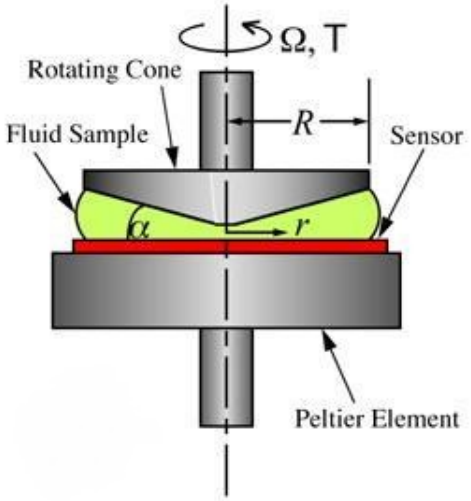

Figure 17: Schematic diagram showing Cone-Plate system set-up

16.2.Rheometer Parameters

The parameter settings for each test run on the Anton Paar Rheometer were maintained throughout the entire experiment. Motor adjustments, air check and quality control procedures were carried out on the Anton paar Rheometer to map the internal friction of the rheometer, maintain consistency of results and ensure that they operated within safe limits. Once the rheomenter was switched on, It was initialized and temperature was set to be constant at 20^oC and normal forces was always reset to zero prior to any experimental run.

The pipette volume was set at 620 ml and extreme care was taken to ensure that the polymer samples were free of bubbles and placed at the center of the sensor plate. At this volume, the fluid between the cone-plate was evenly distributed and there was virtually no need of trimming the edges of the fluid between the rotating cone and the sensor element. It was however noted that during amplitude sweeps for various polymers at 0 g/l salt concentration, the region on Linear Visco-Elasticity (LVE) was easily demarcated and there was "noise" disturbances at frequencies ranging from 10^{-2} to 10^0. A strain amplitude of 10 % was within the LVE limit for all polymers investigated.

CHAPTER FOUR

Results and Discussions

Graphical plots were made from the data measured from the Anton Paar rheometer. For situations where the measured data were irregular and not consistent with established trends, measurements were repeated. Analysis were made based on the desired concentration of the polymer solution and not the true concentration. This was done to establish a common base and make the analysis easy and relative. One major challenge in rheological experiment is determining the concentrations that would be termed "dilute, semi-dilute and concentrated" fluids different behaviour is expected at different concentrations. For the purpose of this work, measurements taken at concentrations of 200 and 500 ppm were termed dilute concentration polymers, semi-dilute concentrations were taken at 1000 ppm while 1500 and 2000 ppm were termed concentrated solutions.

It is important to point out that measurements taken at dilute concentrations/high salinity values, showed highly unsteady data which had significant "noise". These measurements were repeated and in situations where these noises persisted, the data were cleaned or discarded. Due to the large number of figures and charts, a significant majority of the charts on which the discussion is based on are placed in the appendix section. It is however advised that the reader of this theses refer to the appropriate charts in the appendix section as referenced in the text.

16.3.Effect of Concentration on Storage and Loss Modulus (G' and G")

Figure 18, shows a plot of storage modulus against frequency at salt concentration of 0 g/l at different polymer concentrations of 200, 500, 1000, 1500 and 2000 ppm, for the commercial EOR polymer Flopaam 5115 VHM. It is observed that storage modulus, G' increases with a corresponding increase in concentration at the same frequency. Also, Storage modulus increases with increase in frequency of oscillation. It is however noteworthy that all

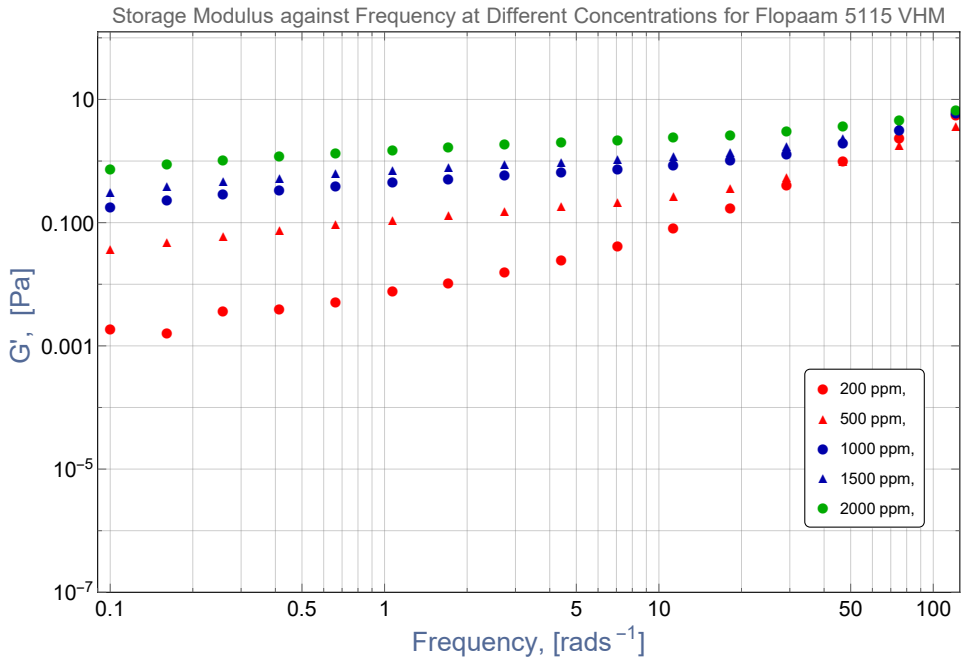

Figure 18: Storage Modulus G', plotted against angular frequency ω, at different polymer concentrations, and 0 g/l salt concentration for the commercial EOR polymer, Flopaam 5115 VHM.

different concentrations tend to converge at a single value at higher frequency values. This trend was replicated in Flopaam AN-125 VHM [Figure 40], and Flopaam 5115 VLM [Figure 65]. This trend is consistent with the C-FENE-P model as shown in Figure 20 (a).

Figure 19 shows the relationship between loss modulus and frequency as a function of concentration for Flopaam 5115 VLM. It is observed that an increase in concentration corresponds to an increase in loss modulus G''. Loss modulus increases with a corresponding increase in the angular frequency. This trend is very similar to the what was obtained in Flopaam 5115 VHM [Figure 40], Flopaam AN-125 VHM [Figure 51,], and Flopaam AN-125 VLM [Figure 73] samples tested in this experiment. This trend is consistent with C-FENE-P Model in Figure 20 (b).

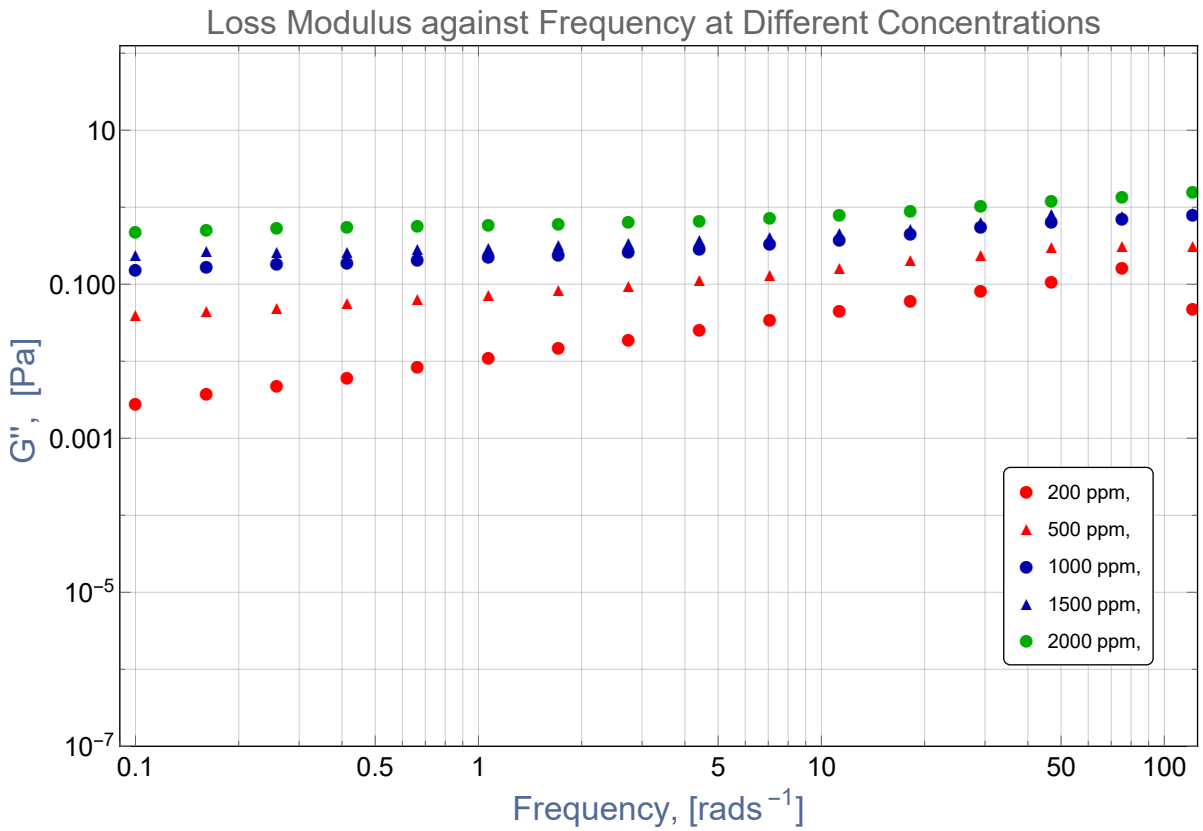

Figure 19: Loss Modulus G'', plotted against angular frequency ω, at different polymer concentrations, and 0g/l salt concentration for the commercial EOR polymer, Flopaam 5115 VLM.

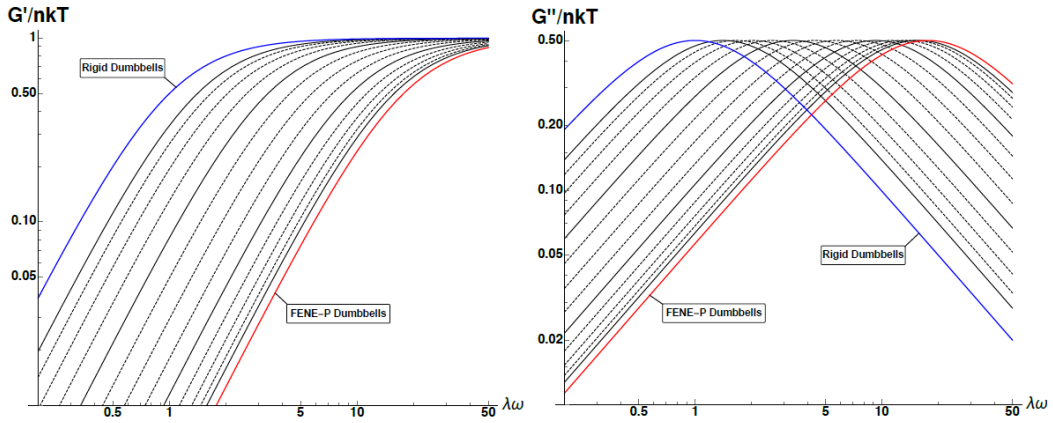

Figure 20: The scaled G' (a) and G'' (b) of the C-FENE-P Dumbbell and Rigid Dumbbell models in SAOS flow, plotted as functions of the experimental dimensionless frequency ω [Shogin, 2019].

16.4.Effects of Salinity/Concentration on Storage and Loss Modulus

Plots were made for five concentrations 200, 500, 1000, 1500 and 2000 ppm all at 10, 20, 30 and 35 g/l salinity. Figure 27, 28, 29, 30, 31 shows the plots for 35g/l salinity for Flopaam 5115 VHM. It is generally observed that Storage and Loss modulus are monotonously increasing functions of angular frequency with a positive slope. At low angular frequencies, the viscous components dominates the viscoelatic properties of Flopaam 5115 VHM. This trend prevailed irrespective of the salinity and polymer concentration.

Figure 21 shows that a progressive increase in salinity corresponds to a progressive decrease in storage modulus at the same angular frequency values as we move from 0, 10, 20, 30 and to 35 g/l salt concentration for Flopaam 5115 VHM. At lower ranges of angular frequency (0.1 to 5 rad/sec), salinity changes tends to be significant, however as the frequency increases above 10 rad/seconds, there is no much observable changes in the storage modulus as all varying concentrations of salt converge into a straight line with similar slope values. The two possible explanation for this convergence at high angular frequency are: Firstly, changes in the flow regime and turbulence and Secondly, the effect of salinity on storage modulus may be insignificant at very high angular frequencies. Similar plots for concentrations of 200, 1000, 1500 and 2000 ppm shows that the angular frequency at which they converge increases with a corresponding increase in polymer concentration as shown in Figure 36, 37, 38, 39.

As stated, the loss modulus is an increasing function of angular frequency. From Figures 22, 23, 24, 25, and 26 which corresponds to 200, 500, 1000, 1500 and 2000 ppm respectively, for the commercial EOR polymer Flopaam 5115 VHM, It is observed that salt concentration has a profound effect on the loss modulus G''. A progressive increase in salt concentration leads to a progressive decrease in the loss modulus G'' at a corresponding angular frequency. This trend is replicated in Flopaam AN-125 VHM polymer, Figures 58, and 59 and it is consistent with the C-FENE-P model at low angular frequency [Figure 20b].

Comparisons were drawn with the C-FENE-P model predictions Figure (34), and laboratory experiments Figure (35), to compare the graphical signature. Linear plots of G' and

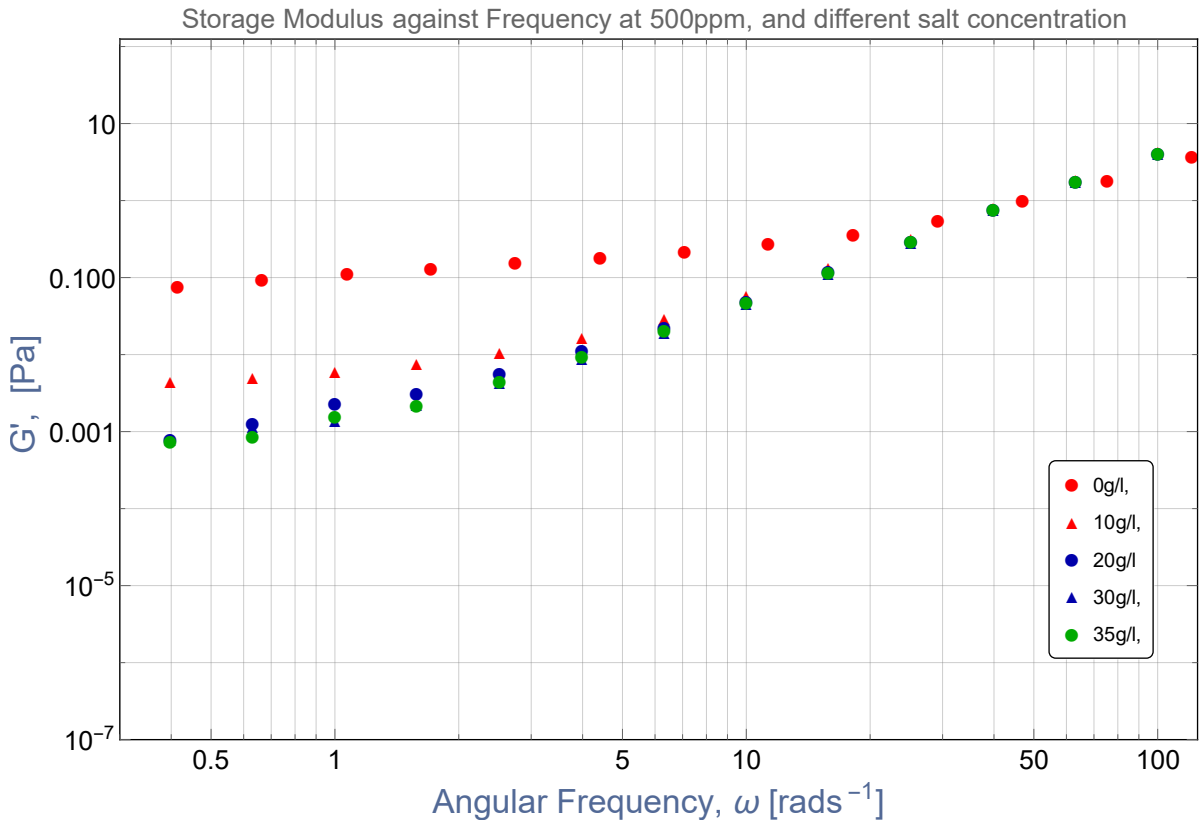

Figure 21: Storage Modulus G', plotted against angular frequency ω, at 500 ppm polymer concentration, and 0, 10, 20, 30, 35 g/l salt concentration for the commercial EOR polymer, Flopaam 5115 VHM

G'' for Flopaam 5115 VHM, plotted as functions of the angular frequency ω for salt concentration of 35 g/l as shown in Figure (35) displays a high degree of correlation with the prediction made by the C-FENE-P model. At high frequency values, the storage modulus, G' becomes relatively constant and approaches a plateau value, while the loss modulus, G'' tends towards having a negative slope. From the C-FENE-P model, Both storage G' and loss G'' start off by having a positive slope before they intersect at relatively low angular frequencies and hence they diverge. The experimental results was not within the angular frequency range where the relative constant value (plateau value) of G' could be observed as predicted by the C-FENE-P model Figure (34), however it showed the points where G'' commenced the negative slope which is consistent with the C-FENE-P model prediction.

It was challenging to resolve the storage modulus G' at very low angular frequencies to determine the relationship $G' \sim \omega^2$ but plots shows a trend that it starts resembling a straight line relationship.

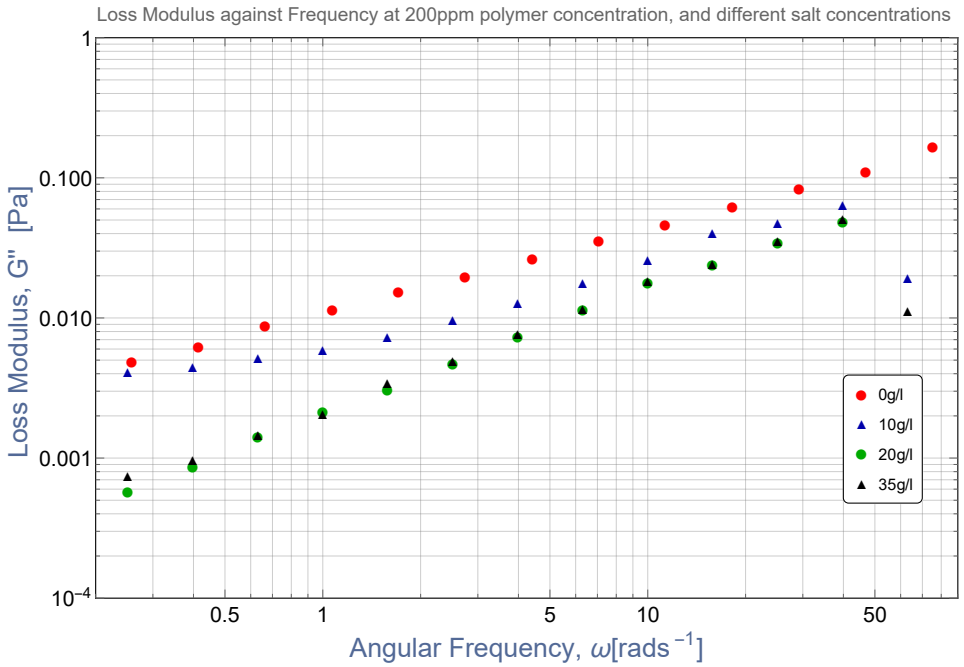

Figure 22: Loss Modulus, G'' as a function of angular frequency for the commercial EOR polymer Flopaam 5115 VHM at 20^oC, 200 ppm polymer concentration, and different Salt concentrations.

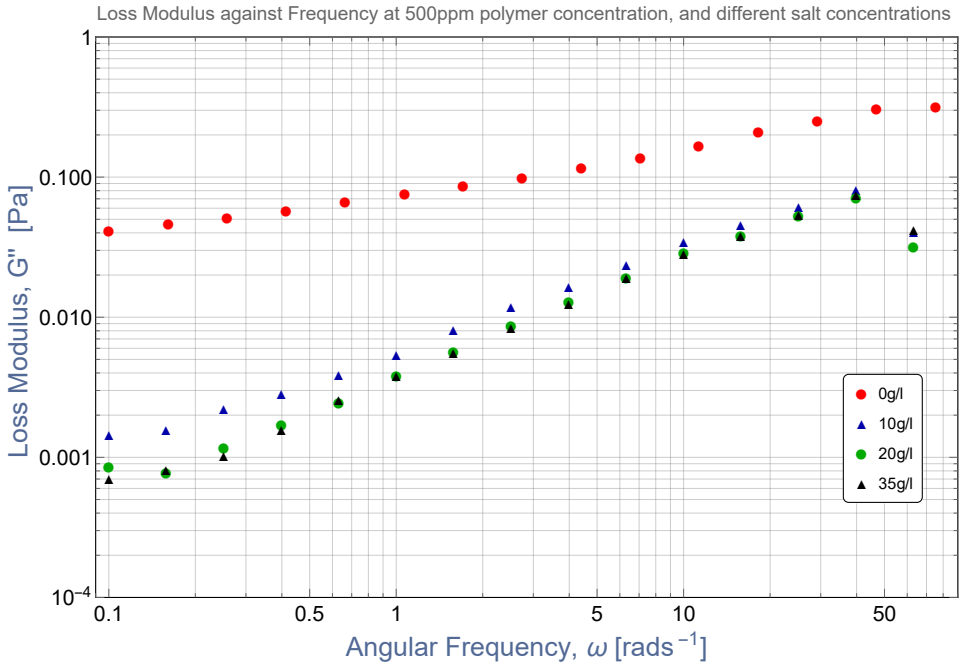

Figure 23: Loss Modulus, G'' as a function of angular frequency for the commercial EOR polymer Flopaam 5115 VHM at 20^oC, 500 ppm polymer concentration, and different Salt concentrations.

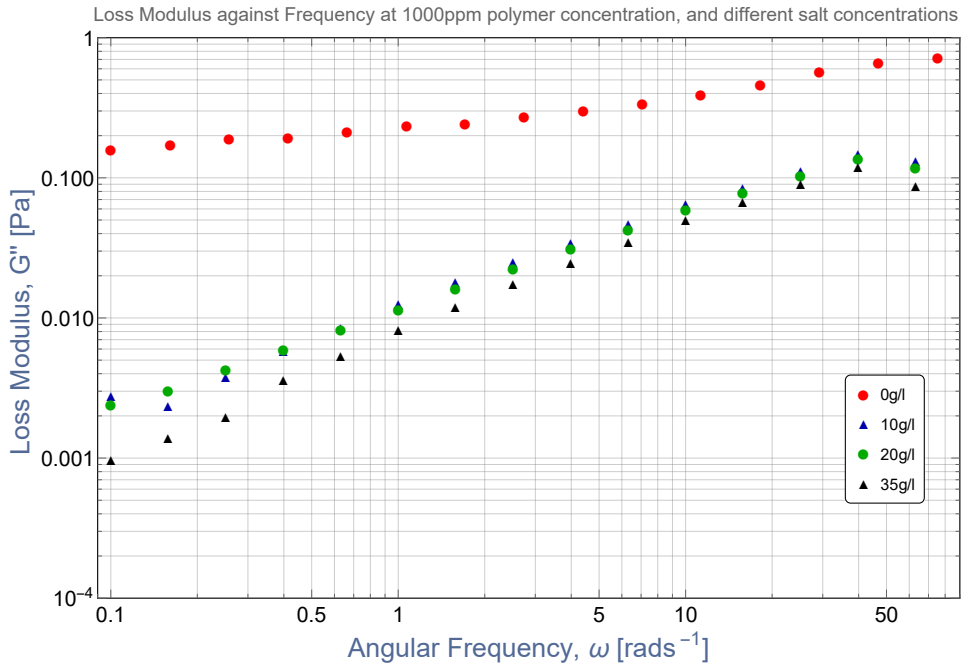

Figure 24: Loss Modulus, G'' as a function of angular frequency for the commercial EOR polymer Flopaam 5115 VHM at 20^oC, 1000ppm polymer concentration, and different Salt concentrations.

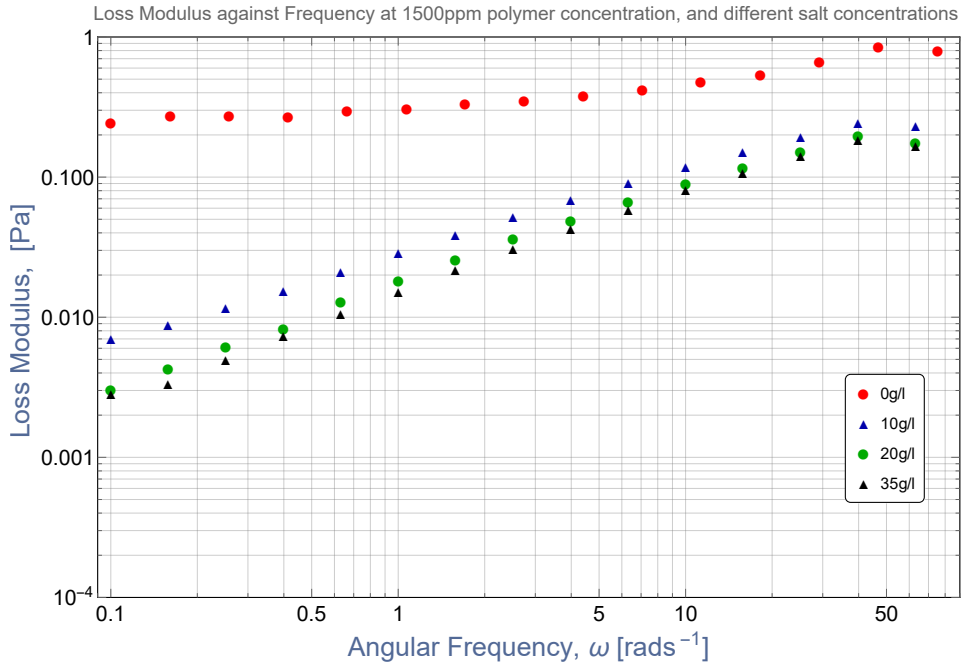

Figure 25: Loss Modulus, G'' as a function of angular frequency for the commercial EOR polymer Flopaam 5115 VHM at 20^oC, 1500 ppm polymer concentration, and different Salt concentrations.

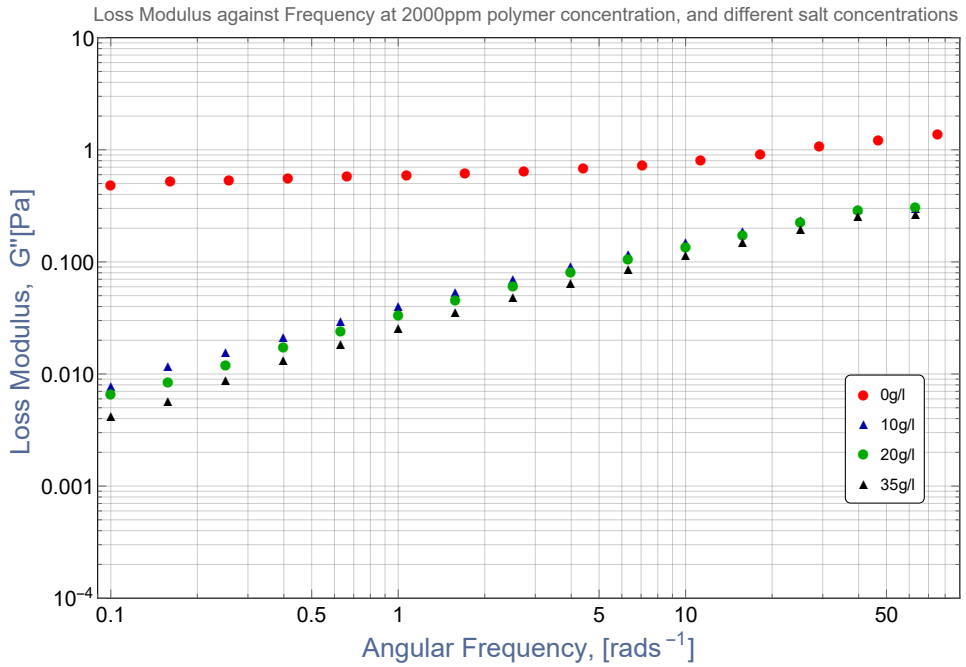

Figure 26: Loss Modulus, G'' as a function of angular frequency for the commercial EOR polymer Flopaam 5115 VHM at 20^oC, 2000 ppm polymer concentration, and different Salt concentrations.

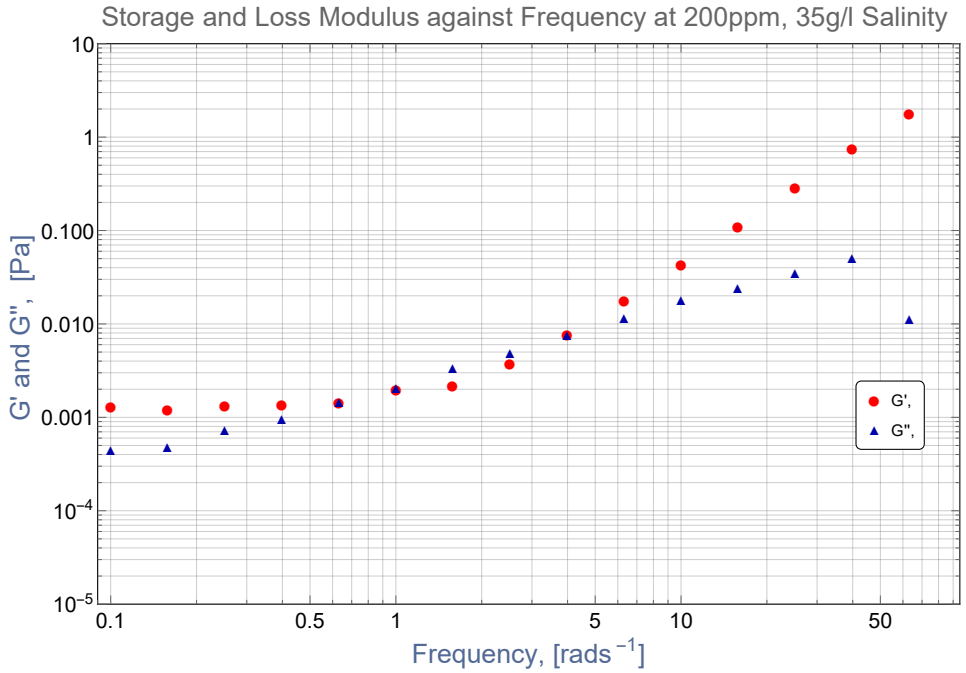

Figure 27: Storage and Loss Modulus against frequency at 200 ppm concentrations, and 35 g/l Salinity for Flopaam 5115 VHM.

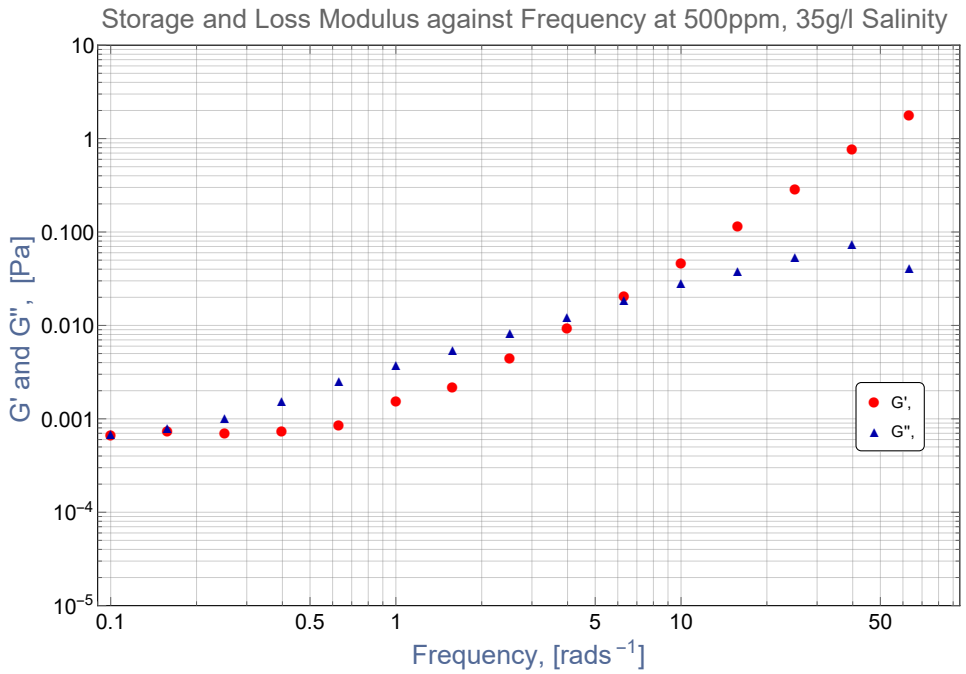

Figure 28: Storage and Loss Modulus against frequency at 500 ppm concentrations, and 35g/l Salinity for Flopaam 5115 VHM.

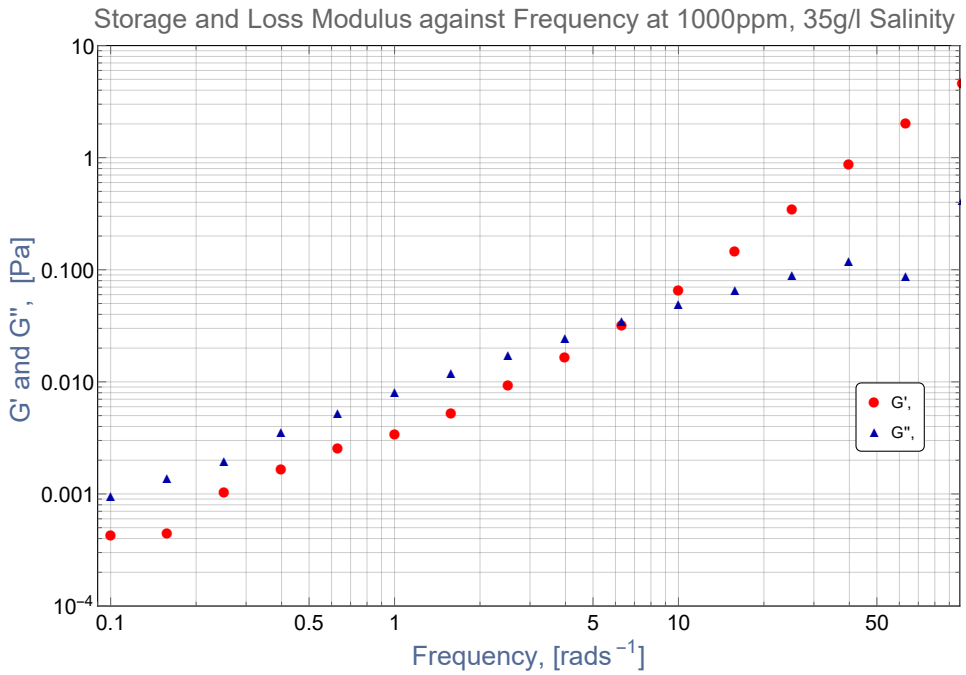

Figure 29: Storage and Loss Modulus against frequency at 1000 ppm concentrations, and 35 g/l Salinity for Flopaam 5115 VHM.

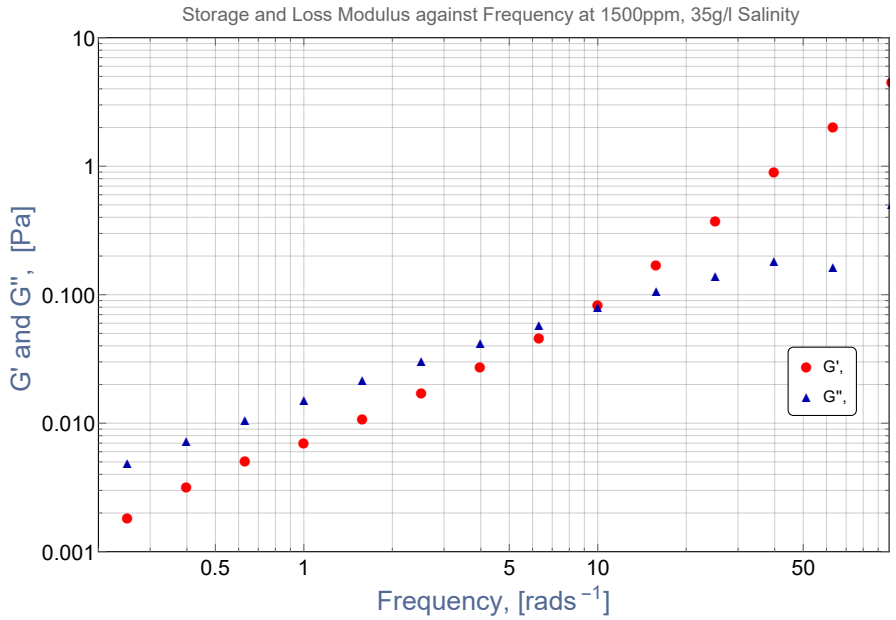

Figure 30: Storage and Loss Modulus against frequency at 1500ppm concentrations, and 35 g/l Salinity for Flopaam 5115 VHM.

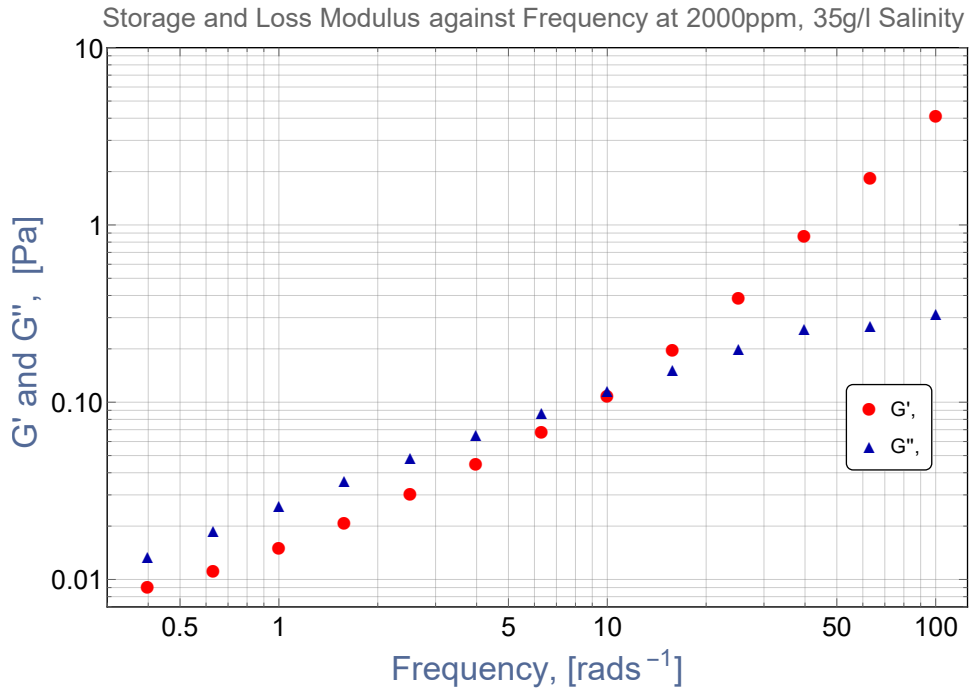

Figure 31: Storage and Loss Modulus against frequency at 2000 ppm concentrations, and 35 g/l Salinity for Flopaam 5115 VHM.

16.5.Effects of Concentration and salinity on Cross Over Angular frequency

The value of angular frequency at $G'' = G'$ was between the ranges of 1 to 15 rad/sec for all measured concentrations of Flopaam 5115 VHM at 10, 20, 30, and 35 g/l salinity. At low concentrations,(200 and 500 ppm) it ranged between 1 to 5 rad/sec irrespective of the salt concentration while for intermediate to high concentration, it was between 5 to 15 rad/sec for the measured salt concentrations as illustrated in Figures 27, 28, 29, 30, 31 for 35 g/l salt concentration. A similar trend is observed for Flopaam AN-125 VHM as shown in Figures 53 54, 55, 56, and 57. This range is relatively low and it suggests that the polymer has a high average molar mass with its molecules being less flexible and mobile.

The change in angular cross over frequency values occurs horizontally, parallel to the x-axis. The cross-over angular frequency increases to the right in the presence of salt irrespective of the salt concentration. It is however important to note that the cross over angular frequency value decreases with a corresponding increase in concentration for a polymer solution measured at zero salt concentration. It shifts towards the left of the curve for Flopaam 5115 VHM Figures 41, 42, 43, 44, 45. Similar trend occurs in Flopaam AN-125 VHM.

It was observed that the cross over angular frequency for Flopaam 5115 VLM showed a different trend. It is observed from Figure 67, 68, 69, 70 and 71, that at low and intermediate polymer concentrations (200, 500, 1000 ppm), the storage and loss modulus curves do not intersect and hence, there are no cross over angular frequencies. At higher polymer concentrations (1500 and 2000 ppm), the curves intersected and the cross over frequency tends to increase to the right with an increase in concentration irrespective of the salt concentration.

At the cross over frequency (i.e the frequency at which $G'' = G'$), the loss modulus changes and starts having a negative slope while the storage modulus maintains its positive slope. The experimental range for the angular frequency used in this experiment did not make it possible to reach the so called G' plateau value where the storage modulus, G' becomes relatively constant and flattens out. It could be inferred that G_p (Plateau value)

would be obtained at sufficiently higher frequencies. These suggests a greater degree of entanglements among the molecules which invariable indicates that Flopaam 5115 VHM is made up of longer molecules and has a higher average molar mass [Mezger, 2011].

16.6.Effect of Concentration on Complex Viscosity coefficient

Plots of complex viscosity $\eta*$ against angular frequency ω, for Flopaam AN-125 VHM [Figure 60] shows that an increase in concentration corresponds to an increase in complex viscosity. Note that at frequency values of above 10 rad/s, there is an increase in the complex viscosity value for the fluid at 200 ppm. As concentration increases, the this increase in complex viscosity shifts to the right of the graph and occurs at a later frequency for higher concentrations 500, 1000, 1500 and 2000 ppm. This is replicated for Flopaam 5115 VHM. It can be observed that an increase in concentration shifts this transition phase to the right. This means that the transition occurs at a higher frequency with corresponding increase in the concentration of the polymer. This trend goes against conventional trends as complex viscosity does not increase with a increase in frequency.

This increase in viscosity that corresponds to an increase in frequency is as a result of high turbulence experienced as the transition from laminar to turbulent flow (change in flow regime) occurs in the fluid sample as it is subjected to large vibrations at higher frequencies in the rheometer. Since the flow regime changes at this point, the measurements done beyond this point are affected and are not relevant.

16.7.Effect of Salinity on Complex Viscosity coefficients

The effect of salinity on In-phase and Out-of phase complex viscosity coefficients, η' and η'' were observed for Flopaam AN-125. Linear plots at salt concentrations (0 g/l) [Figure 33] showed that the in-phase and out-of-phase component decreases at a slow rate at high angular frequency.

While the In-phase complex viscosity η', in the C-FENE-P model [Figure 32] trends with laboratory measurements , the Out-of-phase complex viscosity η'' does not trend as it is totally in opposite to the measurements in the laboratory at all polymer concentrations

once salt was introduced into the mixture. It is observed for Flopaam AN-125 VHM, from Figures 61, 62, 63, 64 that the Out-of-phase complex viscosity coefficient η'' begins to increase slightly and have a positive slope as angular frequency increases in the presence of salt, irrespective of the salt concentration. An increase in salt concentration provokes instabilities or secondary flow and the growing or increase in η'' is an indication of this instability. The above trend was consistent with experimental measurements of Flopaam 5115 VHM [Figure 46, 47, 48, 49, and 50] at a salt concentration of 35 g/l, and all other Flopaam polymers measured. However, this is not consistent with the prediction made by the C-FENE-P model [Figure 32].

From the FENE -P model, the idea that the point of intersection between η' and η'' occurs at the point where η'' is maximum [Figure 32] is not consistent with laboratory experiments as shown in the Figures 46, 47, 48, 49 and 50. It is expected because the dumbbell models undergo complex oscillation in SAOS flows and representing theses flows as simple oscillations of a dumbbell is an oversimplification [Shogin, 2019]. Also, and the region of very low angular frequencies is not being resolved in the experiments to monitor how η'' increases.

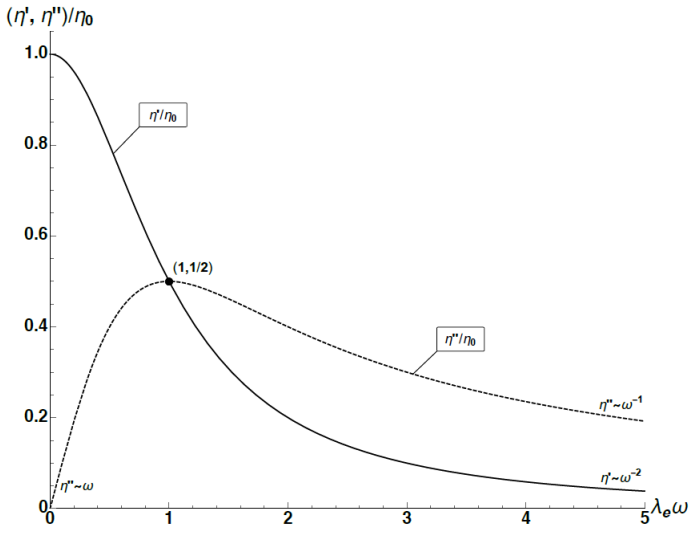

Figure 32: The scaled η' and η'' of the C-FENE-P dumbbells in SAOS flow, plotted as functions of the experimental dimensionless frequency ω [Shogin, 2019].

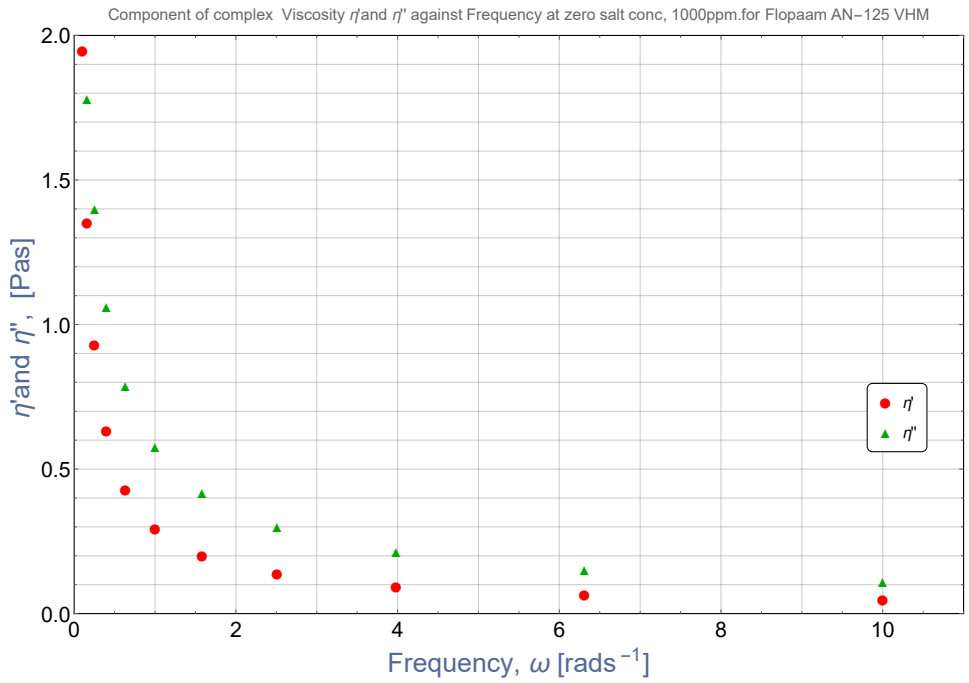

Figure 33: Linear plots of η' and η'' coefficients of complex viscosity, as a function of angular frequency ω for the commercial EOR polymer Flopaam AN-125 VHM at 20^oC, 1000 ppm polymer concentration, and zero Salt concentration.

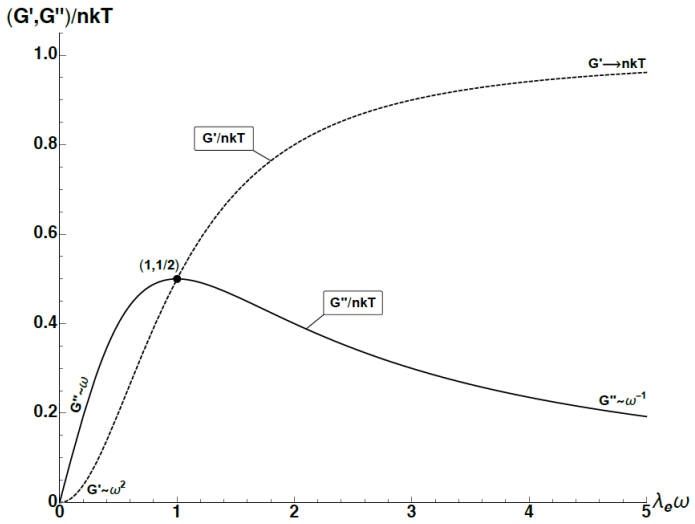

Figure 34: The scaled G' and G'' of the C-FENE-P dumbbells in SAOS flow, plotted as functions of the experimental dimensionless frequency ω [Shogin, 2019].

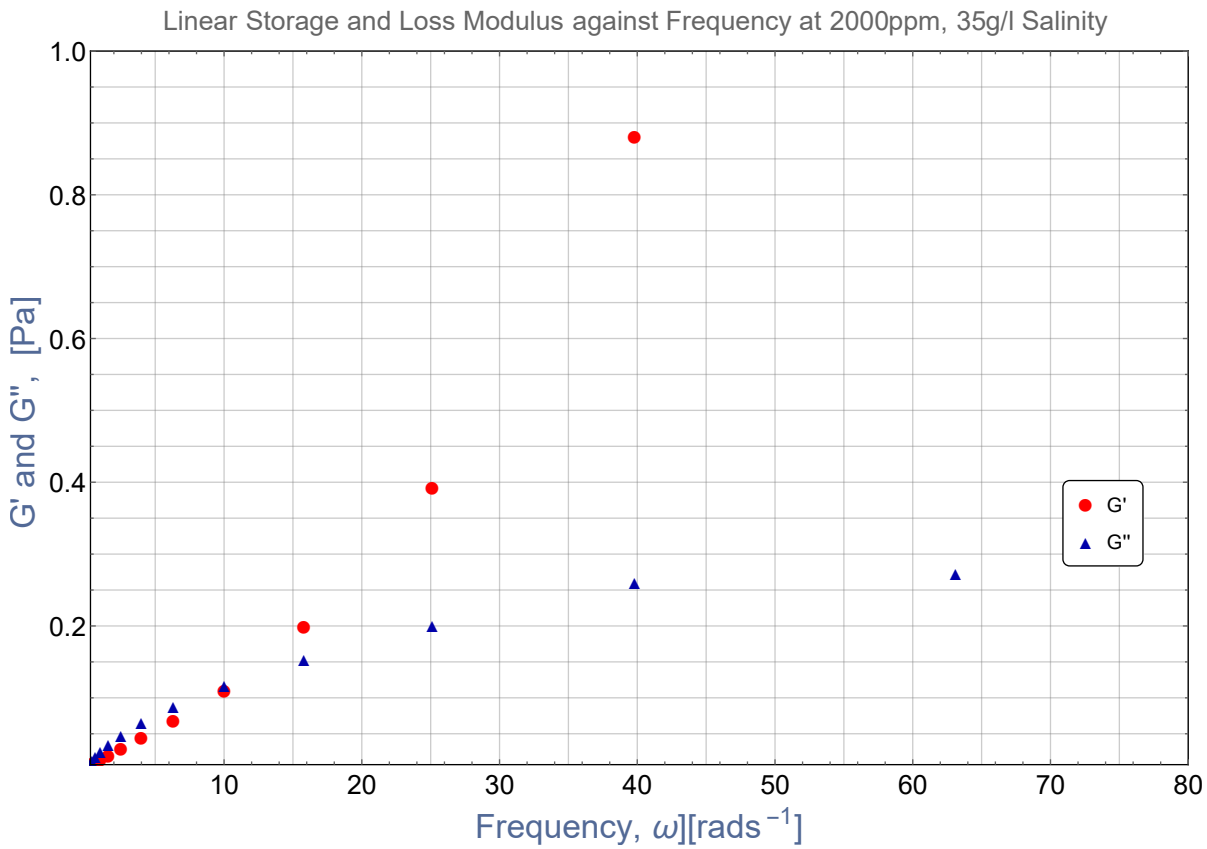

Figure 35: G' and G'' for Flopaam 5115 VHM, plotted as functions of the angular frequency ω for Salt concentration of 35 g/l.

CHAPTER FIVE

Conclusion and Recommendation

17.Summary

This research experiment was proposed to understand the impact of salinity on Small Amplitude Oscillatory Shear (SAOS) material functions of EOR Flopaam ploymers. The results were compared with predictions made by an advanced non-Newtonian fluid model (C-FENE-P Dumbbells). Material functions such as the shear modulus, bulk modulus, and complex viscosity (In-Phase and Out of phase) were measured for four polymer samples, Flopaam 5115-VHM, Flopaam 5115-VLM, Flopaam AN-125-VHM, and Flopaam AN-125-VLM. The experiments were designed to suit the proposed objectives. From the results obtained from the experiments, and the data analysed in the preceding chapter, the following conclusions are drawn.

17.1.Conclusions consistent with the C-FENE-P model

1. Indeed, G' and G'' increases with concentration at all fixed angular frequency ω in accordance with the C-FENE-P model. This increase is close to linear at low concentrations and faster than linear at high concentrations. This is possibly due to increased interaction between the polymer-polymer molecules.

2. G' and G'' increases with corresponding increase in angular frequency within the range of measured angular frequency .

3. A progressive increase in salinity corresponds to progressive decrease in G' and G'' at a fixed frequency. .

4. At high frequencies, Storage modulus G' tends towards having a constant plateau value (G_p) and the loss modulus tends towards having a negative slope.

5. At higher frequencies, G' and G'' are relatively insensitive to salt concentration.

6. An increase in salt concentration corresponds to an increase in the slope of G' at a fixed angular frequency ω which reaches a constant value that is independent of salt concentration.

7. The cross-over angular frequency increases in the presence of salt irrespective of the salt concentration.

8. An increase in salinity moves the cross over frequency towards higher angular frequency values.

17.2.Conclusions not consistent with the C-FENE-P model

1. The In-phase component η' of the complex viscosity coefficient is well predicted by the C-FENE-P model at both low and high angular frequency values, However the model fails to properly predict the behaviour of the Out-of-phase component η'' of complex viscosity at high frequency as laboratory experiments.

   An increase in Salt concentration changes the flow regime, provokes instability which occurs in the form of secondary flows and turbulence. The growth/increase in the Out-of phase complex viscosity coefficient η'' is an indication of this instability. This phenomenon is not consistent with the C-FENE-P, and its is also not consistent with any other model and theoretical prediction as this is an anomaly. By physical reasons, η'' ought to tend towards zero. This anomaly might be explained by instability provoked by increased salt concentrations.

2. At higher polymer concentration, it is less likely to have instability and changes in flow regimes because their is an increased interaction between the polymer molecules. This interaction stabilize the flow. On the other hand, at low concentrations and increased salt concentrations the flow breaks down at relatively lower angular frequencies.

3. The C-FENE-P model predicts that the point of intersection where $\eta' = \eta''$ occurs at the point where η'' is maximum. This is not in agreement with experiments and it is expected because the dumbbell models undergo complex oscillation in

SAOS flows and representing theses flows as simple oscillations of a dumbbell is an oversimplification.

4. In the absence of salt, the cross-over frequency decreases with a corresponding increase in polymer concentration. The plausible explanation to this phenomenon is the role of polymer-polymer molecule interactions.

17.3.Remarks

At low polymer concentrations, the cross-over angular frequency is not easily noticed within the range of angular frequencies investigated. However, at higher polymer concentrations, irrespective of salt concentration, the cross-over angular frequency for Flopaam polymers are within the range of 1 to 15 rad/s.

18.Recommendations for further study

1. Regions of lower frequencies should be resolved. Experiments should be conducted by extending the frequency ranges. The rheometer settings should be adjusted to special regimes, More time should be allocated to accommodate this.

2. To reduce the effect of instability, changes in flow regimes and turbulence in the rheometer during measurements at high angular frequencies, the measuring time allocated to each measurement point should be increased to improve the accuracy of the results.

3. Cone-Plate measuring elements has its advantages and disadvantages. One of the disadvantages of the cone-plate measuring element is having a fixed gap width between the cone plate and the element. This contributes negatively to measurements at hight angular frequencies by increasing instability. Parallel plate has an adjustable gap which can improve stability of the flow at high angular frequency. Future experiments should be conducted using a parallel plate system to account for extremely low and high angular frequency measurements.

4. Future experiments should be conducted with other inorganic salts of Calcium, Barium and Magnesium to validate the conclusions reached in this work.

5. The effect and role of divalent cations in salts should be studied in-depth.

6. Large Amplitude Oscillatory Shear (LAOS) tests should be investigated in the non-linear viscoelastic region.

7. The C-FENE-P dumbbell model should be extended to a Bead-Spring-Chain version in order to make better quantitative predictions (example: G'/G'' intersection).

Appendix

A.Formulas for polymer Sample Preparation

The following formulas were employed while preparing the solutions to calculate the required concentration of dilute and concentrated polymer solutions.

A.1.Preparation of Concentrated Solutions

Theoretical evaluation of the required mass of polymer, g:

$$M_p = \frac{cM_s \times 10^{-6}}{1 - c \times 10^{-}6} \left[\frac{\text{g} \cdot \text{ppm}}{\text{ppm}}\right] \tag{A.1}$$

Practical calculation of the true concentration of polymer, ppm:

$$c = \frac{M_p}{M_p M_s} \times 10^{-6} \tag{A.2}$$

Where:

M_p= measured mass of polymer

M_s = measured mass of the solvent.

c = Desired concentration

A.2.Preparation of Dilute Solution

Theoretical mass of the concentrated polymer, g:

$$M_c = \left[\frac{c}{c_0} m\right] \tag{A.3}$$

Where:

c = Desired concentration of the diluted solution, ppm

c_o = True concentration of the polymer solution, ppm

m = Desired total mass of the diluted solution,g

To evaluate the Total Mass of the diluted solution required, ppm:

$$m = \left[\frac{M_c c_o}{c}\right] \tag{A.4}$$

Where:

c_o=True concentration of the concentrated solution, ppm

M_c= Mass of the concentrated polymer taken in practice, g

c=The desired concentration of the diluted solution, ppm

While to Evaluate the True Concentration of the diluted solution, ppm

$$c = \left[\frac{M_c c_o}{m}\right] \tag{A.5}$$

Where: M_c=Mass of the concentrated polymer taken in practice, g

c_o= True concentration of the concentrated solution, ppm

m= Measured mas of the diluted solution, g

B.Tables

B.1.Concentrated stock solution Data for Flopaam polymer Solutions at 0 g/l salt concentration

	5115 VHM	5115 VLM	AN-125 VHM	AN-125 VLM
Desired Concentration [ppm]	10,000	10,000	10,000	10,000
Required Mass of water [ml]	500	500	705.50	200
Required mass of Polymer [g]	5.06	5.06	7.13	2.02
Measured mass of Polymer [g]	5.07	5.05	7.14	2.06
Measured mass of solvent [g]	500.05	498.21	705.59	200.29
True Concentration [ppm]	10,008.50	9,995.59	10,017.80	10,181.40

Table 1: Stock solution data for all Flopaam Polymers at 0g/l Salt Concentration .

B.2.Concentrated stock solution Data for Flopaam polymer Solutions at 35 g/l salt concentration

	5115 VHM	5115 VLM	AN-125 VHM	AN-125 VLM
Desired Concentration [ppm]	10,000	10,000	10,000	10,000
Required Mass of Brine [l]	500	500	400	400
Required mass of Polymer [g]	5.06	5.06	4.04	4.04
Measured mass of Polymer [g]	5.08	5.05	4.04	4.04
Measured mass of solvent [g]	500.60	499.52	400.38	400.21
True Concentration [ppm]	10,045.90	9999.80	9989.61	9993.82

Table 2: Stock solution data for all Flopaam Polymers prepared with 35 g/l Brine.

B.3.Dilute solution Data for Flopaam 5115 VHM polymer Solutions at different salt concentration

Desired Concentration [ppm]	200	500	1000	1500	2000
Actual Measured mass of Stock Polymer [g]	1.07	2.49	4.99	7.53	10.05
Total Measured mass of diluted Polymer [g]	53.98	49.90	50.64	50.28	50.35
True Concentration [ppm]	198.39	499.42	1000.45	1498.89	1997.72

Table 3: Dilute solution data for Flopaam 5115 VHM at 0 g/1000 ml Salinity.

Desired Concentration [ppm]	200	500	1000	1500	2000
Actual Measured mass of Stock Polymer [g]	0.57	1.42	2.53	3.76	4.95
Total Measured mass of diluted Polymer [g]	28.90	28.64	25.86	25.44	25.02
True Concentration [ppm]	197.98	498.215	982.37	1485.22	1987.32

Table 4: Dilute solution data for Flopaam 5115 VHM at 10 g/1000ml Salinity.

Desired Concentration [ppm]	200	500	1000	1500	2000
Actual Measured mass of Stock Polymer [g]	0.51	1.26	2.48	3.78	5.37
Total Measured mass of diluted Polymer [g]	25.61	25.31	24.99	25.34	26.96
True Concentration [ppm]	196.43	498.09	996.863	1498.43	2000.80

Table 5: Dilute solution data for Flopaam 5115 VHM at 20 g/1000 ml Salinity.

Desired Concentration [ppm]	200	500	1000	1500	2000
Actual Measured mass of Stock Polymer [g]	1.15	2.45	2.67	3.77	4.41
Total Measured mass of diluted Polymer [g]	58.18	51.66	27.33	25.24	25.91
True Concentration [ppm]	198.55	476.39	981.35	1493.87	1981.61

Table 6: Dilute solution data for Flopaam 5115 VHM at 30 g/1000 ml Salinity.

Desired Concentration [ppm]	200	500	1000	1500	2000
Actual Measured mass of Stock Polymer [g]	0.5	1.27	2.44	3.72	5.05
Total Measured mass of diluted Polymer [g]	25.22	25.57	24.51	25.05	25.36
True Concentration [ppm]	199.15	498.91	1000.40	1491.71	1999.50

Table 7: Dilute solution data for Flopaam 5115 VHM at 35 g/1000 ml Salinity.

B.4.Dilute solution Data for Flopaam 5115 VLM polymer Solutions at different salt concentration

Desired Concentration [ppm]	200	500	1000	1500	2000
Actual Measured mass of Stock Polymer [g]	1.01	2.55	5.02	7.53	10.04
Total Measured mass of diluted Polymer [g]	50.60	50.64	50.32	50.95	50.18
True Concentration [ppm]	199.51	503.33	997.17	1498.14	1999.91

Table 8: Dilute solution data for Flopaam 5115 VLM at 0 g/1000 ml Salinity.

Desired Concentration [ppm]	200	500	1000	1500	2000
Actual Measured mass of Stock Polymer [g]	0.53	1.25	2.61	3.80	5.05
Total Measured mass of diluted Polymer [g]	26.48	24.99	26.11	25.96	25.44
True Concentration [ppm]	200.14	499.19	999.21	1463.76	1985.02

Table 9: Dilute solution data for Flopaam 5115 VLM at 10 g/1000 ml Salinity.

Desired Concentration [ppm]	200	500	1000	1500	2000
Actual Measured mass of Stock Polymer [g]	0.54	1.30	2.54	3.77	5.00
Total Measured mass of diluted Polymer [g]	27.01	25.70	25.38	25.11	25.02
True Concentration [ppm]	199.92	505.80	1000.77	1501.36	1997.56

Table 10: Dilute solution data for Flopaam 5115 VLM at 20 g/1000 ml Salinity.

Desired Concentration [ppm]	200	500	1000	1500	2000
Actual Measured mass of Stock Polymer [g]	0.52	1.26	2.62	3.75	5.01
Total Measured mass of diluted Polymer [g]	25.90	25.14	26.06	25.45	25.03
True Concentration [ppm]	200.76	501.18	1005.35	1473.45	2001.56

Table 11: Dilute solution data for Flopaam 5115 VLM at 30 g/1000 ml Salinity.

Desired Concentration [ppm]	200	500	1000	1500	2000
Actual Measured mass of Stock Polymer [g]	0.49	1.26	2.56	3.75	5.11
Total Measured mass of diluted Polymer [g]	25.58	25.13	25.55	25.11	25.55
True Concentration [ppm]	191.55	501.58	1001.94	1493.40	1999.96

Table 12: Dilute solution data for Flopaam 5115 VLM at 35 g/1000 ml Salinity.

B.5.Dilute solution Data for Flopaam AN-125 VHM polymer Solutions at different salt concentration

Desired Concentration [ppm]	200	500	1000	1500	2000
Actual Measured mass of Stock Polymer [g]	0.57	1.34	2.43	4.03	5.03
Total Measured mass of diluted Polymer [g]	28.43	27.18	24.27	26.88	25.24
True Concentration [ppm]	200.84	493.88	1003.02	1501.92	1996.42

Table 13: Dilute solution data for Flopaam AN-125 VHM at 0 g/1000 ml Salinity.

Desired Concentration [ppm]	200	500	1000	1500	2000
Actual Measured mass of Stock Polymer [g]	0.61	1.31	2.47	4.02	5.18
Total Measured mass of diluted Polymer [g]	30.90	26.29	25.74	26.80	26.01
True Concentration [ppm]	197.14	497.58	958.59	1498.44	1989.47

Table 14: Dilute solution data for Flopaam AN-125 VHM at 10 g/1000 ml Salinity.

Desired Concentration [ppm]	200	500	1000	1500	2000
Actual Measured mass of Stock Polymer [g]	0.54	1.29	2.50	3.80	5.00
Total Measured mass of diluted Polymer [g]	26.98	25.69	24.96	25.41	25.02
True Concentration [ppm]	199.94	501.61	1000.56	1493.33	1994.73

Table 15: Dilute solution data for Flopaam AN-125 VHM at 20 g/1000 ml Salinity.

Desired Concentration [ppm]	200	500	1000	1500	2000
Actual Measured mass of Stock Polymer [g]	0.53	1.26	2.49	3.78	5.02
Total Measured mass of diluted Polymer [g]	26.41	25.22	24.95	25.17	25.46
True Concentration [ppm]	200.47	499.08	996.95	1500.23	1969.67

Table 16: Dilute solution data for Flopaam AN-125 VHM at 30 g/1000 ml Salinity.

Desired Concentration [ppm]	200	500	1000	1500	2000
Actual Measured mass of Stock Polymer [g]	0.54	1.25	2.25	3.86	5.00
Total Measured mass of diluted Polymer [g]	26.81	24.97	25.18	25.70	25.59
True Concentration [ppm]	201.20	498.68	983.88	1494.57	1951.10

Table 17: Dilute solution data for Flopaam AN-125 VHM at 35 g/1000 ml Salinity.

B.6.Dilute solution Data for Flopaam AN-125 VLM polymer Solutions at different salt concentration

Desired Concentration [ppm]	200	500	1000	1500	2000
Actual Measured mass of Stock Polymer [g]	0.51	1.22	2.51	3.77	4.95
Total Measured mass of diluted Polymer [g]	26.02	25.01	25.53	25.75	25.45
True Concentration [ppm]	199.55	494.85	1001.34	1490.58	1980.19

Table 18: Dilute solution data for Flopaam AN-125 VLM at 0 g/1000 ml Salinity.

Desired Concentration [ppm]	200	500	1000	1500	2000
Actual Measured mass of Stock Polymer [g]	0.50	1.28	2.52	3.82	5.02
Total Measured mass of diluted Polymer [g]	25.08	25.59	25.19	25.48	25.66
True Concentration [ppm]	199.23	499.88	999.77	1498.29	1955.14

Table 19: Dilute solution data for Flopaam AN-125 VLM at 10 g/1000 ml Salinity.

Desired Concentration [ppm]	200	500	1000	1500	2000
Actual Measured mass of Stock Polymer [g]	0.51	1.30	2.50	3.79	5.04
Total Measured mass of diluted Polymer [g]	25.35	25.83	25.05	25.25	25.22
True Concentration [ppm]	201.05	502.98	.997.38	1500.06	1997.18

Table 20: Dilute solution data for Flopaam AN-125 VLM at 20 g/1000 ml Salinity.

Desired Concentration [ppm]	200	500	1000	1500	2000
Actual Measured mass of Stock Polymer [g]	0.58	1.28	2.54	3.76	5.00
Total Measured mass of diluted Polymer [g]	28.98	25.60	25.32	25.20	25.04
True Concentration [ppm]	200.01	499.69	1002.54	1491.14	1995.57

Table 21: Dilute solution data for Flopaam AN-125 VLM at 30 g/1000 ml Salinity.

Desired Concentration [ppm]	200	500	1000	1500	2000
Actual Measured mass of Stock Polymer [g]	0.50	1.29	2.52	3.82	5.00
Total Measured mass of diluted Polymer [g]	25.00	25.63	25.37	25.57	25.05
True Concentration [ppm]	199.87	503.00	992.68	1493.01	1994.77

Table 22: Dilute solution data for Flopaam AN-125 VLM at 35 g/1000 ml Salinity.

C.Figures for FLOPAAM 5115 VHM

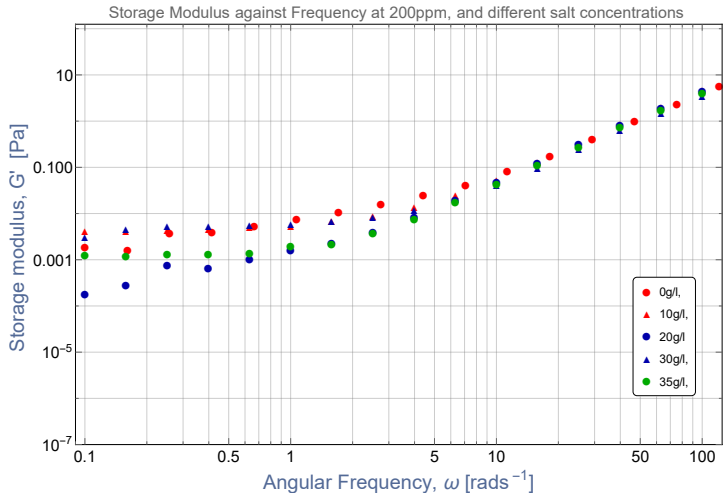

Figure 36: Storage Modulus against angular frequency at different Salt concentrations, 200 ppm for Flopaam 5115 VHM.

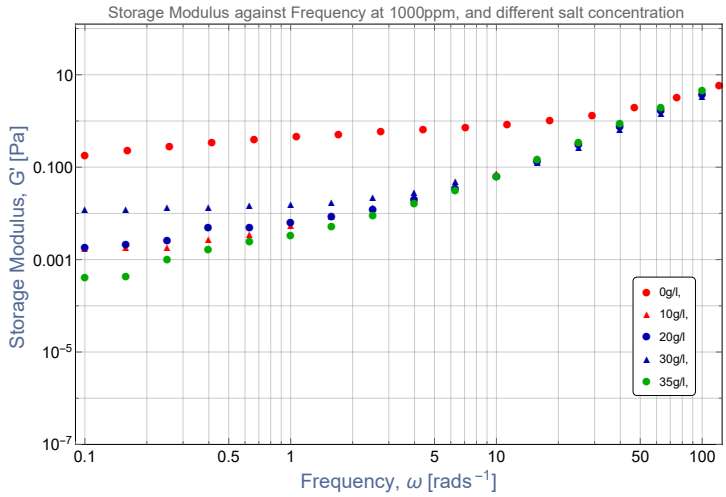

Figure 37: Storage Modulus against angular frequency at different Salt concentrations, 1000 ppm for Flopaam 5115 VHM.

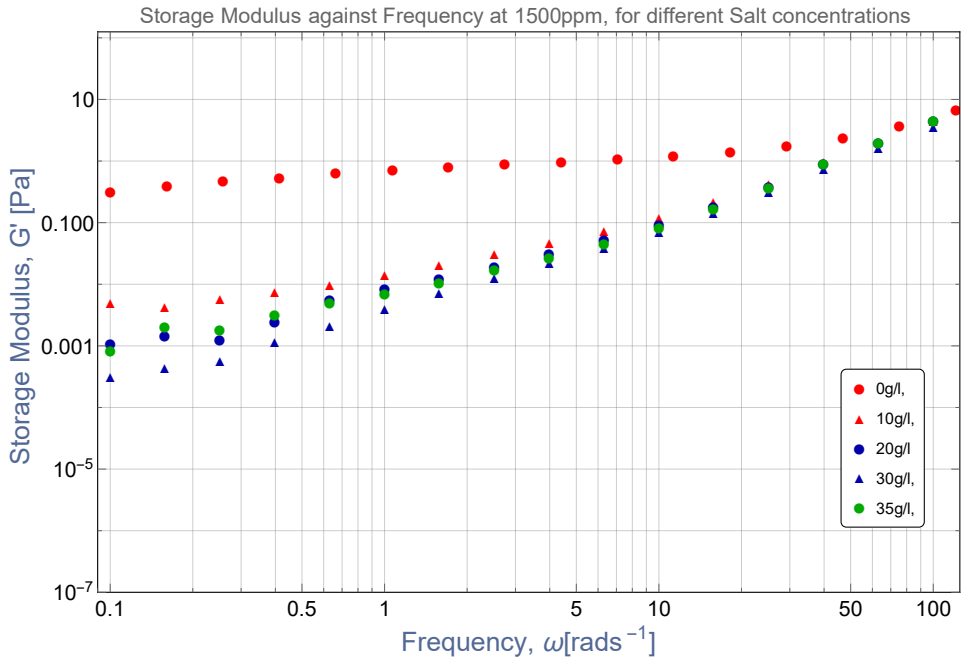

Figure 38: Storage Modulus against angular frequency at different Salt concentrations, 1500 ppm for Flopaam 5115 VHM.

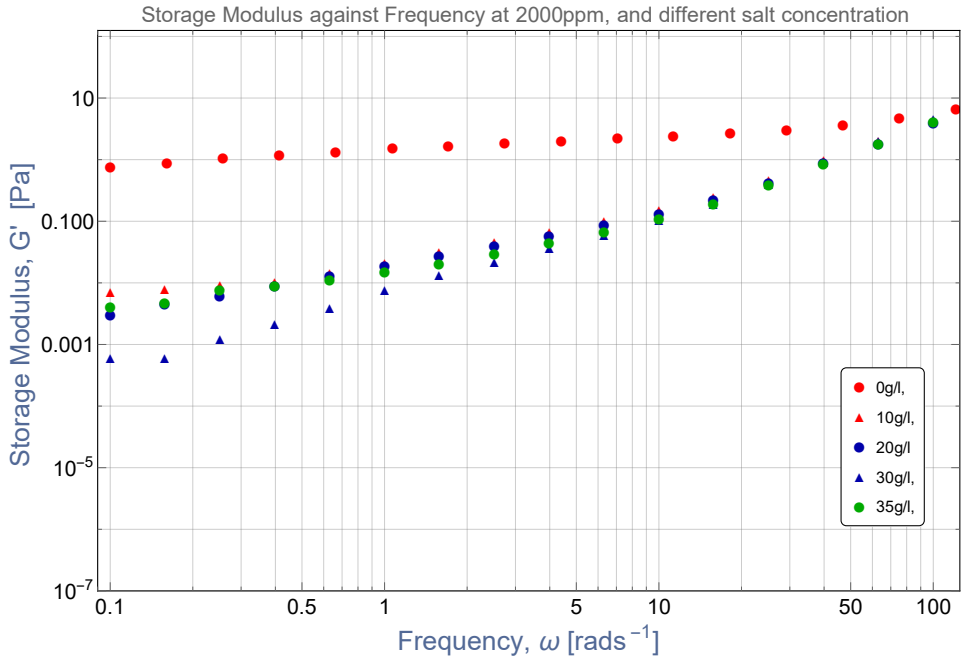

Figure 39: Storage Modulus against angular frequency at different Salt concentrations, 2000 ppm for Flopaam 5115 VHM.

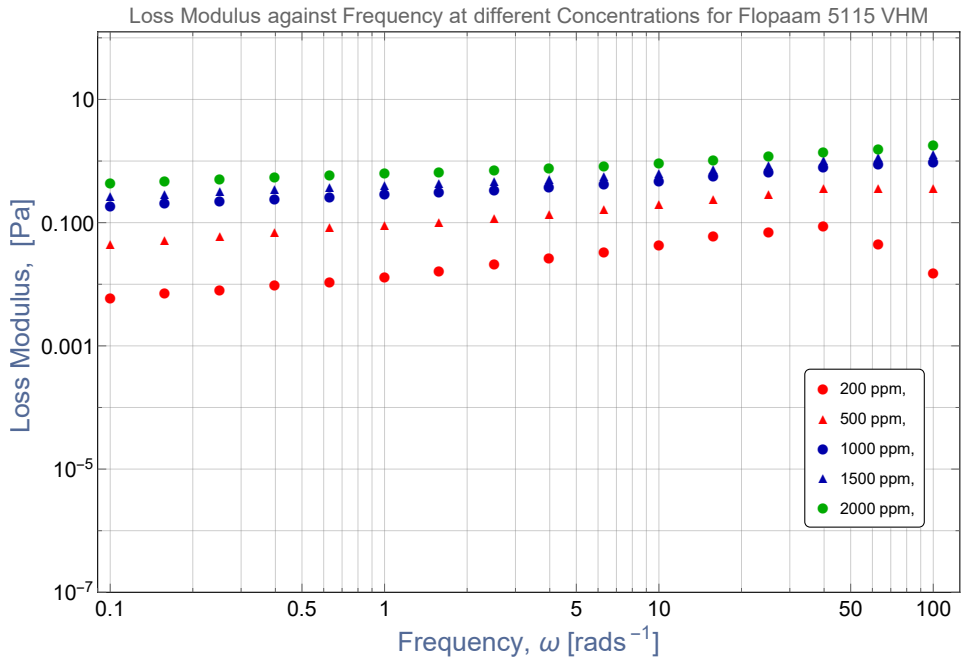

Figure 40: Loss modulus G" plotted against angular frequency ω at different polymer concentrations, and zero salt concentration for the commercial EOR polymer,for Flopaam 5115 VHM.

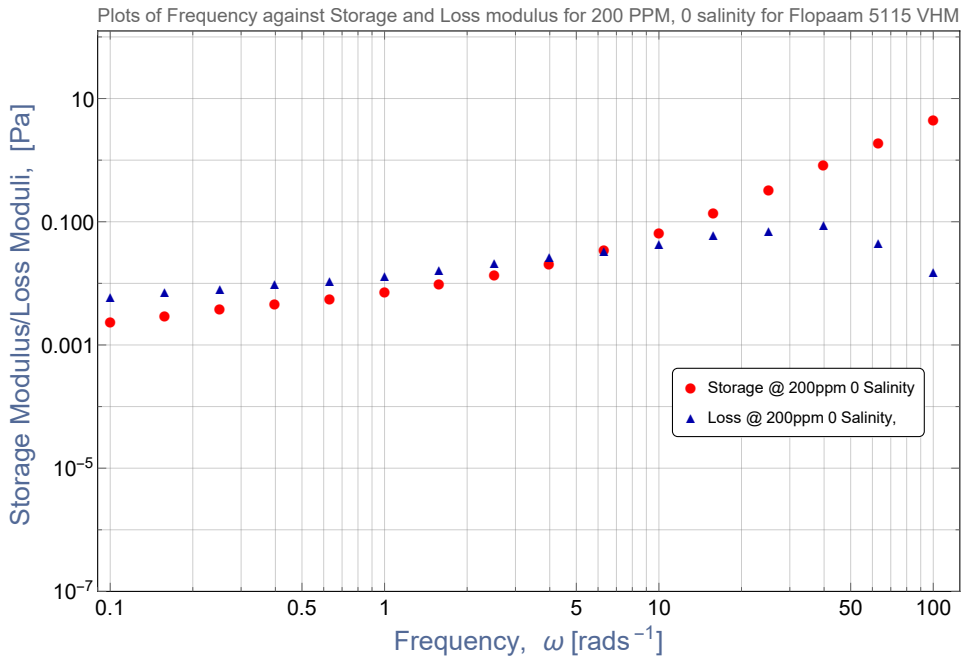

Figure 41: Storage and Loss Modulus against frequency at 200ppm concentrations, and zero salt concentration for the commercial EOR polymer Flopaam 5115 VHM.

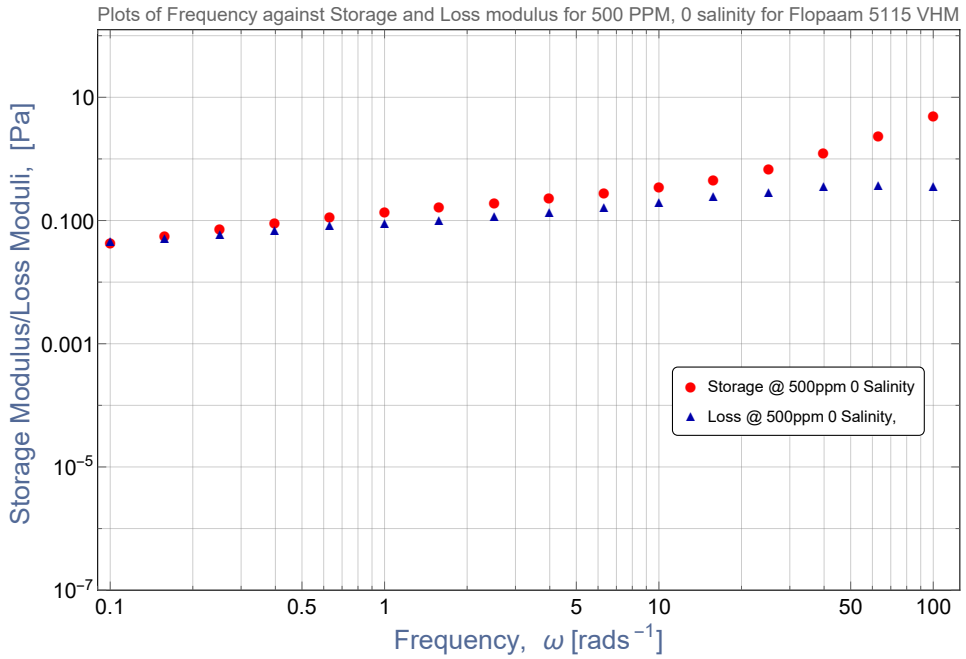

Figure 42: Storage and Loss Modulus against frequency at 500 ppm concentrations, and 0 g/l salt concentration for the commercial EOR polymer Flopaam 5115 VHM.

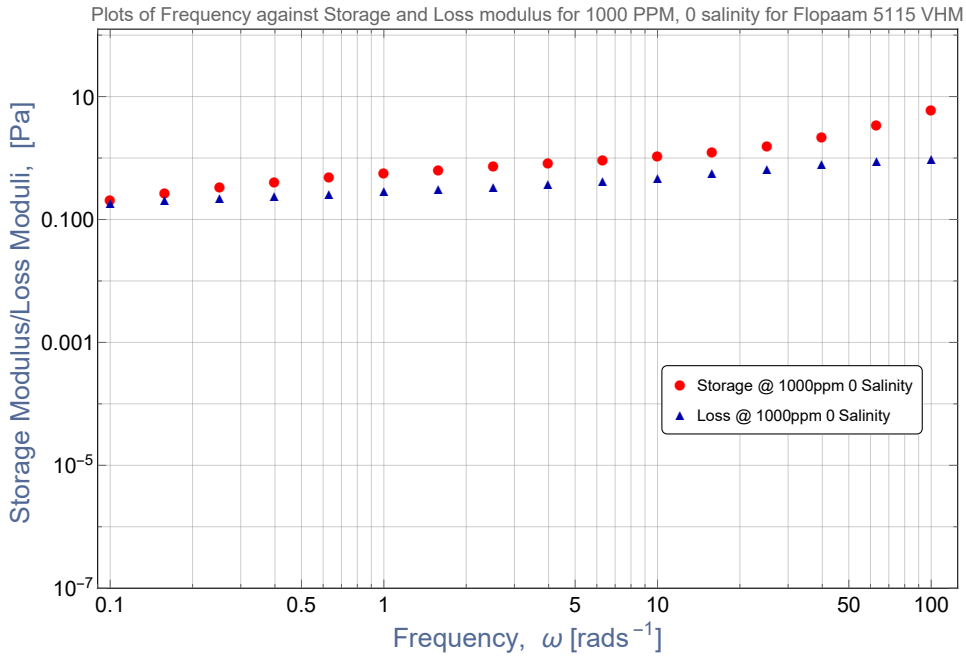

Figure 43: Storage and Loss Modulus against frequency at 1000 ppm concentrations, and 0 g/l salt concentration for the commercial EOR polymer Flopaam 5115 VHM.

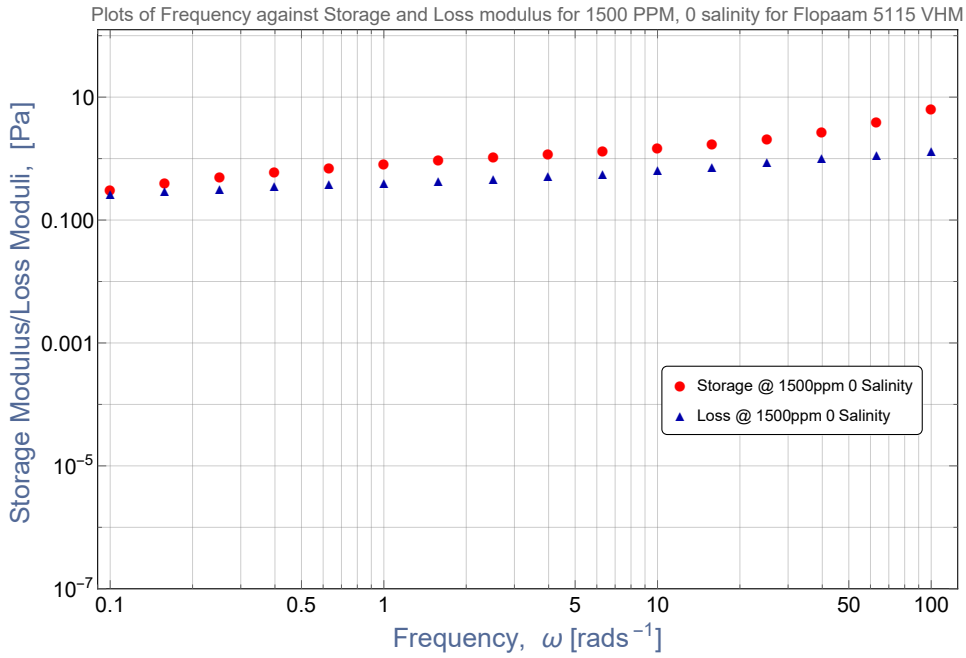

Figure 44: Storage and Loss Modulus against frequency at 1500 ppm concentrations, and 0 g/l salt concentration for the commercial EOR polymer Flopaam 5115 VHM.

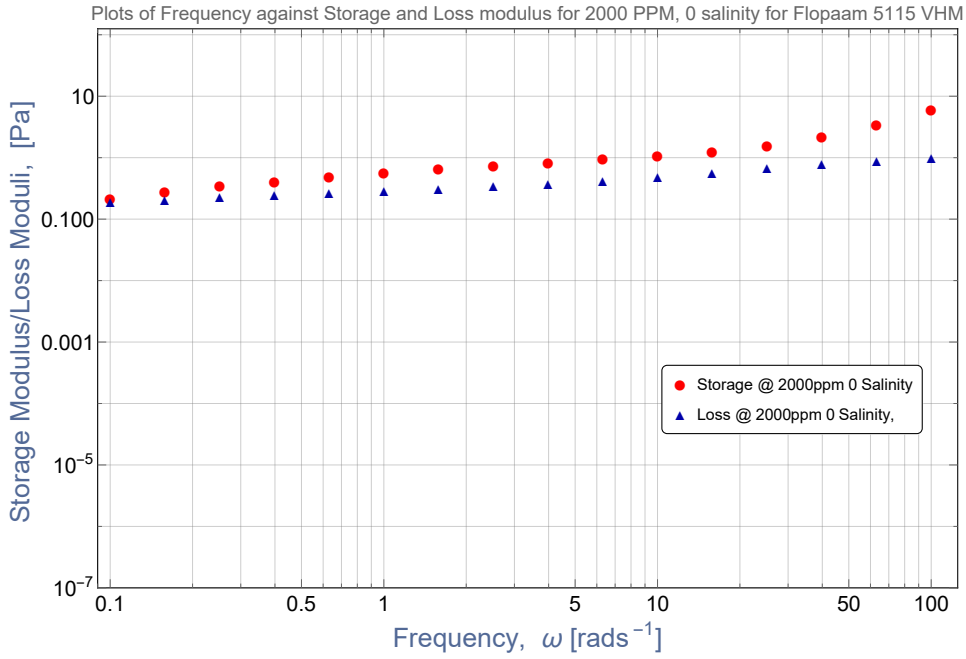

Figure 45: Storage and Loss Modulus against frequency at 2000 ppm concentrations, and 0 g/l salt concentration for the commercial EOR polymer Flopaam 5115 VHM.

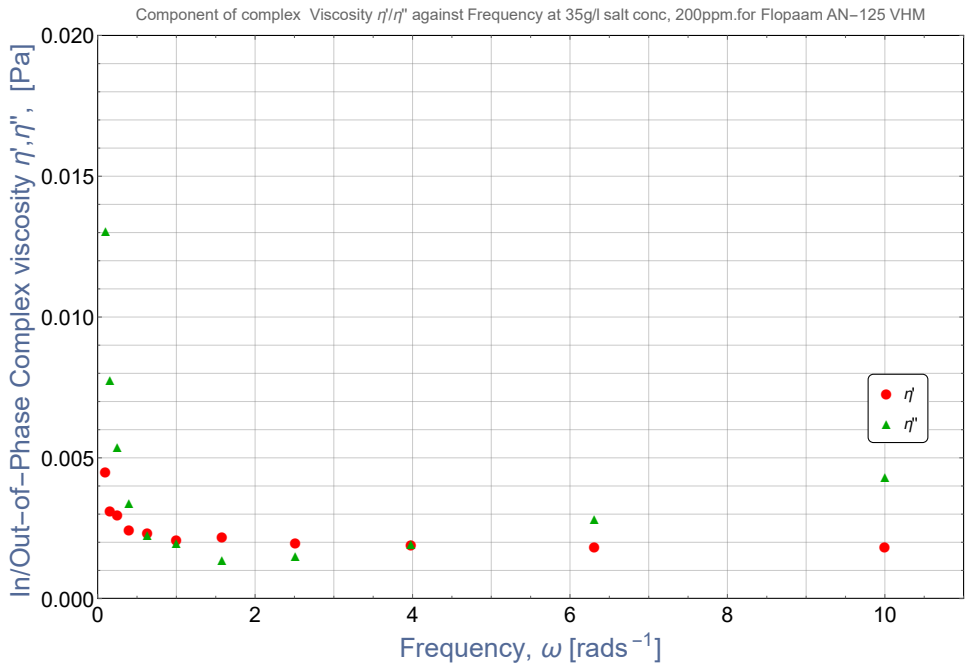

Figure 46: Linear plots of η' and η'' coefficients of complex viscosity, as a function of angular frequency for the commercial EOR polymer Flopaam 5115 VHM at 20^oC, 200 ppm polymer concentration, and 35 g/l Salt concentration.

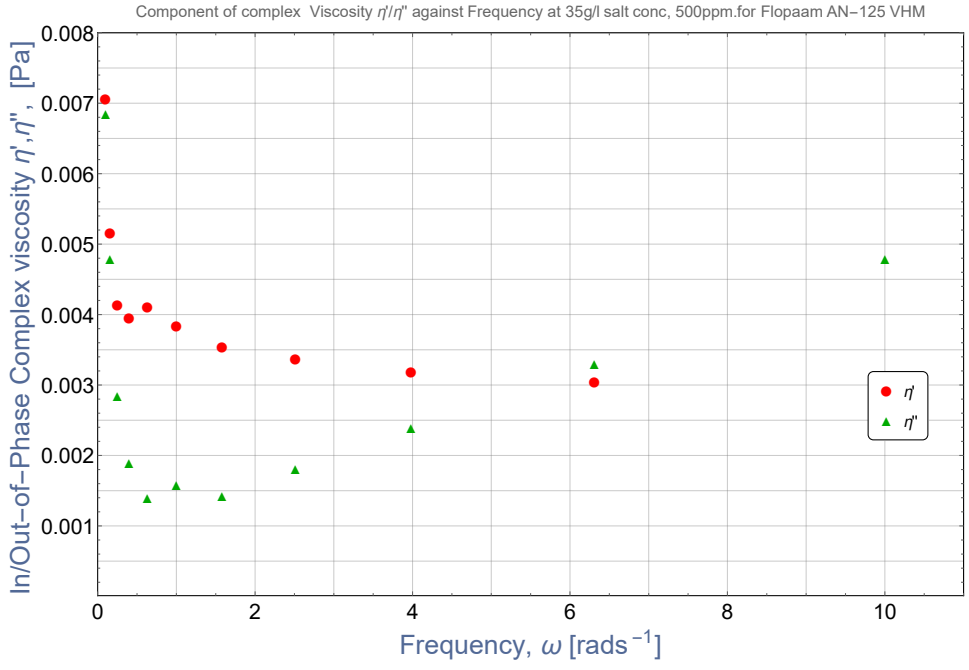

Figure 47: Linear plots of η' and η'' coefficients of complex viscosity, as a function of angular frequency for the commercial EOR polymer Flopaam 5115 VHM at 20^oC, 500 ppm polymer concentration, and 35 g/l Salt concentration.

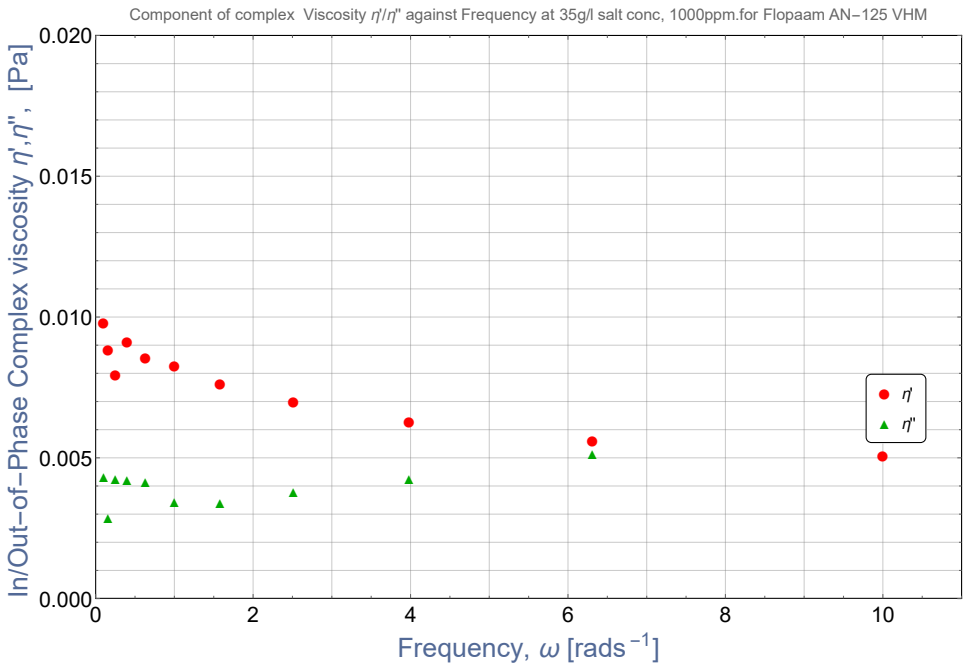

Figure 48: Linear plots of η' and η'' coefficients of complex viscosity, as a function of angular frequency for the commercial EOR polymer Flopaam 5115 VHM at 20^oC, 1000 ppm polymer concentration, and 35 g/l Salt concentration.

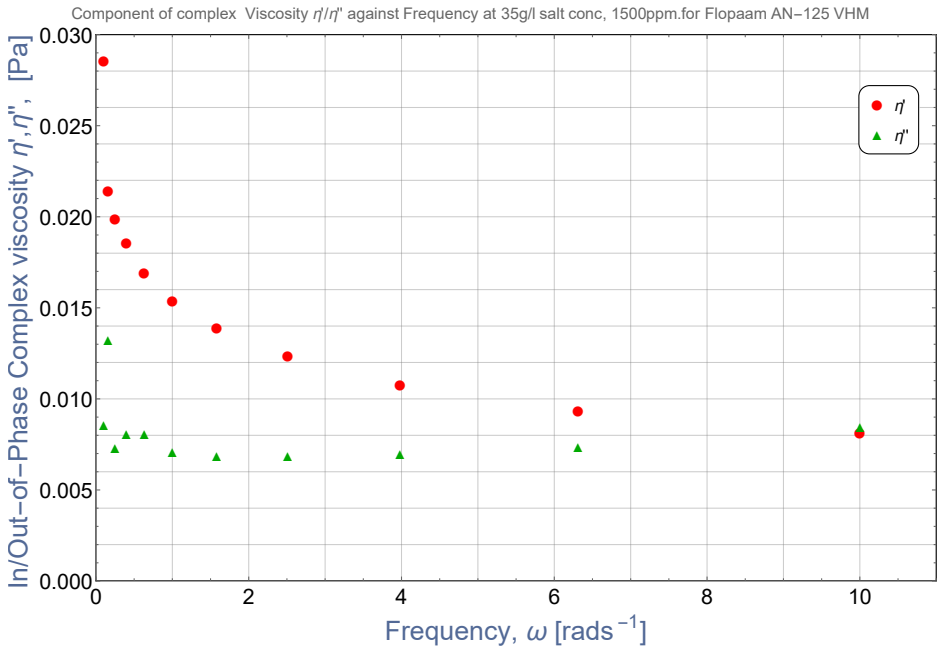

Figure 49: Linear plots of η' and η'' coefficients of complex viscosity, as a function of angular frequency for the commercial EOR polymer Flopaam 5115 VHM at 20^oC, 1500 ppm polymer concentration, and 35 g/l Salt concentration.

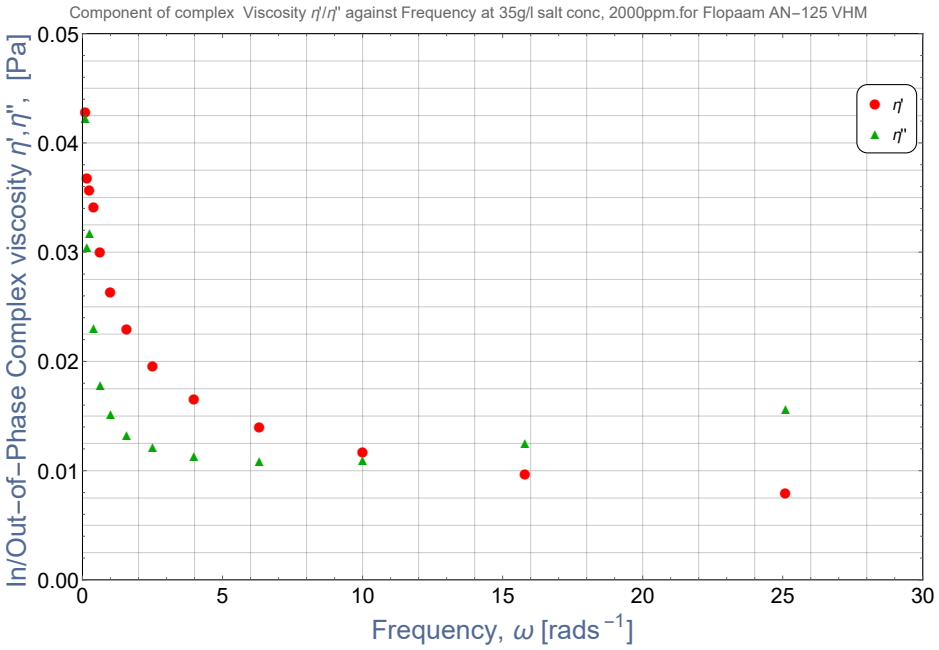

Figure 50: Linear plots of η' and η'' coefficients of complex viscosity, as a function of angular frequency for the commercial EOR polymer Flopaam 5115 VHM at 20^oC, 2000 ppm polymer concentration, and 35 g/l Salt concentration.

D.Figures for FLOPAAM AN-125 VHM

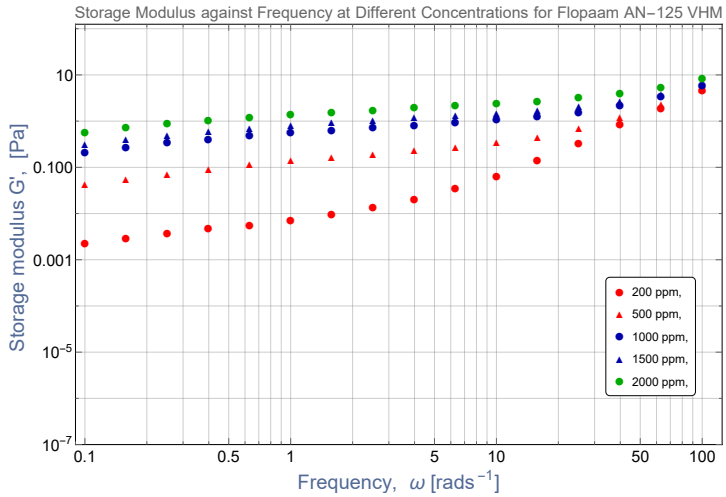

Figure 51: Storage Modulus G' plotted against angular frequency ω at different polymer concentrations, and 0 g/l salt concentration for the commercial EOR polymer, Flopaam AN-125 VHM.

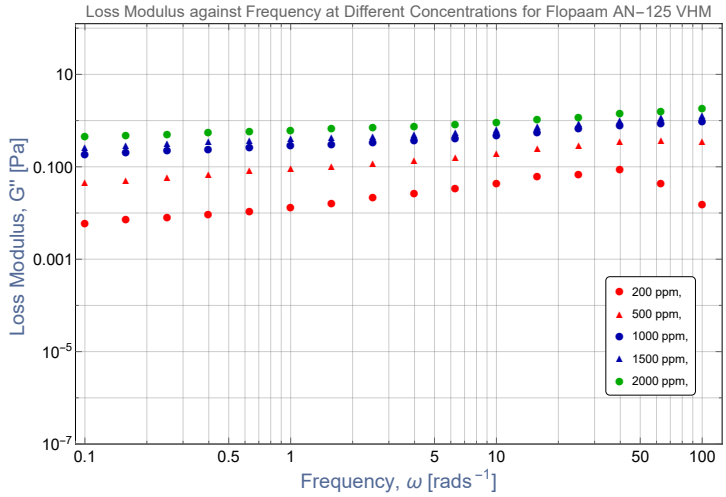

Figure 52: Loss modulus G" plotted against angular frequency ω at different polymer concentrations, and 0 g/l salt concentration for the commercial EOR polymer, Flopaam AN-125 VHM.

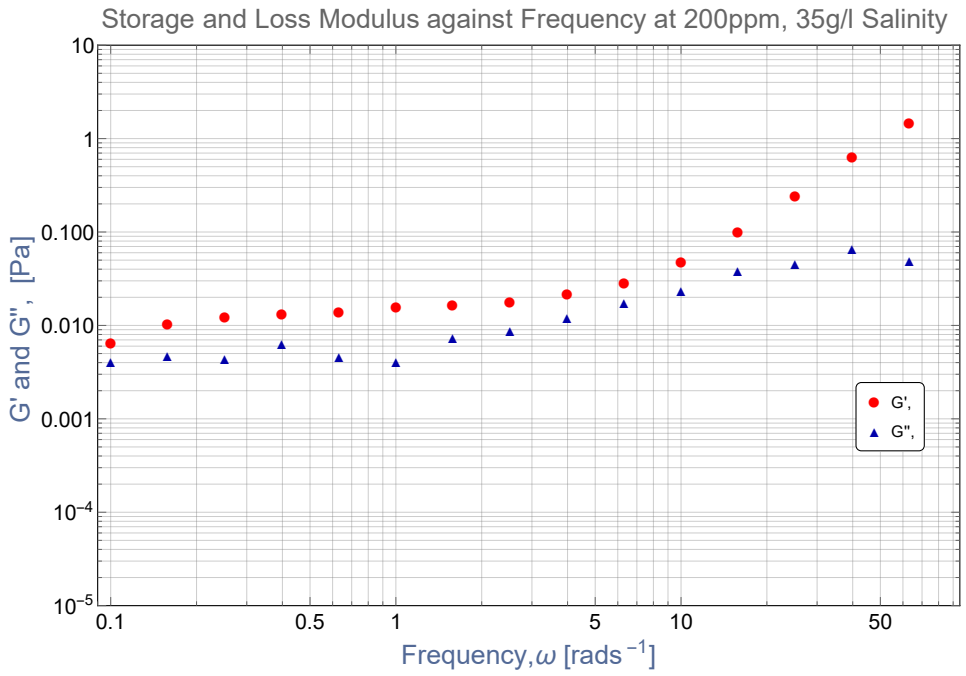

Figure 53: Storage and Loss Modulus against frequency at 200 ppm concentrations, and 35 g/l salt concentration for the commercial EOR polymer Flopaam AN-125 VHM.

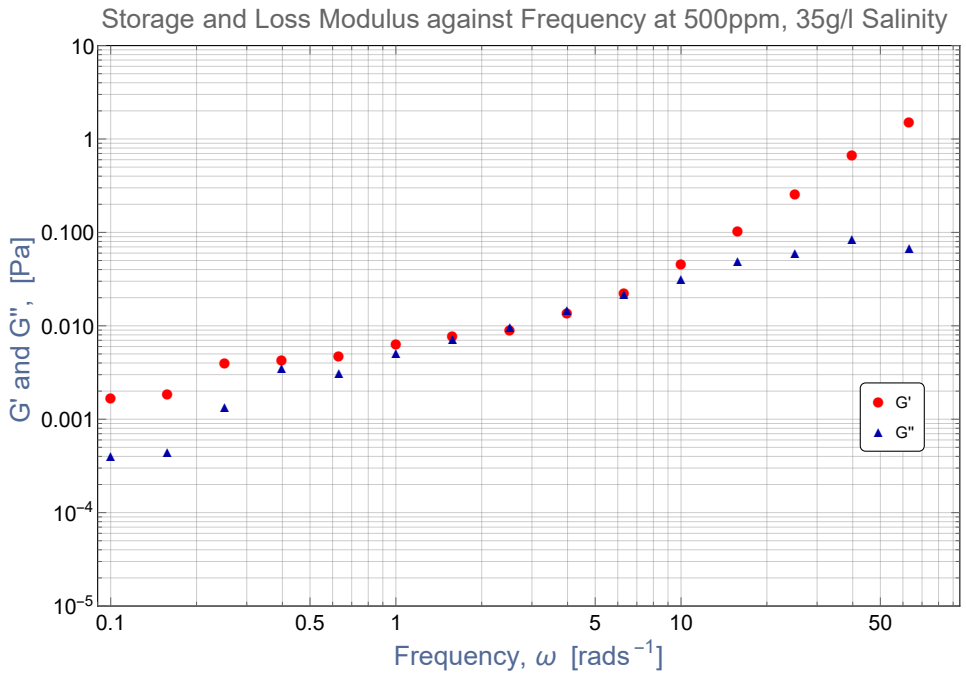

Figure 54: Storage and Loss Modulus against frequency at 500 ppm concentrations, and 35 g/l salt concentration for the commercial EOR polymer Flopaam AN-125 VHM.

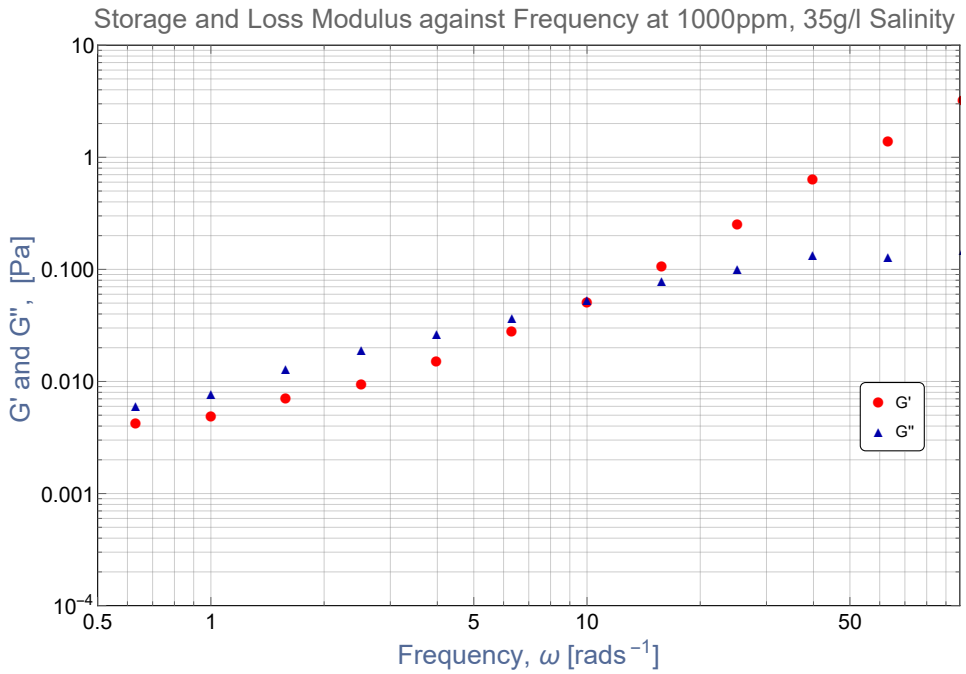

Figure 55: Storage and Loss Modulus against frequency at 1000 ppm concentrations, and 35 g/l salt concentration for the commercial EOR polymer Flopaam 5115 VHM.

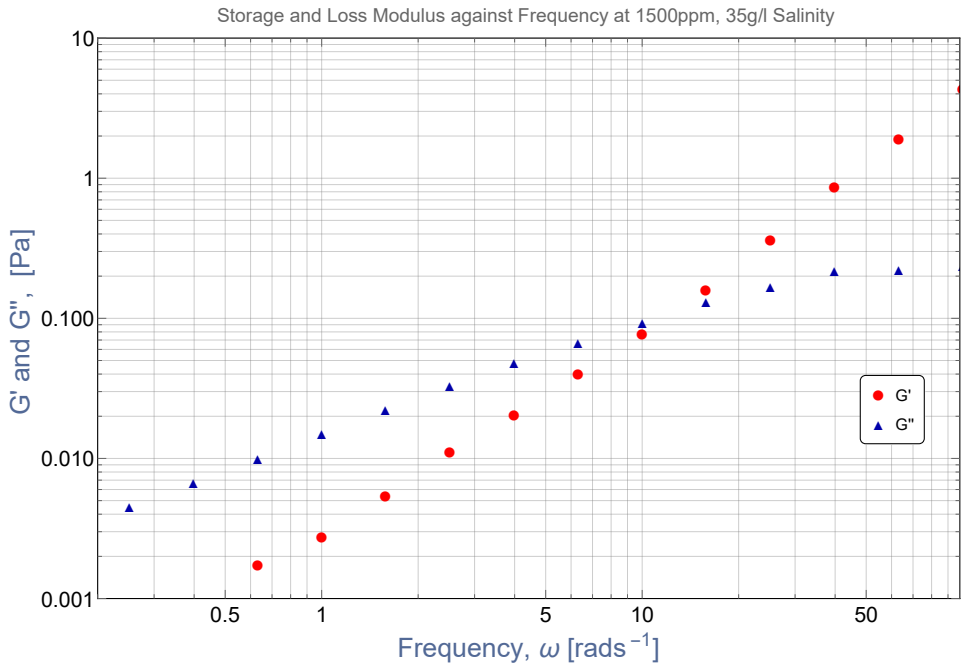

Figure 56: Storage and Loss Modulus against frequency at 1500 ppm concentrations, and 35 g/l salt concentration for the commercial EOR polymer Flopaam AN-125 VHM.

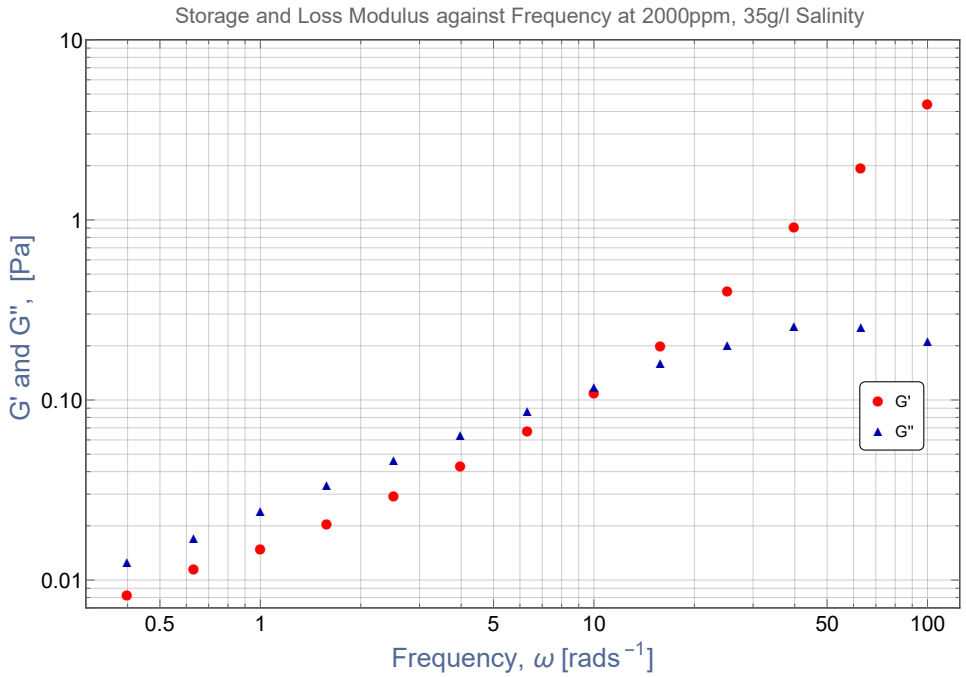

Figure 57: Storage and Loss Modulus against frequency at 2000 ppm concentrations, and 35 g/l salt concentration for the commercial EOR polymer Flopaam AN-125 VHM.

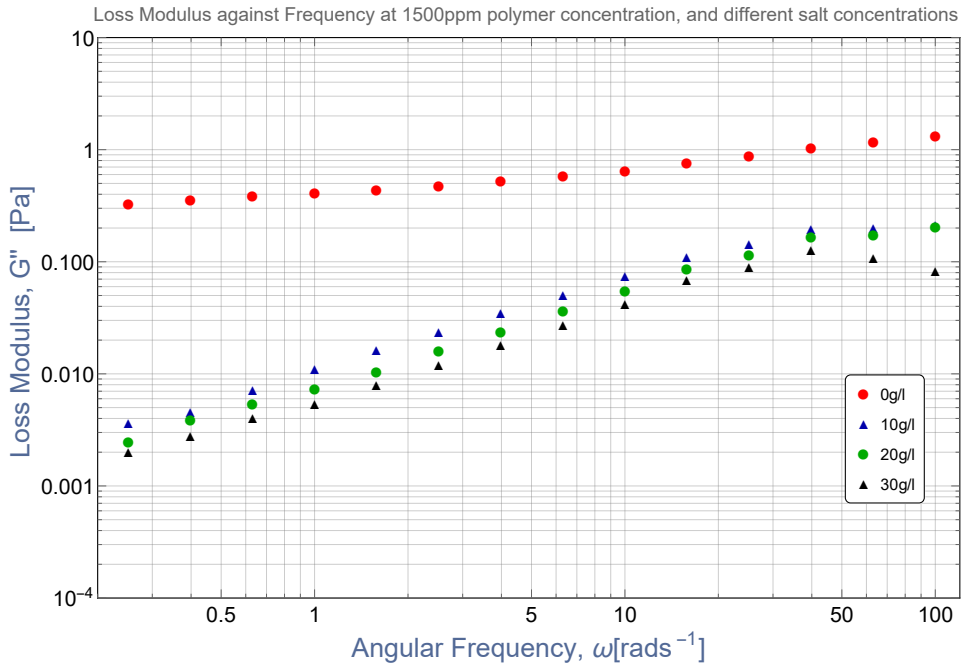

Figure 58: Loss Modulus, G'' as a function of angular frequency for the commercial EOR polymer Flopaam AN-125 VHM at 20^oC, 1500 ppm polymer concentration, and different Salt concentrations.

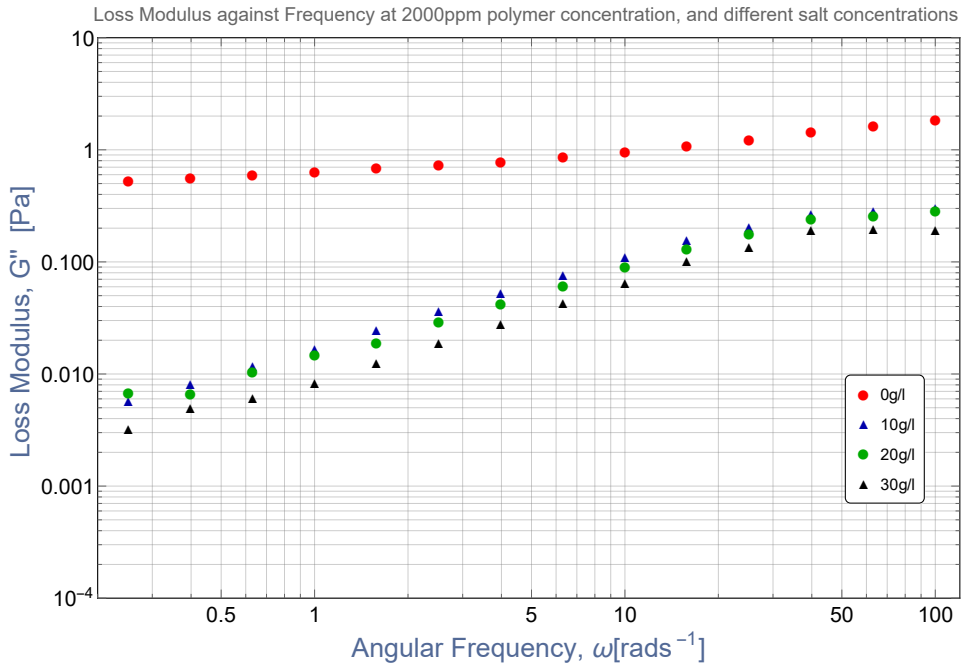

Figure 59: Loss Modulus, G'' as a function of angular frequency for the commercial EOR polymer Flopaam AN-125 VHM at 20^oC, 2000 ppm polymer concentration, and different Salt concentrations.

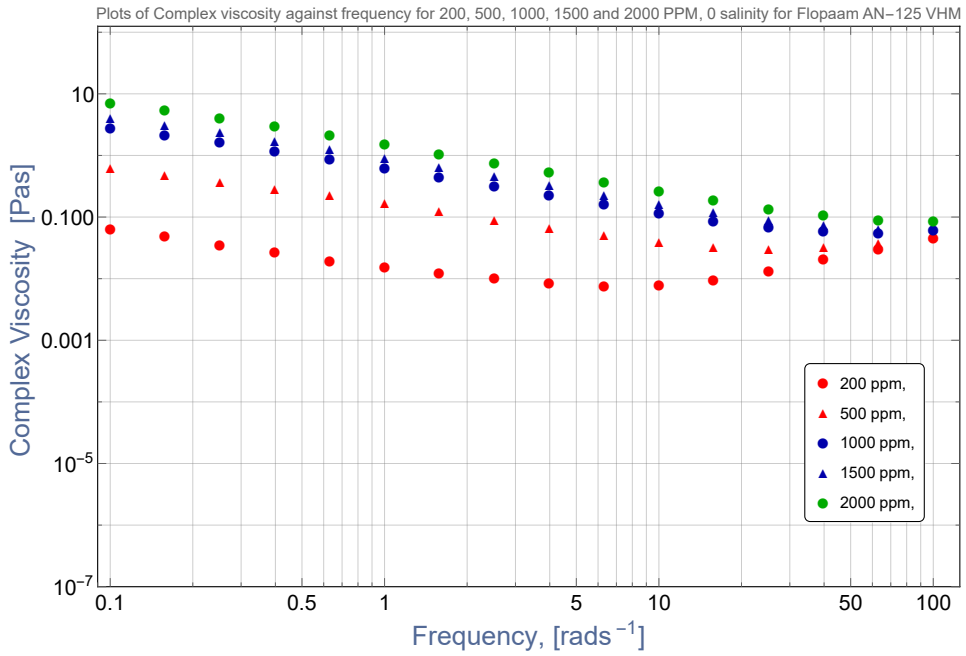

Figure 60: Complex Viscosity, $\eta*$ as a function of angular frequency for the commercial EOR polymer Flopaam AN-125 VHM at 20^oC, different polymer concentration, and different zero Salt concentration.

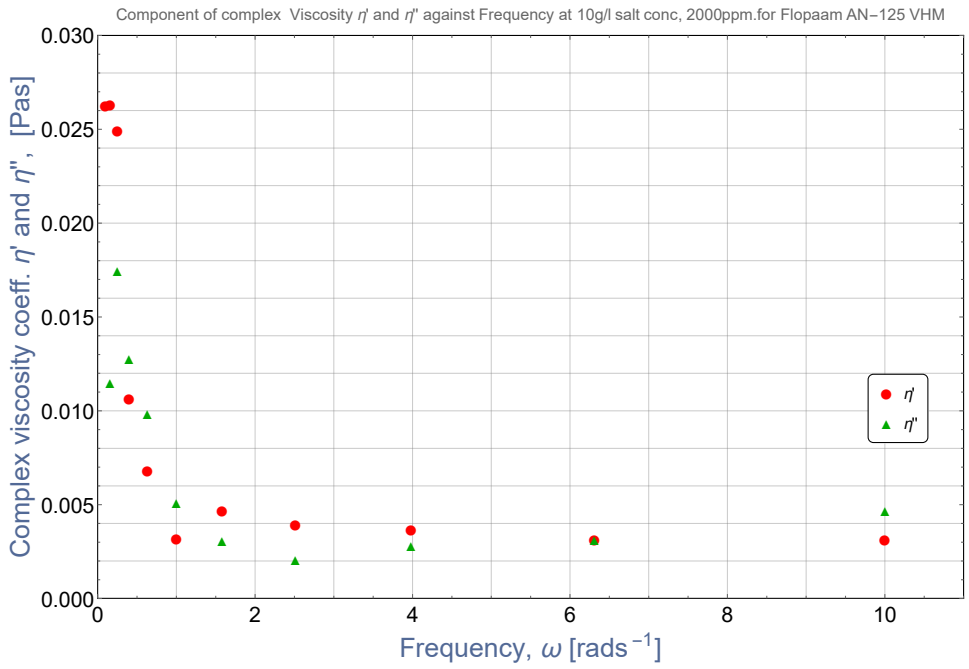

Figure 61: Linear plots of η' and η'' coefficients of complex viscosity, as a function of angular frequency for the commercial EOR polymer Flopaam AN-125 VHM at 20^oC, 2000 ppm polymer concentration, and 10 g/l Salt concentration.

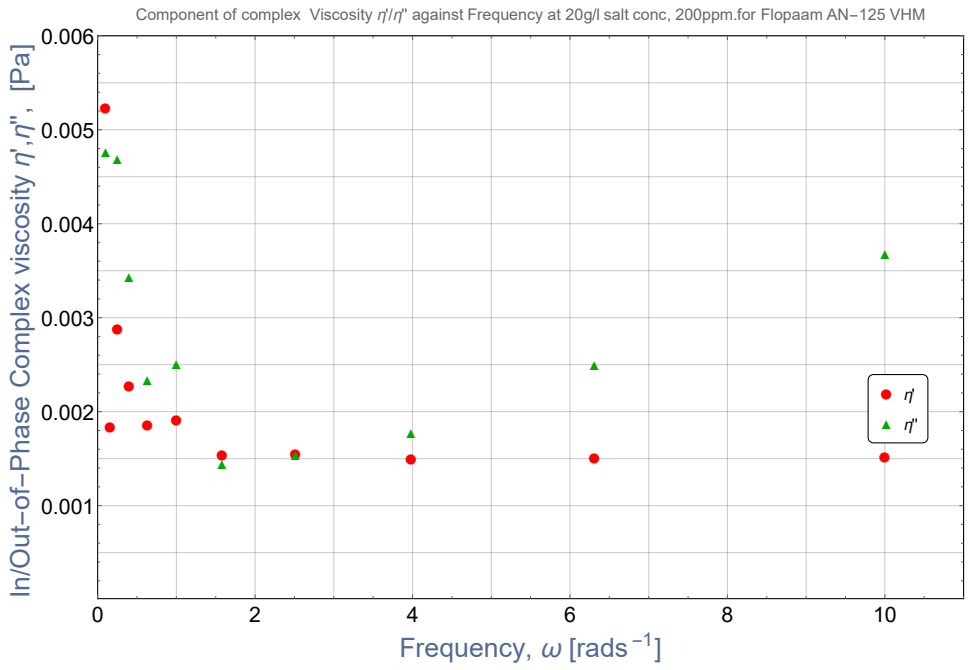

Figure 62: Linear plots of η' and η'' coefficients of complex viscosity, as a function of angular frequency for the commercial EOR polymer Flopaam AN-125 VHM at 20^oC, 200 ppm polymer concentration, and 20 g/l Salt concentration.

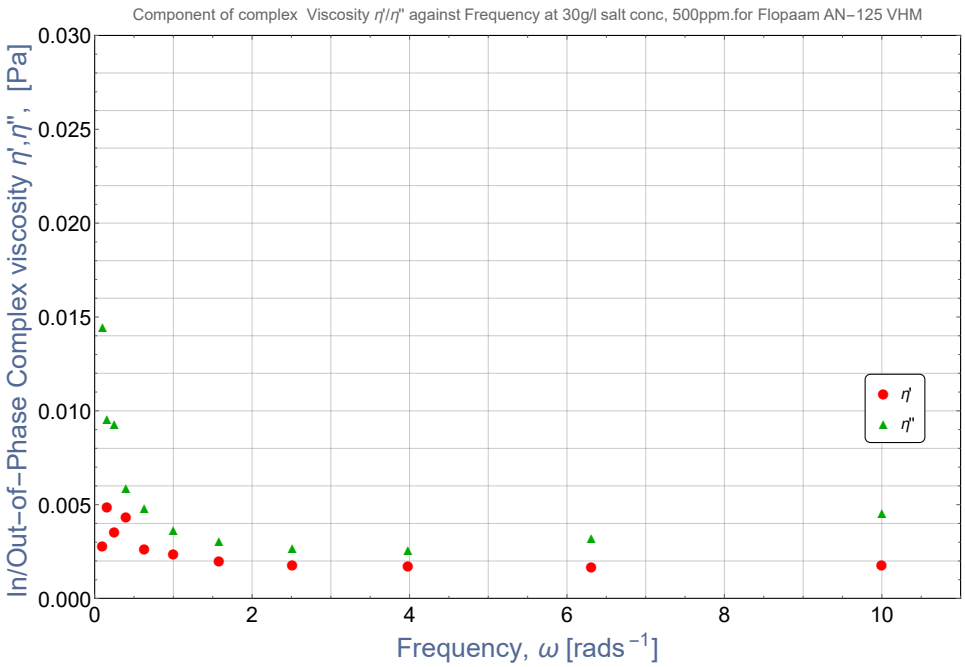

Figure 63: Linear plots of η' and η'' coefficients of complex viscosity, as a function of angular frequency for the commercial EOR polymer Flopaam AN-125 VHM at 20^oC, 500 ppm polymer concentration, and 30 g/l Salt concentration.

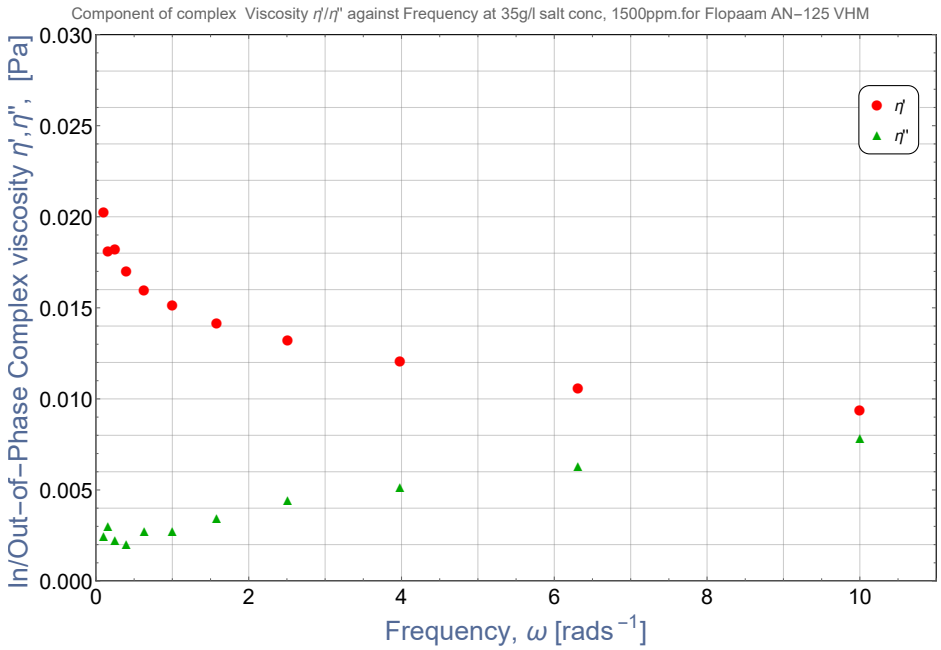

Figure 64: Linear plots of η' and η'' coefficients of complex viscosity, as a function of angular frequency for the commercial EOR polymer Flopaam AN-125 VHM at 20^oC, 1500 ppm polymer concentration, and 35 g/l Salt concentration.

E.Figures for FLOPAAM 5115 VLM

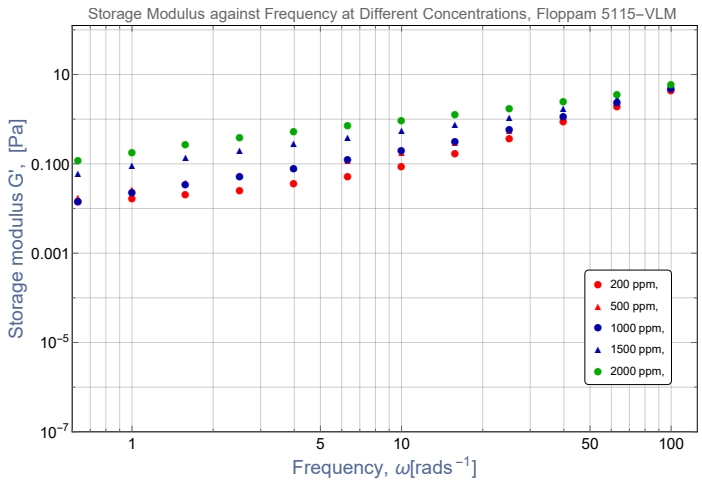

Figure 65: Storage Modulus G', plotted against angular frequency ω,at 20^oC, at different polymer concentrations, and 0 g/l salt concentration for the commercial EOR polymer, Flopaam 5115 VLM.

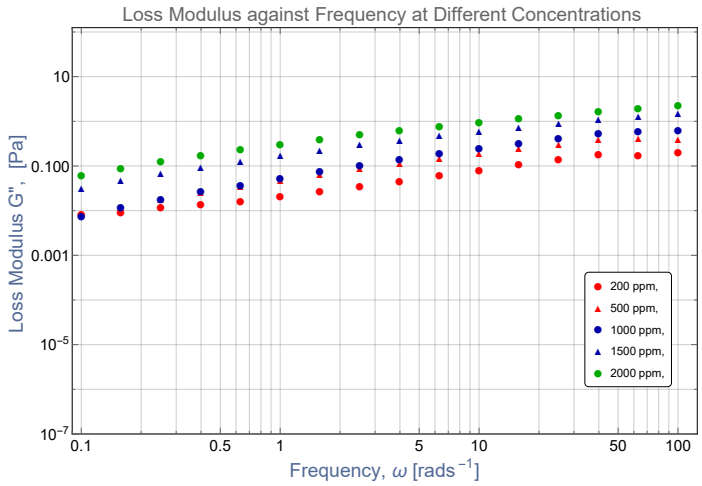

Figure 66: Loss Modulus G'', plotted against angular frequency ω, at 20^oC, at different polymer concentrations, and 0 g/l salt concentration for the commercial EOR polymer, Flopaam 5115 VLM.

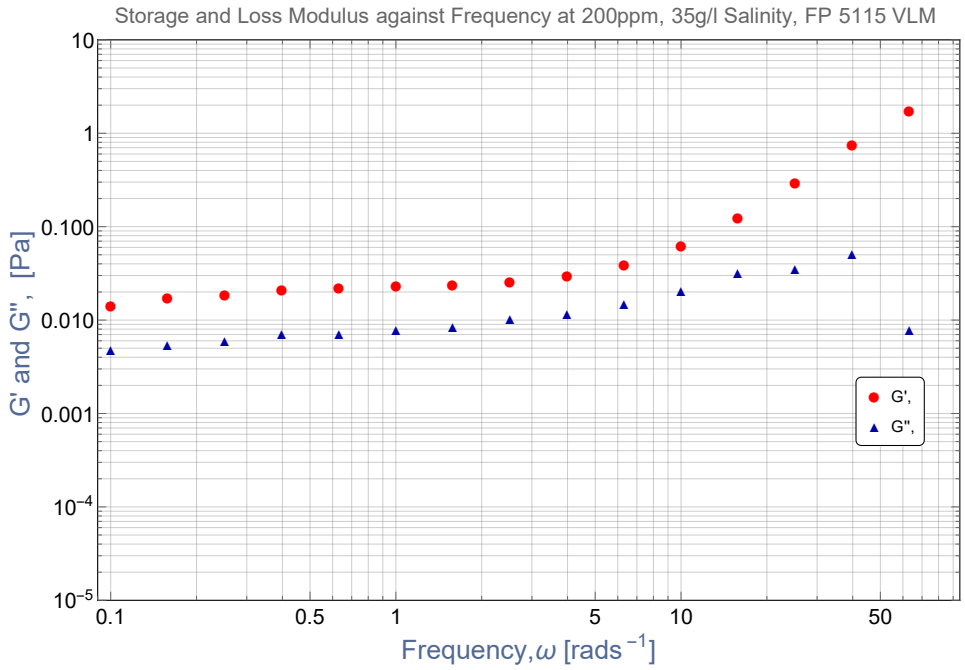

Figure 67: Storage and Loss Modulus against frequency at 200 ppm polymer concentration, and 35 g/l salt concentration for the commercial EOR polymer Flopaam 5115 VLM.

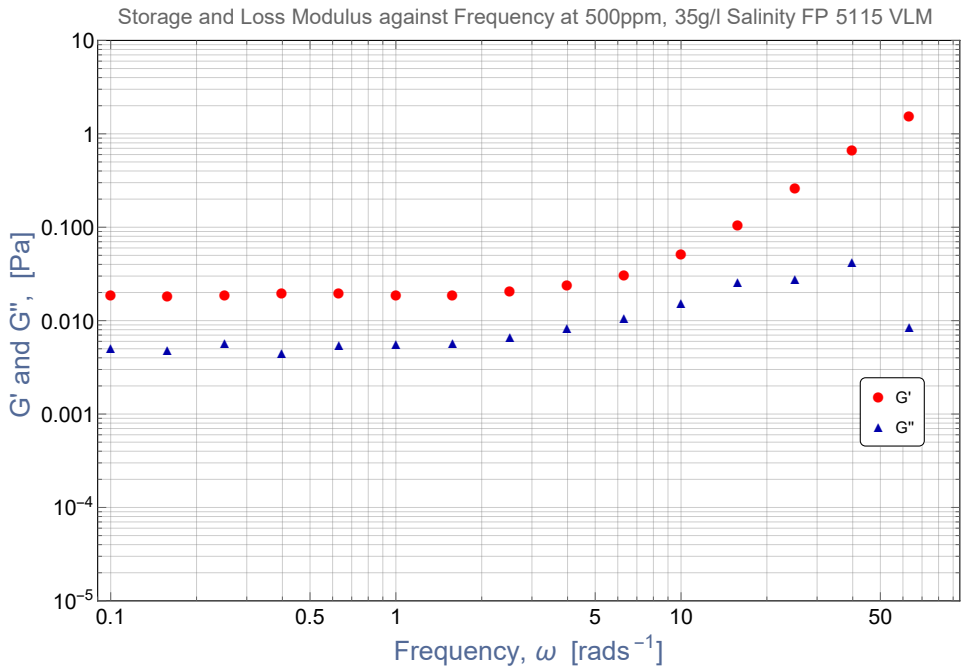

Figure 68: Storage and Loss Modulus against frequency at 500 ppm polymer concentration, and 35 g/l salt concentration for the commercial EOR polymer Flopaam 5115 VLM.

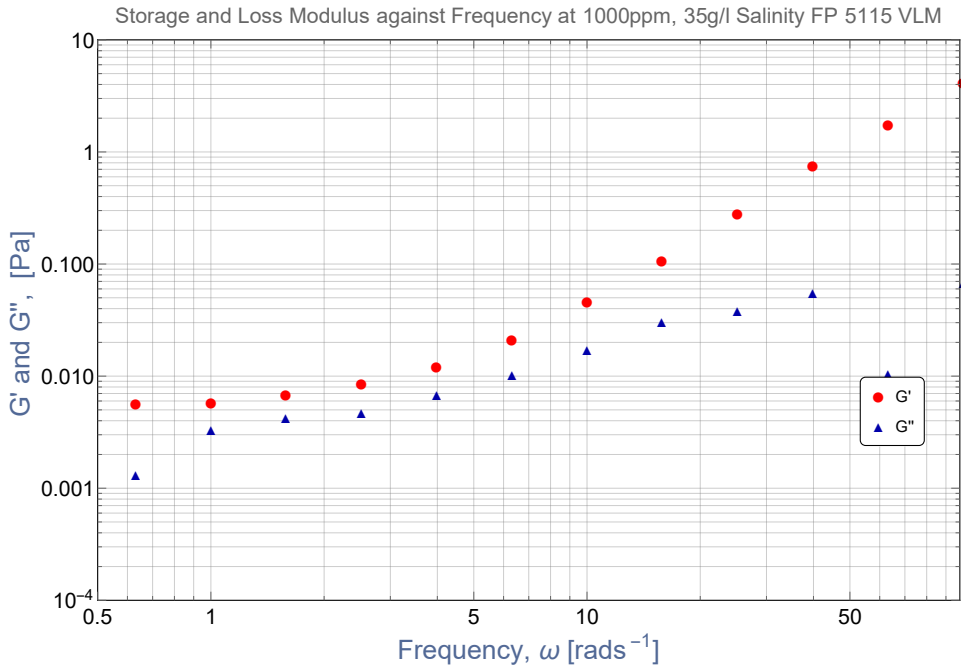

Figure 69: Storage and Loss Modulus against frequency at 1000 ppm polymer concentrations, and 35 g/l salt concentration for the commercial EOR polymer Flopaam 5115 VLM.

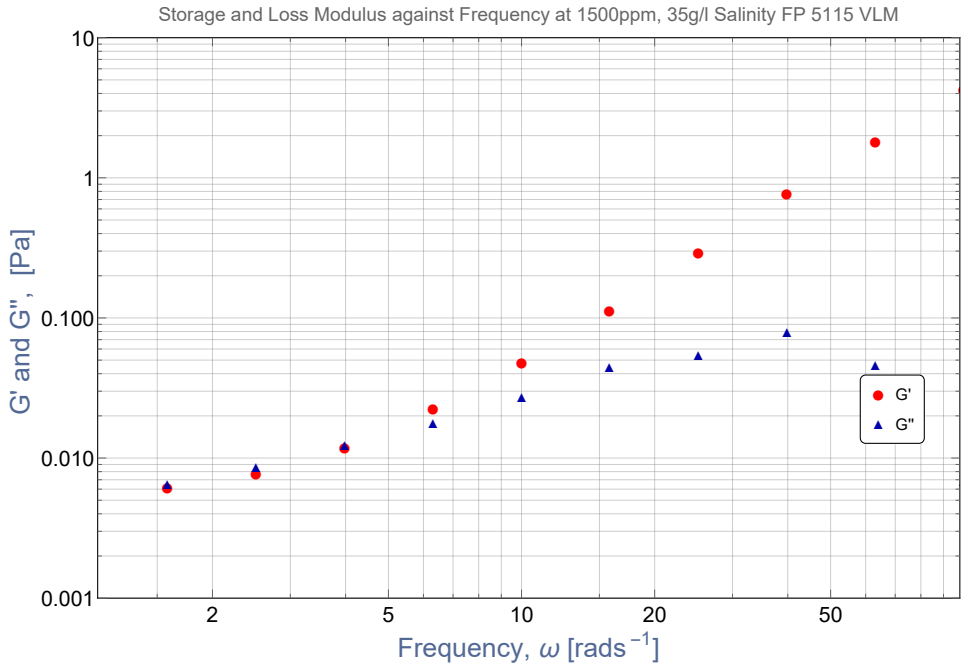

Figure 70: Storage and Loss Modulus against frequency at 1500 ppm polymer concentrations, and 35 g/l salt concentration for the commercial EOR polymer Flopaam 5115 VLM.

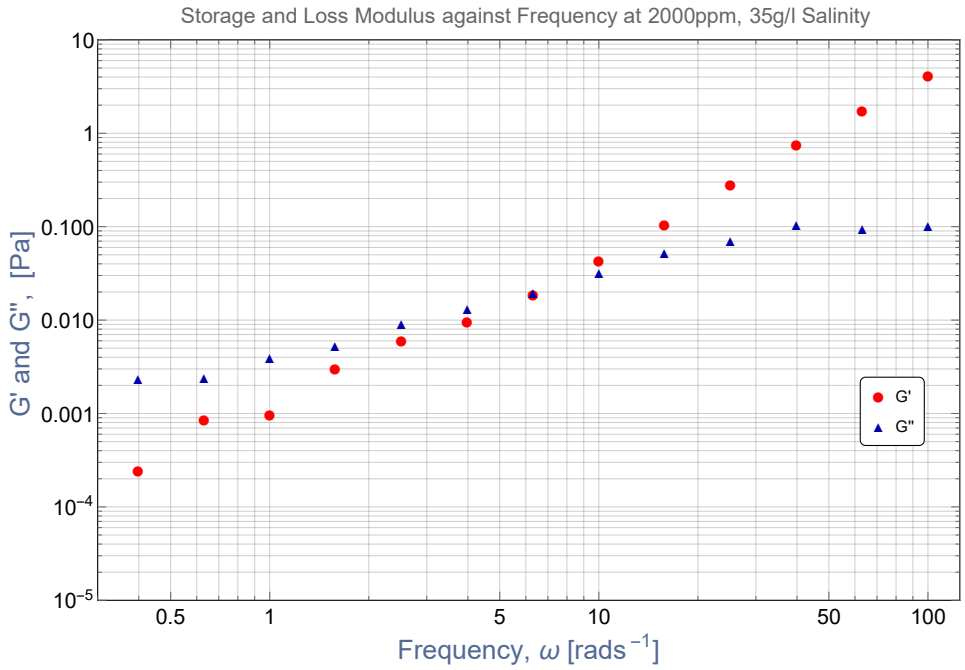

Figure 71: Storage and Loss Modulus against frequency at 2000 ppm polymer concentrations, and 35 g/l salt concentration for the commercial EOR polymer Flopaam 5115 VLM.

F.Figures for FLOPAAM AN-125 VLM

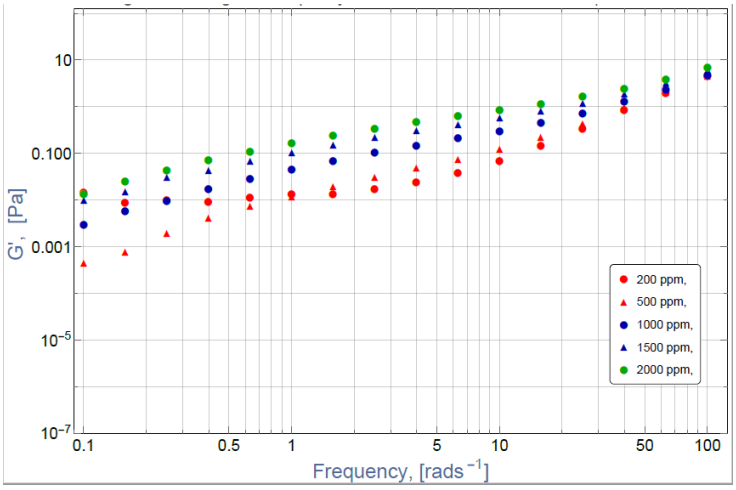

Figure 72: Storage Modulus G', plotted against angular frequency ω,at 20^oC, at different polymer concentrations, and 0 g/l salt concentration for the commercial EOR polymer, Flopaam AN-125 VLM.

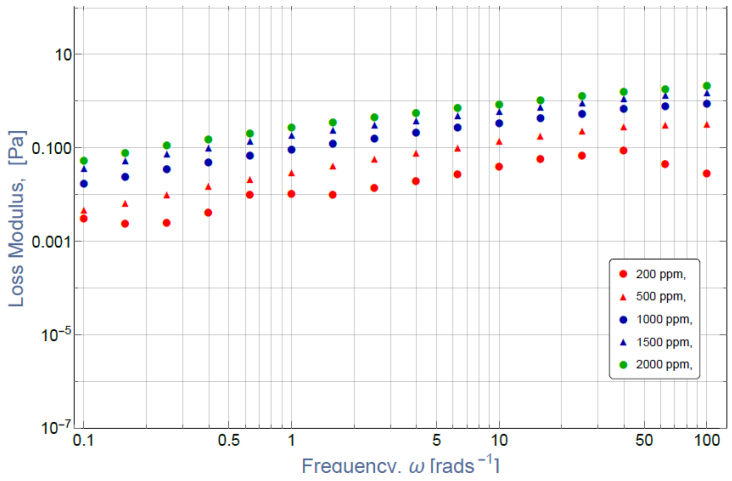

Figure 73: Loss Modulus G', plotted against angular frequency ω,at 20^oC, at different polymer concentrations, and 0 g/l salt concentration for the commercial EOR polymer, Flopaam AN-125 VLM.

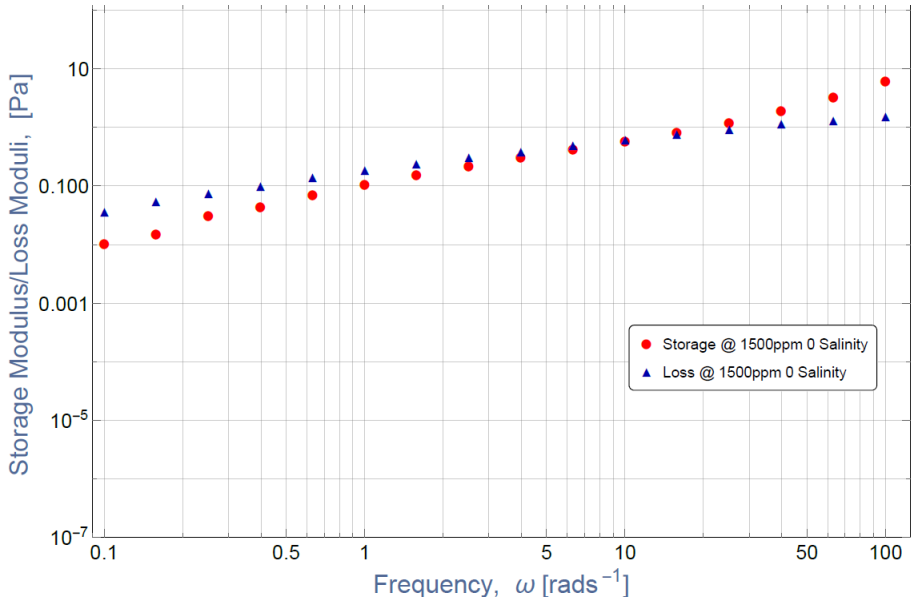

Figure 74: Storage and Loss Modulus against frequency at 1500 ppm polymer concentrations, and 0 g/l salt concentration for the commercial EOR polymer Flopaam AN-125 VLM.

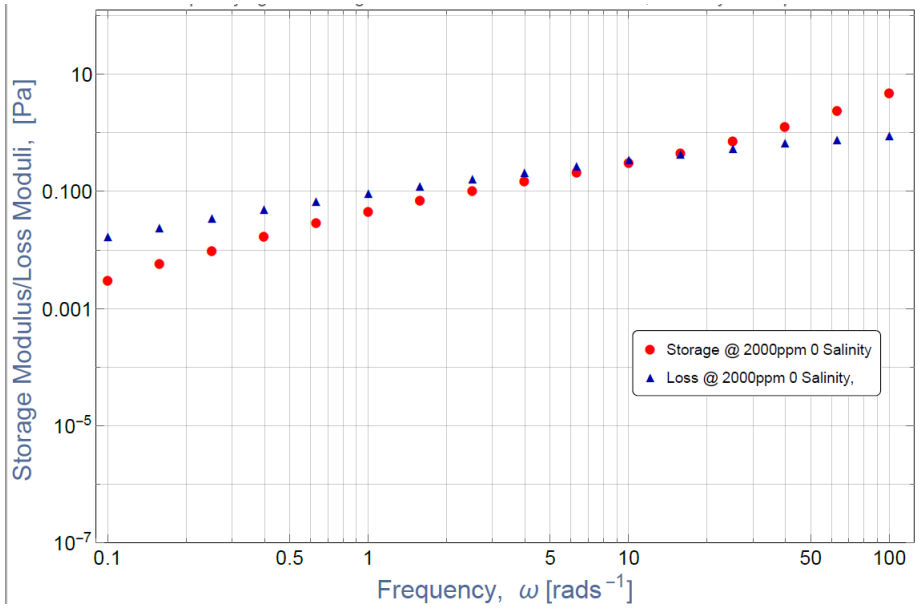

Figure 75: Storage and Loss Modulus against frequency at 2000 ppm polymer concentrations, and 0 g/l salt concentration for the commercial EOR polymer Flopaam AN-125 VLM.

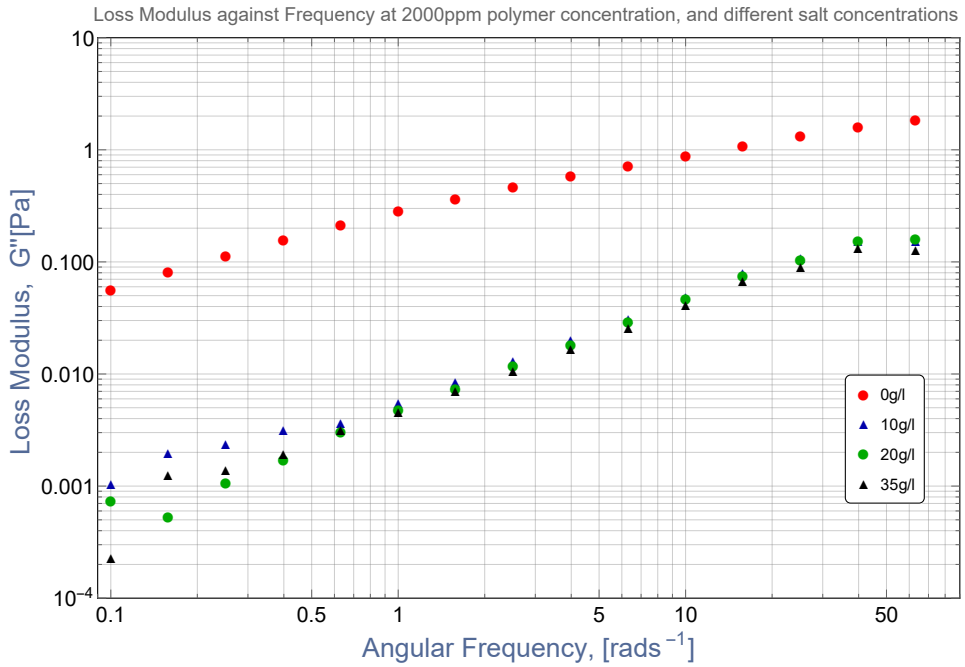

Figure 76: Loss Modulus G'', plotted against angular frequency ω, at 20^oC, at polymer concentrations 2000 ppm, and different salt concentration for the commercial EOR polymer, Flopaam AN-125 VLM.

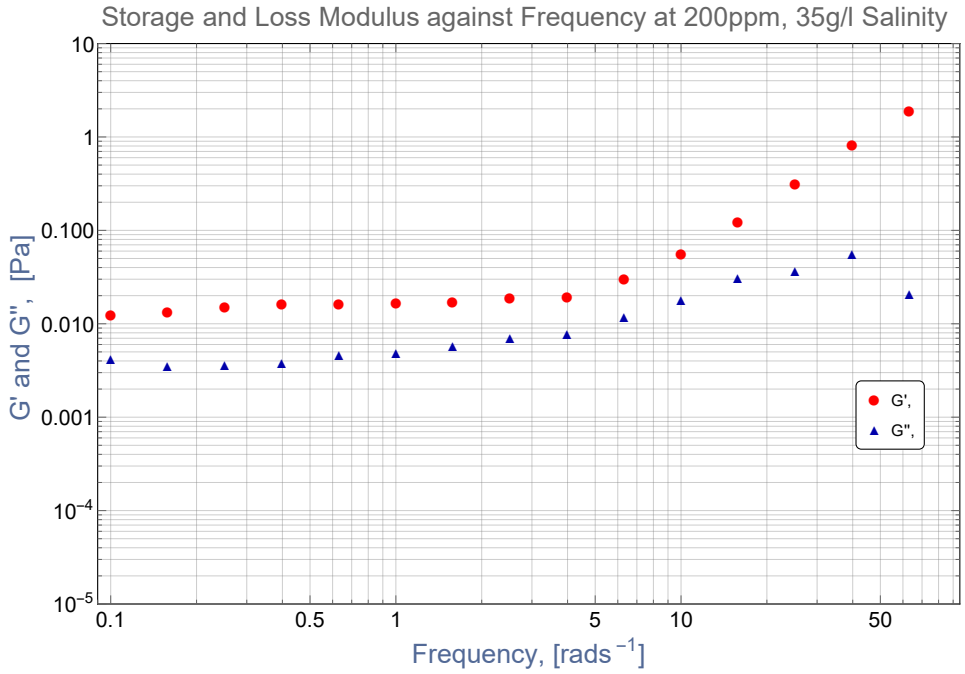

Figure 77: Storage and Loss Modulus against frequency at 200 ppm polymer concentration, and 35 g/l salt concentration for the commercial EOR polymer Flopaam AN-125 VLM.

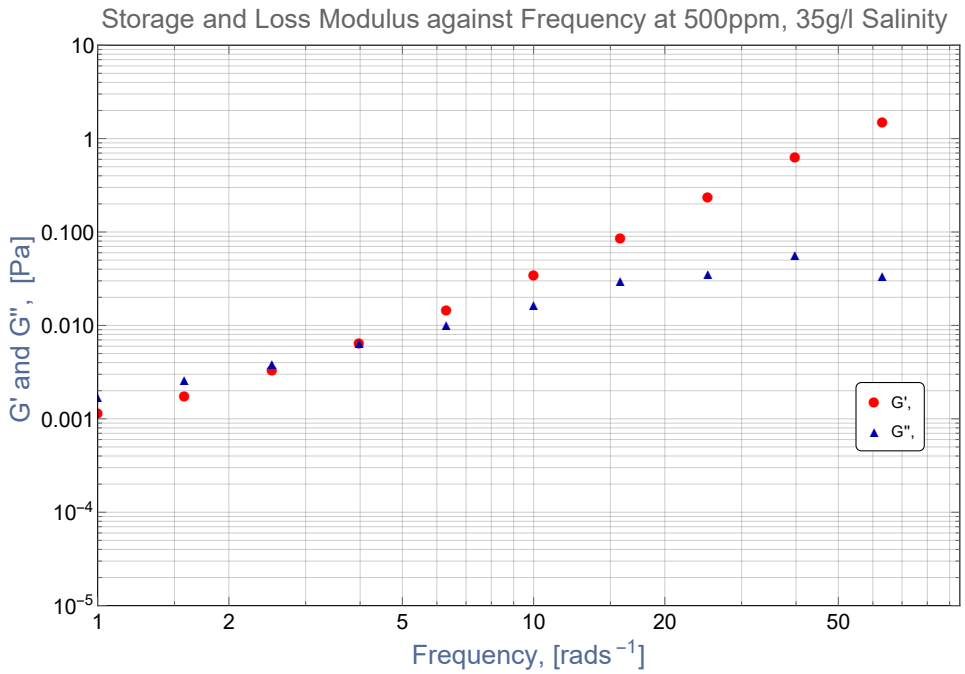

Figure 78: Storage and Loss Modulus against frequency at 500 ppm polymer concentration, and 35 g/l salt concentration for the commercial EOR polymer Flopaam AN-125 VLM.

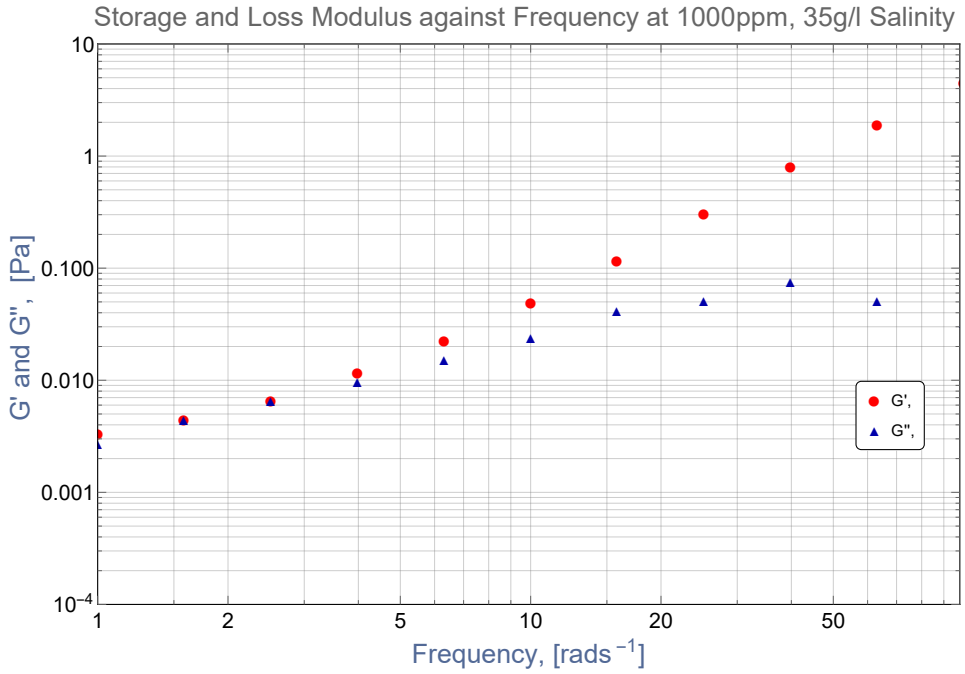

Figure 79: Storage and Loss Modulus against frequency at 1000 ppm polymer concentration, and 35 g/l salt concentration for the commercial EOR polymer Flopaam AN-125 VLM.

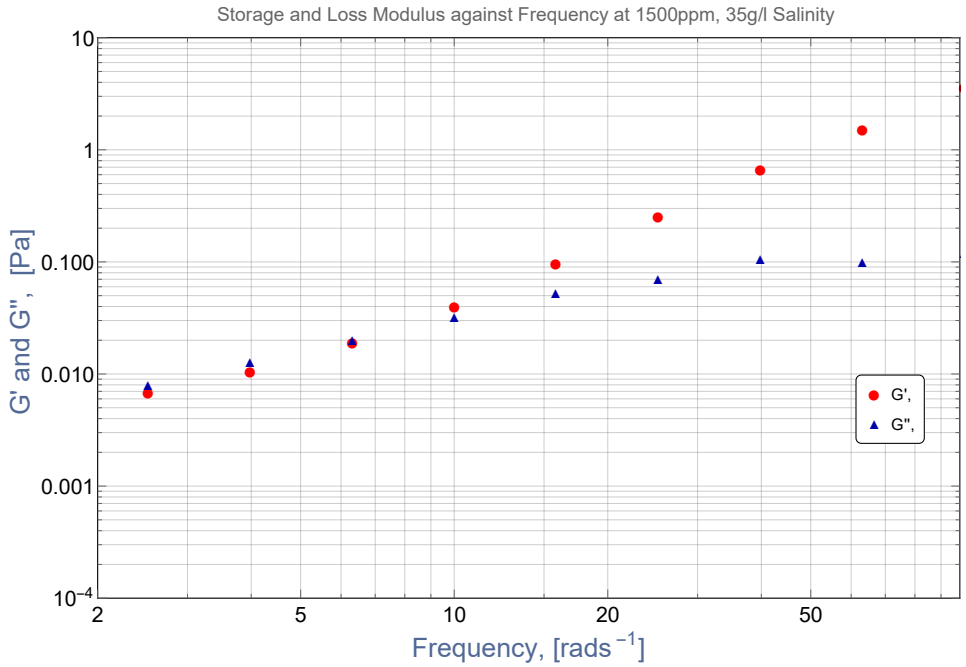

Figure 80: Storage and Loss Modulus against frequency at 1500 ppm polymer concentration, and 35 g/l salt concentration for the commercial EOR polymer Flopaam AN-125 VLM.

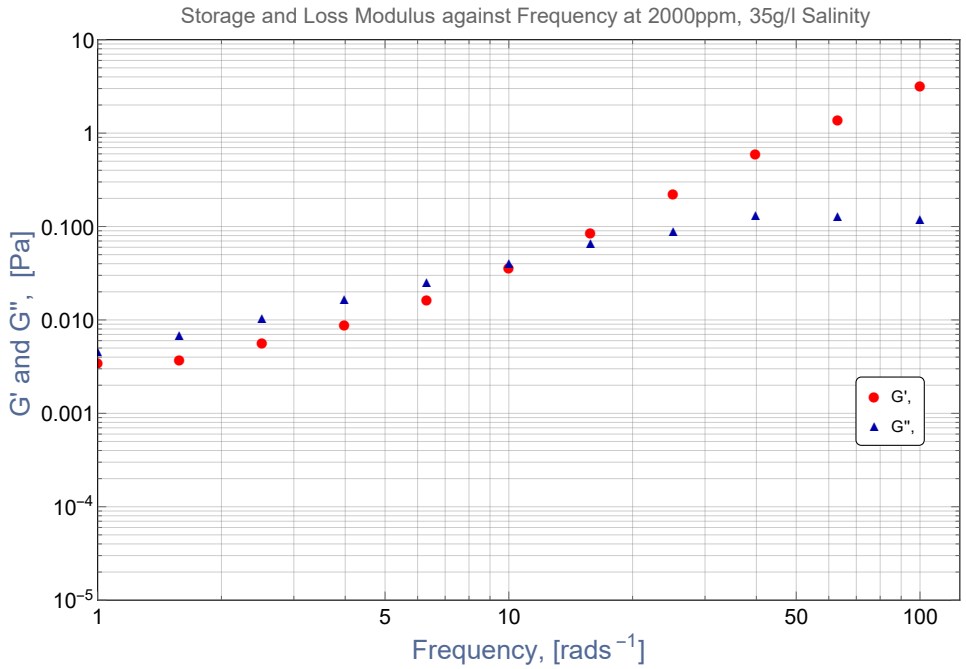

Figure 81: Storage and Loss Modulus against frequency at 2000 ppm polymer concentration, and 35 g/l salt concentration for the commercial EOR polymer Flopaam AN-125 VLM.

References

[Ait-Kadi et al., 1987] Ait-Kadi, A., Carreau, P., and Chauveteau, G. (1987). Rheological properties of partially hydrolyzed polyacrylamide solutions. *Journal of Rheology*, 31(7):537–561.

[Armstrong, 1974] Armstrong, R. C. (1974). Kinetic theory and rheology of dilute solutions of flexible macromolecules. i. steady state behavior. *The Journal of Chemical Physics*, 60(3):724–728.

[Bird et al., 1987a] Bird, R. B., Armstrong, R. C., and Hassager, O. (1987a). Dynamics of polymeric liquids. Vol. 1: Fluid mechanics.

[Bird et al., 1987b] Bird, R. B., Curtiss, C., and Armstrong, R. (1987b). 0. hassager, dynamics of polymeric liquids, vol. 2, kinetic theory.

[Borthakur et al., 1995] Borthakur, A., Rahman, M., Sarmah, A., and Subrahmanyam, B. (1995). Partially hydrolyzed polyacrylamide for enhanced oil-recovery. *RESEARCH AND INDUSTRY*, 40(2):90–94.

[Chilcott and Rallison, 1988] Chilcott, M. and Rallison, J. M. (1988). Creeping flow of dilute polymer solutions past cylinders and spheres. *Journal of Non-Newtonian Fluid Mechanics*, 29:381–432.

[Du et al., 2004] Du, Y., Guan, L., et al. (2004). Field-scale polymer flooding: lessons learnt and experiences gained during past 40 years. In *SPE International Petroleum Conference in Mexico*. Society of Petroleum Engineers.

[Dunlap and Leal, 1984] Dunlap, P. and Leal, L. (1984). The charged dumbbell model for dilute polyelectrolyte solutions in strong flows. *Rheologica acta*, 23(3):238–249.

[Dupuis et al., 1994] Dupuis, D., Lewandowski, F., Steiert, P., and Wolff, C. (1994). Shear thickening and time-dependent phenomena: the case of polyacrylamide solutions. *Journal of non-newtonian fluid mechanics*, 54:11–32.

[Falode and Afolabi, 2011] Falode, F. and Afolabi, F. (2011). Simulation study of polymer flooding performance: effect of clay minerals. *Journal of Petroleum & Coal*, 53(3):206–211.

[Ferry, 1980] Ferry, J. D. (1980). *Viscoelastic properties of polymers*. John Wiley & Sons.

[Graessley, 1974] Graessley, W. W. (1974). The entanglement concept in polymer rheology. In *The entanglement concept in polymer rheology*, pages 1–179. Springer.

[Herrchen and Öttinger, 1997] Herrchen, M. and Öttinger, H. C. (1997). A detailed comparison of various fene dumbbell models. *Journal of Non-Newtonian Fluid Mechanics*, 68(1):17–42.

[Hyun et al., 2011] Hyun, K., Wilhelm, M., Klein, C. O., Cho, K. S., Nam, J. G., Ahn, K. H., Lee, S. J., Ewoldt, R. H., and McKinley, G. H. (2011). A review of nonlinear oscillatory shear tests: Analysis and application of large amplitude oscillatory shear (laos). *Progress in Polymer Science*, 36(12):1697–1753.

[Jeldres et al., 2018] Jeldres, R. I., Piceros, E. C., Wong, L.-s., Leiva, W. H., Herrera, N., and Toledo, P. G. (2018). Dynamic moduli of flocculated kaolinite sediments: effect of salinity, flocculant dose, and settling time. *Colloid and Polymer Science*, 296(12):1935–1943.

[Lake, 1989] Lake, L. W. (1989). Enhanced oil recovery.

[Larson, 1999] Larson, R. G. (1999). The structure and rheology of complex fluids (topics in chemical engineering). *Oxford University Press, New York• Oxford*, 86:108.

[Lee et al., 2009] Lee, S., Kim, D. H., Huh, C., Pope, G. A., et al. (2009). Development of a comprehensive rheological property database for eor polymers. In *SPE Annual Technical Conference and Exhibition*. Society of Petroleum Engineers.

[Lutskina, 2018] Lutskina, M. (2018). Describing viscosity of ior polymer solutions with differential non-newtonian fluid models. Master's thesis, University of Stavanger, Norway.

[Martínez-Vázquez et al., 2010] Martínez-Vázquez, F. J., Perera, F. H., Miranda, P., Pajares, A., and Guiberteau, F. (2010). Improving the compressive strength of bioceramic robocast scaffolds by polymer infiltration. *Acta Biomaterialia*, 6(11):4361–4368.

[Mezger, 2011] Mezger, T. (2011). The rheology handbook (vincentz network. *Hanover, Germany*.

[Morgan and McCormick, 1990] Morgan, S. E. and McCormick, C. L. (1990). Water-soluble polymers in enhanced oil recovery. *Progress in polymer science*, 15(1):103–145.

[Morrison et al., 2001] Morrison, F. A. et al. (2001). *Understanding rheology*. Topics in Chemical Engineering.

[Ninomiya and Fujita, 1957] Ninomiya, K. and Fujita, H. (1957). Stress-relaxation behavior of polyvinyl acetate films. *Journal of Colloid Science*, 12(2):204–229.

[Okubo et al., 2001] Okubo, T., Kimura, H., and Hatta, T. (2001). Rheo-optics of colloidal crystals. In *Studies in Surface Science and Catalysis*, volume 132, pages 387–390. Elsevier.

[Paar, 2011] Paar, A. (2011). Anton Paar Equipment Laboratory Manual. pages 1–20.

[Rashidi et al., 2010] Rashidi, M., Blokhus, A. M., and Skauge, A. (2010). Viscosity study of salt tolerant polymers. *Journal of applied polymer science*, 117(3):1551–1557.

[Rigelesaiyin et al., 2018] Rigelesaiyin, J., Diaz, A., Li, W., Xiong, L., and Chen, Y. (2018). Asymmetry of the atomic-level stress tensor in homogeneous and inhomogeneous materials. *Proceedings of the Royal Society A: Mathematical, Physical and Engineering Sciences*, 474(2217):20180155.

[Seright et al., 2009] Seright, R., Seheult, M., and Talashek, T. (2009). Injectivity characteristics of eor polymers, spe res eng: 783-792. Technical report, SPE-115142-PA.

[Shogin, 2019] Shogin, D. (2019). Fluid dynamics class notes.

[Shogin et al., 2017] Shogin, D., Amundsen, P., Hiorth, A., and Madland, M. (2017). Rheology of polymeric flows in circular pipes, slits and capillary bundles: analytical solutions from kinetic theory. In *IOR Norway 2017—19th European Symposium on Improved Oil Recovery*.

[SNF, 2004] SNF (2004). Floppams for enhanced oil recovery brochure. pages 1–20.

[Stanislavskiy, 2018] Stanislavskiy, V. (2018). Investigating the impact of solvent salinity on the viscometric functions of ior polymers. Master's thesis, University of Stavanger, Norway.

[Stavland A., 2013] Stavland A., Hilde J., S. D. (2013). When will polymer viscosity be a design criterion for eor polymer flooding? In *IEA-EOR 34th Annual Sympossium, Stavanger Norway*.

[Stokes and Evans, 1997] Stokes, R. J. and Evans, D. F. (1997). *Fundamentals of interfacial engineering*. John Wiley & Sons.

[Sukpisan et al., 1998] Sukpisan, J., Kanatharana, J., Sirivat, A., and Wang, S. (1998). The specific viscosity of partially hydrolyzed polyacrylamide solutions: Effects of degree of hydrolysis, molecular weight, solvent quality and temperature. *Journal of Polymer Science Part B: Polymer Physics*, 36(5):743–753.

[Tam and Tiu, 1990] Tam, K. and Tiu, C. (1990). Role of ionic species and valency on the steady shear behavior of partially hydrolyzed polyacrylamide solutions. *Colloid and polymer science*, 268(10):911–920.

[Thien and Tanner, 1977] Thien, N. P. and Tanner, R. I. (1977). A new constitutive equation derived from network theory. *Journal of Non-Newtonian Fluid Mechanics*, 2(4):353–365.

[Wang et al., 2009] Wang, D., Dong, H., Lv, C., Fu, X., Nie, J., et al. (2009). Review of practical experience by polymer flooding at daqing. *SPE Reservoir Evaluation & Engineering*, 12(03):470–476.

[Warner Jr, 1972] Warner Jr, H. R. (1972). Kinetic theory and rheology of dilute suspensions of finitely extendible dumbbells. *Industrial & Engineering Chemistry Fundamentals*, 11(3):379–387.

[Wedgewood et al., 1991] Wedgewood, L. E., Ostrov, D. N., and Bird, R. B. (1991). A finitely extensible bead-spring chain model for dilute polymer solutions. *Journal of non-newtonian fluid mechanics*, 40(1):119–139.

[Wever et al., 2011] Wever, D., Picchioni, F., and Broekhuis, A. (2011). Polymers for enhanced oil recovery: a paradigm for structure–property relationship in aqueous solution. *Progress in Polymer Science*, 36(11):1558–1628.

[Winter and Chambon, 1986] Winter, H. H. and Chambon, F. (1986). Analysis of linear viscoelasticity of a crosslinking polymer at the gel point. *Journal of rheology*, 30(2):367–382.

Miscellaneous

NPD (2018).(http://www.npd.no/en/Publications/Norwegian-Continental-Shelf/No-1-2017/Immobile-oil/). Accessed 30th March 2019

Chegg (2019). https://www.chegg.com/homework-help/questions-and-answers/simple-shear-flow-parallel-plates-consider-flow-incompressible-newtonian-fluid-parallel-pl-q14690247. Accessed 30th March 2019